

Master Erasmus Mundus in  
Colour in Informatics and Media Technology (CIMET)



*UGR* | Universidad  
de Granada



Colour Visualisation of Hyperspectral Images in Art  
Restoration

Master Thesis Report

Presented by

Ailin Chen

and defended at

Gjøvik University College

12/07/2013

Academic Supervisor(s): Prof. Jon Y. Hardeberg  
Ferdinand Deger

Jury Committee: Prof. Eva M. Valero Benito – Universidad de Granada  
Dr Pertti Silfsten – University of Eastern Finland



# Colour Visualisation of Hyperspectral Images in Art Restoration

Ailin Chen

12/07/2013

## Abstract

A large number of research and practices related to hyperspectral imaging in cultural heritage have been carried out in the past. The development of colour visualisation of paintings, especially in the field of hyperspectral imaging has been substantially invigorating for art restoration. Not only art restorers but also spectators are benefiting from hyperspectral imaging and its applications greatly. The thesis presented therefore is motivated by the ever-progressing hyperspectral imaging in the art conservation area and tries to examine its implementations in art paintings in order to serve the best for the conservators as well as museum visitors. Two main arenas of hyperspectral imaging are particularly discussed, the visualisation of the invisible information from the hyperspectral images defined in the report and the fusion of the invisible and the visible information. Related research in terms of colour visualisation of hyperspectral imaging such as the application of false colour in art paintings is also briefly discussed.

Two groups of hyperspectral data are utilised accordingly in the project. Data are acquired with two hyperspectral cameras in the spectral ranges of Visible and Near-Infrared (VNIR) as well as Short-Wavelength Infrared (SWIR), and are **based on Norwegian artist Edvard Munch's** painting *The Scream* that is held at the National Gallery in Oslo. The software used for data processing in this project is ENVI and Matlab.

Comprehensive analyses of literature were executed to construct a concrete foundation for pertinent aspects of hyperspectral imaging techniques. One piece of software inspired by previous researched work is devised for the purpose of this research. One psychophysical experiment conducted by a group of observers in order to determine the best method with respect to invisible information. The result effectively corroborated the research hypotheses and assisted the resolution of the proposed research perplexities. The information obtained in SWIR region displayed more discernible invisible information. A consultation with an expert restorer from the National Gallery in terms of the images applied for the psychophysical experiment was performed. The discussed outcome coincides with the result obtained from the psychophysical experiment and disclosed several interesting facts not only for the author but also for the expert.

The applied fusion technique combining the visible and invisible regions provided an intriguing result in terms of perceptual attributes. Further research about false colour representation also produced interesting outcomes.

The researched directions as well as the obtained results can be used as reference accordingly for the art restorer and museum visitors for conservation as well as education purposes.

## **Preface**

First of all I would like to express my gratitude and deepest respect to my supervisors, Prof. Jon Y. Hardeberg and Ferdinand Deger as well as Dr Sony George. Without their invaluable advice, guidance and encouragement this research would not have been possible.

My most sincere respect, love and gratitude go to my family: my parents Shijun Chen and Xuding Tong, my sister Yanni Chen and my brother Xiaoyong Chen. Thank you all for believing in me, for your sacrifice, support and unconditional love in every step of my life.

A special acknowledgement goes to all the lecturers from CIMET who assisted me during my MSc study and made possible this research.

Special thanks to all my friends that supported my study and research. Their invaluable friendship, encouragement and advice helped me to make the research successful.

Finally, I want to dedicate this dissertation to my beloved husband, Edgar Ramon Sanchez Galicia. Thank you very much for your love, support and patience on those very long days of this endeavour.

## Contents

Abstract .....	i
Preface.....	ii
Contents .....	iii
List of Figures.....	v
List of Tables .....	vii
List of Abbreviations.....	viii
1 Introduction .....	1
1.1 Background.....	1
1.1.1 Significance of Research.....	1
1.2 Research Objectives.....	2
1.2.1 Research Questions and Hypotheses .....	2
1.2.2 Presupposed Resolutions Towards Issues Raised .....	3
1.3 Thesis Methodology.....	3
1.3.1 Research Method.....	3
1.3.2 Data Source.....	4
1.4 Chapter Structure .....	4
1.5 Conclusion .....	4
2 Literature Review.....	6
2.1 Understanding Spectral Imaging .....	6
2.2 Spectral Images vs. Spectral Curves.....	6
2.3 Multispectral Imaging vs. Hyperspectral Imaging .....	6
2.4 Other Conservation Technologies .....	7
2.5 Invasive Techniques .....	8
2.6 Non-Invasive Techniques .....	8
2.7 Algorithms for Hyperspectral Imagery in Conservation of Paintings.....	9
2.8 Conclusion .....	10
3 Methodology.....	11
3.1 Object of Study.....	11
3.1.1 Background.....	11
3.1.2 Data Acquisition .....	13
3.1.3 Data Pre-Processing .....	17
3.1.4 Data After Pre-Processing .....	19
3.2 Research Orientation.....	19
3.2.1 <b>What is “Invisible” Information?</b> .....	19

3.2.2	<b>Seeing the “Invisible” Information</b> .....	23
3.2.3	Principal Component Analysis.....	23
3.2.4	Independent Component Analysis.....	25
3.2.5	Minimum Noise Fraction.....	28
3.2.6	Images for Comparison.....	30
3.2.7	Embedding Invisible Information into the VIS Region.....	30
3.3	Evaluation.....	37
3.3.1	Psychophysical Experiment.....	37
3.3.2	Experimental Criteria.....	37
3.3.3	Choice of Observations.....	39
3.3.4	Observers and Setting.....	42
3.3.5	<b>Comparison Between Natural Colour Images and Munch’s Image</b> .....	43
3.4	Conclusion.....	45
4	Results and Discussion.....	46
4.1	Results.....	46
4.1.1	Psychophysical Experiment.....	46
4.1.2	<b>Comparison between Natural Colour Images and Munch’s Image</b> .....	61
4.2	Discussion.....	63
4.2.1	Success.....	63
4.2.2	Failure.....	77
4.3	Conclusion.....	80
5	Conclusions.....	81
6	Future Work.....	84
	Bibliography.....	85
	Appendix A.....	91

## List of Figures

Figure 1: Electromagnetic spectrum [9].	2
Figure 2: Multispectral/Hyperspectral Comparison [13].	7
Figure 3: Four versions of <i>The Scream</i> [39].	12
Figure 4: Artefacts found in <i>The Scream</i> [43].	14
Figure 5: Hyperspectral cameras used for data acquisition [44].	14
Figure 6: Hyperspectral image acquisition [42].	15
Figure 7: HySpex VNIR-1600 acquisition principle [45].	15
Figure 8: Hyperspectral data processing flow [46].	17
Figure 9: Image warping process [46].	18
Figure 10: Image stitching [46].	18
Figure 11: Hyperspectral data from <i>The Scream</i> [46].	19
Figure 12: Active infrared night vision [47].	20
Figure 13: RGB photograph of <i>The Scream</i> .	21
Figure 14: 4 <sup>th</sup> IC processed with ICA of SWIR data.	22
Figure 15: RGB, IR, Raking and UK versions of <i>The Scream</i> [43].	23
Figure 16: Images from <i>The Scream</i> using PCA.	24
Figure 17: ICA processed versions of <i>The Scream</i> .	27
Figure 18: MNF processed versions of <i>The Scream</i> .	29
Figure 19: SWIR and VNIR set of data.	30
Figure 20: Fusion Level [30].	31
Figure 21: Transformation proposed by Tsagaris.	34
Figure 22: Transformation to RGB.	36
Figure 23: Details of interest.	40
Figure 24: Details from Table 5.	42
Figure 25: Modified process proposed.	44
Figure 26: VNIR-30cm data from <i>The Scream</i> .	47
Figure 27: Detail 1: Second coat of paint by the artist.	49
Figure 28: Psychophysical results for Detail 1.	50
Figure 29: Detail 2: Tilted 4-shaped “scratch”.	51
Figure 30: Psychophysical results for Detail 2.	52
<b>Figure 31: Detail 3: Hook shaped “scratch”.</b>	53
Figure 32: Psychophysical results for Detail 3.	54
<b>Figure 33: Detail 4: Horizontal “scratch”.</b>	55
Figure 34: Psychophysical results for Detail 4.	56
Figure 35: Detail 5: A tallow dropping.	57
Figure 36: Psychophysical results for Detail 5.	58
Figure 37: Detail 6: Cluster of tallow droppings.	59
Figure 38: Psychophysical results for Detail 6.	60
Figure 39: Summary of best and worst results.	60
Figure 40: Linear transformation using 100 images with natural colours.	62
Figure 41: Linear transformation based on an RGB photo.	62
Figure 42: SWIR_IC1 image of <i>The Scream</i> selected by the restorer.	67
Figure 43: SWIR_IC3 image of <i>The Scream</i> selected by the restorer.	68
Figure 44: SWIR_IC4 image of <i>The Scream</i> selected by the restorer.	69
Figure 45: SWIR_MNF5 image of <i>The Scream</i> selected by the restorer.	70
Figure 46: SWIR_MNF6 image of <i>The Scream</i> selected by the restorer.	71
Figure 47: SWIR_PC1 image of <i>The Scream</i> selected by the restorer.	72



Figure 48: SWIR\_PC2 image of *The Scream* selected by the restorer. .... 73  
Figure 49: VNIR\_IC3 image of *The Scream* selected by the restorer. .... 74  
Figure 50: VNIR\_MNF1 image of *The Scream* selected by the restorer. .... 75  
Figure 51: False colour image generated with the best images from psychophysical experiment.  
..... 76  
Figure 52: ICA output of detail 2. .... 78  
Figure 53: ICA output of detail 3. .... 78  
Figure 54: ICA output of detail 5. .... 79

## List of Tables

Table 1: Specifications of hyperspectral cameras used [44]. .....	16
Table 2: Characteristics of pre-processed data. ....	19
Table 3: Statistical values resulting for the set of images studied. ....	32
Table 4: Categories used for the psychophysical experiment. ....	38
Table 5: Selected details for the psychophysical experiment. ....	41
Table 6: Notation to describe processed images from details of interest. ....	48

## List of Abbreviations

CC	Correlation Coefficient
CMF	Colour Matching Function
EEG	Electroencephalogram
ERP	Event-Related Potential
HPLC	High-Performance Liquid Chromatography
ICA	Independent Component Analysis
IR	Infrared
IRR	Infrared Reflectography
ITU	International Telecommunication Union
JND	Just Noticeable Difference
LCTF	Liquid Crystal Tuneable Filter
LDA	Linear Discriminant Analysis
MEMC	Maximum Energy Minimum Correlation
MI	Mutual Information
MNF	Minimum Noise Fraction
MOS	Mean Opinion Score
MSE	Minimum Square Error
NAPCA	Noise-Adjusted PCA
OIF	Optimum Index Factor
PCA	Principal Component Analysis
RMSE	Root Mean Square Error
SAM	Spectral Angle Mapper
SEM	Scanning Electron Microscopy
SERS	Surface-Enhanced Raman Spectroscopy
SIFT	Scale-Invariant Feature Transform
SNR	Signal-to-Noise Ratio
SPD	Spectral Power Distribution
SWIR	Short-Wavelength Infrared
UV	Ultraviolet
VIS	Visible
VNIR	Visible and Near-Infrared

# 1 Introduction

## 1.1 Background

Spectral imaging technology was initially developed for the purpose of colour photography dating back to nineteenth century. In the past 40 years, the technology has progressed drastically, mainly in the application areas of astrophysics, remote sensing and terrestrial military. With the advancement of new technologies and resources, more recent implementations occurred in fields such as medical imaging, food engineering and conservation.

Spectral imaging is considered as a branch of spectroscopy and photography. Oftentimes, people tend to dub it directly as a generic term for multispectral, hyperspectral and chemical imaging [1], or even simply as hyperspectral imaging [2, 3]. The basic concept of the aforementioned terms seems to be very similar; a technique applied for spectroscopic image acquisition and analysis where the information across the electromagnetic spectrum is collected, processed and interpreted. However, the factual acquisition procedure and execution conducted differ.

This report briefly introduces the fundamentals of spectral imaging and differentiates it from hyperspectral imaging, and especially concentrates in hyperspectral imaging as well as its applications in the art conservation arena. Art conservation is a broad topic in terms of cultural heritage. Based on the data available, the particular case in terms of colour visualisation of hyperspectral imagery of paintings is studied mainly in this project.

### 1.1.1 Significance of Research

Hyperspectral imaging has been researched in many fields and like other spectral imaging it makes use of the information across the electromagnetic spectrum. Usually, the images are collected and combined to form a three-dimensional hyperspectral data cube for examination.

However, the human eye is unable to perceive such information unless it is further processed to grayscale or colour images in order to satisfy the requirements of human vision system. A plethora of information is often provided by hyperspectral imaging and with the implementation of specialised software, usually remote sensing application software, such as ENVI and OpenEV, researchers are able to apply appropriate algorithms so that important features can be identified and documented. Those features thus can be used by specialists for their respective purposes.

Art restorers need many aspects of training and education to be able to perform art restoration activities [4]. They can only attempt to return the work of art to the previous state based on their knowledge and imagination of the irreplaceable original state. Current hyperspectral imaging technology has provided a great platform for the restorers with further information outside their knowledge, skills and training supplied since most of the hyperspectral imaging data can go beyond the visible region. It is significantly important for the restorers to have the opportunity to associate their conservation work with the supplementary information to achieve better results. Not only the conservation/restoration experts can benefit substantially from the extra information supplied from hyperspectral imaging, but also the museum spectators may be able to gain more knowledge out of it. Gooch [5] in particular noted that:

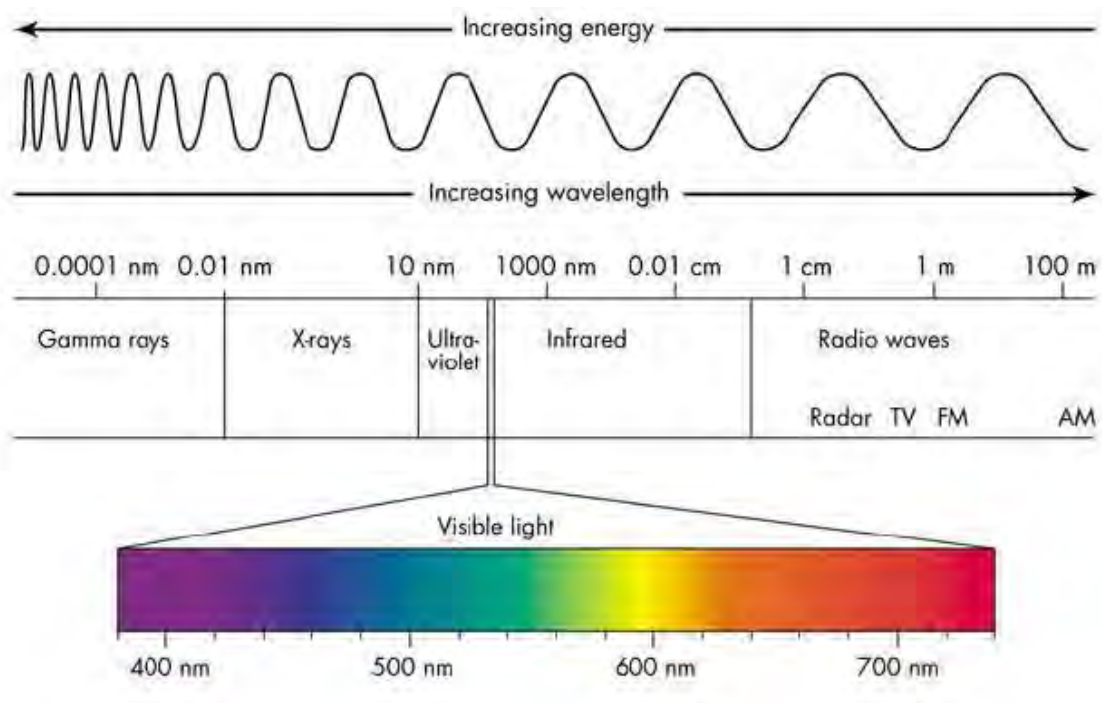
“Retracing the steps of a master artist can be immensely instructive, and help reveal artistic processes, decisions and influences that produced historically important paintings”.

## 1.2 Research Objectives

### 1.2.1 Research Questions and Hypotheses

The research presented in this thesis intends to investigate the application of hyperspectral imaging in paintings mainly for the use of art restorers. The data available for this project has been obtained via a hyperspectral camera HySpex VNIR 160 and HySpex SWIR 320m-e by Norsk Elektro Optikk AS.

The visible portion of the electromagnetic spectrum for human visual system usually is defined approximately between 380 and 780 nanometres [6]. The VNIR part ranges from the wavelength of about 400 to 1400 nanometres [7] whilst the SWIR region encompasses the spectrum between 1400 nanometres and 3000 nanometres [8]. It is identifiable there is information from the data that is located outside the range of human vision. This is particularly evident in SWIR data which includes only information from non-visible region. See Figure 1 for the spectrum range.



**Figure 1: Electromagnetic spectrum [9].**

Questions are hence raised concerning how this non-visible information can be used for the favour of art restoration purpose: *colour visualisation of hyperspectral images in art restoration*.

Further related questions and hypotheses include:

Question 1: What information can be found in the visible region? What information can be found in the infrared region?

Question 2: What can be considered as visible information? What is considered as invisible information?

Question 3: How can the invisible information be exploited?

Question 4: How can invisible information be embedded into the visible region?

Based on the nature of the data and the object of study, a painting for the purposes of this research, it is possible to make the following hypotheses.

Hypothesis 1: There might exist more invisible information in SWIR data than in VNIR data.

Hypothesis 2: There might exist a specific algorithm to best display a particular set of invisible details in the painting.

Hypothesis 3: It might be possible to display a single image with the result of the processed images with the most invisible information.

The thesis and its pertinent questions intend to address the usefulness of the information obtained from the infrared regions so that the information can be explored and applied accordingly by the restorers or the spectators. Concerning the questions raised above, corresponding answers are presupposed thereafter.

### **1.2.2 Presupposed Resolutions Towards Issues Raised**

The development of colorimetry which describes and quantifies the human colour perception has provided the possibility to transform the spectral signals to the three channels that can be visualised by the human eye. Regarding the first part of Question 1 in section 1.2.1, a transformation with the application of Colour Matching Function (CMF) and Gamma correction can be used to make the data available to be viewed by human eye. In terms of the information in the infrared region, mathematical techniques have to be applied in order to extract the most important features due to the abundance supplied. With respect to Question 2, 3 and 4, it is **necessary to define the term “invisible” for this specific project so that** further processing can be performed.

**Since the information would be “invisible”, usual colorimetric procedures might not be feasible.** The possible algorithms considered thus include mathematical methods, false colour imaging as well as image fusion techniques respectively.

## **1.3 Thesis Methodology**

### **1.3.1 Research Method**

The thesis adopts the mixed method approach, which combines quantitative and qualitative orientations to triangulate designated research objectives.

Qualitative research methods include Literature Review and Interview. Literature review is applied to introduce the technological development in hyperspectral imaging. The interview with the expert discloses further information in comparison with the result analysed from the psychophysical experiment with the participants.

The quantitative technique, Psychophysical Experiment, was conducted in order to draw the conclusion for the best method applied in respect to the extracted feature of the data. The detailed implementation of the methodologies is detailed in section 3.

### **1.3.2 Data Source**

Qualitative data demanded from the literature review section was mainly collected from secondary statistics via the Internet and libraries. The interviewee was a conservation expert from the National Gallery in Oslo.

In terms of quantitative resources, the essential data to be processed were collected in the year 2012 by the cultural heritage team and pre-processed and passed on to the author by the same team. The observers for the psychophysical experiment all have academic background and are mostly from the same research group as the author.

## **1.4 Chapter Structure**

The thesis comprises approximately six chapters. Chapter structures and components are illustrated in order *vide infra*.

Chapter 1 provides a general impression and outline for the reader that the thesis will be discussing a research interstice regarding hyperspectral data collected merely with hyperspectral cameras. In particular the comparison and integration between VNIR and SWIR data is introduced.

Chapter 2 interprets previous research work in the areas of hyperspectral imaging, typically its application in conservation field. Other conservation technologies are also compared.

Chapter 3 elaborates the research methods and techniques that are implemented in the thesis in more detail. Important definitions and the usage of those methods are explained.

Chapter 4 contains two main parts. The first part reveals the results analysed from the psychophysical experiment and possible utilisation of the best methods evaluated in terms of specific details in the painting. The second part compares the conclusion obtained from the **psychophysical experiment with the expert restorer's review** of images acquired with the same methods and examines further with a set of images coming from the concluded best methods. The fusion technique applied is also analysed with two examples.

Chapter 5 is the recapitulation of the whole thesis and the accentuation for the most advantageous methods applied in processing of the data in terms of specific details of interest as well as the similarities and differences between the result and the expert review.

Chapter 6 looks into the current problems with respect to the fusion of VNIR and SWIR data and envisages the concluded results to be applied better between the data.

## **1.5 Conclusion**

A large number of researches on the development of hyperspectral imaging have been done in the past years. Hyperspectral imaging has been an important part for the restorers to be able to look at the information outside the visible region, particularly outside their knowledge and

skills. The information processed especially in the infrared region might be significantly interesting not only for the restoration work but also for the museum spectators in terms of educational purpose.

The research presented in this thesis has obtained resources both from direct and secondary statistics. Data collected from VNIR and SWIR regions of the spectrum of a painting were pre-processed and passed onto the author. Based on the nature of the data and the painting, different algorithms are applied on the data. A psychophysical experiment with academic participants as well as an interview with an expert are designed, performed and compared in order to find the best methods.



## 2 Literature Review

### 2.1 Understanding Spectral Imaging

In the late nineteenth century a group of photographic engineers made the attempt to search for a commercially viable colour imaging system. By applying different properties of light and implementing appropriate basic tools like grating and prism, elegant platforms were invented to capture and reproduce the spectra of original scenes. Modern spectral imaging technology mainly is based on CCD cameras with many types of filters in order to capture simultaneously both spectral and spatial information of an object.

As mentioned in section 1, the primary application of spectral imaging was in the areas of remote sensing and terrestrial military back in the early 1990s, and it was described as **“multispectral” imaging originally. The evolutions of materials and resources have led to a leap** in the development and advancement of spectral imaging, not only in spectral resolution but also in its application arena.

Spectral imaging started to gain importance in the conservation field in the past decade. Fischer [10] noted that spectral imaging is based on the extensive implementation of Infrared Reflectography (IRR) in the study of paintings, yet it has extended the capabilities of IRR in diagnostic imaging.

Difference exists in spectral and spatial resolution, interval and contiguousness of bands, number of bands as well as the application, the terms and the techniques applied also differ. The most commonly used terms are multispectral imaging, hyperspectral imaging for spectral images, and full spectral imaging for spectral curves.

### 2.2 Spectral Images vs. Spectral Curves

Image cubes usually represent spectral images, particularly hyperspectral imaging because of its near contiguous spectral resolution. Multispectral and hyperspectral imaging acquire data for every pixel on each spectral band; each pixel acquires many bands along the spectrum whereas full spectral imaging acquires data as spectral curves for one point of interest, and significantly reduces the data rate and volume in comparison with the former [11].

Spectral capture of images usually can be obtained by remote sensing radiometers for multispectral images and spectral camera for hyperspectral images. Spectral measurement of a point can be done by instruments like spectroradiometer or spectrometer. Many types of detectors and filtering or dispersing technologies have been customised for specific spectral imaging systems. Two types of spectral cameras used for acquiring the hyperspectral data for this project are discussed in section 3.1.2.

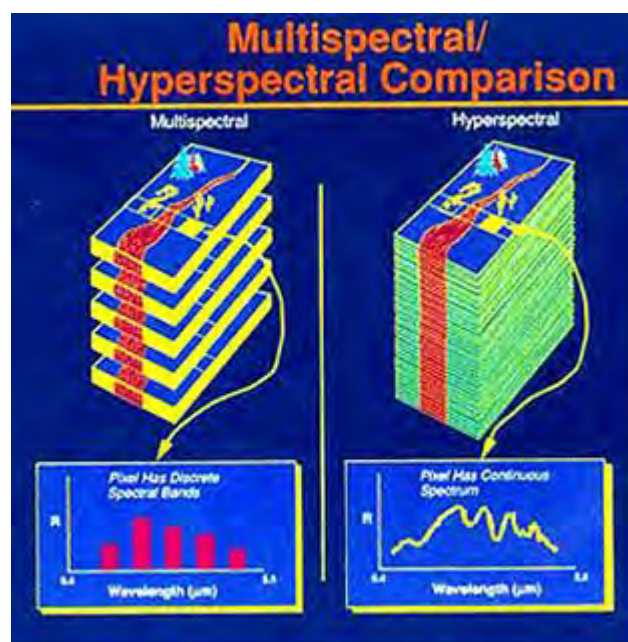
### 2.3 Multispectral Imaging vs. Hyperspectral Imaging

Basically, based on the nature of the measurement, the factors differentiating hyperspectral imaging from multispectral imaging are the interval and the number of bands as well as resolution.

Hyperspectral sensors detect narrow spectral bands along a continuous spectral range usually across the electromagnetic spectrum of ultraviolet (UV), visible (VIS) and infrared (IR) regions.

On the other hand, multispectral sensors deal with discrete and comparatively broader bands than hyperspectral sensors but can also cover the afore-mentioned spectral range. Subsequently, the application of hyperspectral data has the advantage of identifying surface features with a higher spectral resolution than multispectral data [12]. Nevertheless, different types of instruments define the properties of the spatial resolutions of the two imageries; the characteristics of the measurements would be compensating their spectral resolutions respectively. This means that the spatial resolution of multispectral imagery is therefore higher than the counterpart of hyperspectral imagery.

Consider Figure 2 where for each single pixel, the spectral values are discrete and limited to five bands in the multispectral image on the left of the figure. The spectral curve for the hyperspectral image on the right is in contrast continuous and with more bands ranging a whole spectrum in the figure.



**Figure 2: Multispectral/Hyperspectral Comparison [13].**

Shrestha [14] considers that traditionally imagery with more than 10 spectral bands is hyperspectral imagery whilst less than 10 spectral bands is multispectral imagery. However this argument has been ambiguous since Barry [15] noted that the primary difference between multispectral and hyperspectral imagery is the spectral resolution. Both imageries can have the same number of bands but covering different ranges of the spectrum. The ultimate decision for the type of imagery would be depending on the width of the bands; the more contiguous the bands are, the more possibility that it would be categorised as hyperspectral imagery [16].

## 2.4 Other Conservation Technologies

The application of spectral imaging extends from the primary usage of remote sensing to other areas such as medical imaging and art conservation. The analysis of a painting intends to provide important clues for art conservators and restorers. The conservation of paintings

necessitates a good comprehension of material compositions and construction methods applied by the artist.

**The word “pentimenti” especially refers to the hidden layer of the paintings, which usually are traces of previous work or changes made by the artist under the current state of the paintings [5].** A number of analytical techniques can reveal detailed information not limited to the materials used by the artist, but also the history of the painting through layers of the paintings. There are both invasive approaches and non-destructive methods for the study of conservation of paintings.

## **2.5 Invasive Techniques**

The techniques can be destructive where a micro sample of the painting has to be extracted from the painting to be examined. Examples include cross-sectional analysis, Scanning Electron Microscopy (SEM) and High-Performance Liquid Chromatography (HPLC).

For instance, SEM applies electrons to create images instead of light, and amplifies details to several thousand times. Therefore it has much higher magnification than light microscopes and is used to analyse the surface of materials so that the elements of a sample can be identified and the conservation treatments can be studied. This technology requires a processed sample. X-rays are generated when the electrons interact with the atomic structure of the sample material so that the composition of the elements of the sample can be analysed from the X-ray spectrum. The spectrum is considered to resemble the spectrum produced by X-ray fluorescence analysis [17, 18].

## **2.6 Non-Invasive Techniques**

Artworks are unique and precious and have great historical value; even the most cautious sampling of the materials from the artworks can only be done when additional information required is considered to be vital and repetitive sampling is not recommended [19].

Therefore, it is necessary to apply more non-invasive procedures in order to eliminate physical destruction of the paintings. They are usually non-contact spectroscopic techniques and have been applied extensively in the scientific examination and documentation of artworks. Excluding the spectral imaging techniques mentioned previously where spectroscopy and imaging are combined so that spectral acquisition with spatially resolved information can be performed; other methods include X-ray fluorescence spectroscopy, infrared spectroscopy and Raman spectroscopy.

X-ray fluorescence measures the chemical component when the atoms of an element are hit by X-rays of a known energy so that fluorescent X-rays are emitted with its specific characteristic of the elemental composition [20]. In this way, different chemical compositions can be examined. X-ray imaging has been applied successfully to reveal the hidden history of paintings as demonstrated by Gooch [5]; an underlying composition was painted over by the artist in **Picasso’s Half-Length Female Nude**.

Both Infrared spectroscopy and Raman spectroscopy are vibrational spectroscopy and work in a similar way but produce complementary information. They have been applied for pigment mapping. Particularly Raman spectroscopy has become more and more popular in the art

conservation area and is quite applicable for identification of pigments, binding media and varnishes in paintings [21, 22]. When the molecular vibrations of a sample interact with laser light, the laser photons produce shifting energies which signify the information of the vibrational models in the system [22]. Mukhopadhyay [23] documented the usefulness of **Raman spectroscopy in its ability to “unearth all sorts of secrets hidden in artworks and national treasures” resulting in the detection of plant dye madder in an Egyptian painted quiver** with Surface-Enhanced Raman Spectroscopy (SERS).

## **2.7 Algorithms for Hyperspectral Imagery in Conservation of Paintings**

Section 2.2 briefly introduced both destructive and non-destructive techniques in terms of conservation of paintings. Spectral imaging is popular in this research area as it does not need to physically cut off samples from the paintings, i.e. it is non-invasive. Since the data applied in this research is built upon hyperspectral imaging data, the algorithms in terms of hyperspectral imaging for conservation of paintings from previous studies are mentioned below.

The primary purpose of hyperspectral imaging processing is to examine the spectral signatures in order to extract features and distinguish and identify materials. Various methods based on spectral transformation and multivariate statistic techniques are available to conduct the analysis so that the trade-offs among flexibility, accuracy and speed can be fulfilled [10].

A great success has been achieved in the remote sensing field by exploiting computational methods such as multivariate analysis and pattern recognition. Distinguishing spectral features like vegetation and minerals are classified and recognised sufficiently with the applications of Spectral Angle Mapper (SAM), Linear Discriminant Analysis (LDA), Maximum Likelihood and Neural Networks [19, 10].

It appears that extensive research has been done in pigment identification since it has been one of the most important parts in conservation of paintings. Pigment mapping necessitates the usual processes of segmentation and classification. Hyperspectral imaging has had profitable adaptation of the afore-mentioned techniques in pigment mapping for example.

Mathematical investigation such as Principal Component Analysis (PCA) has been widely implemented in hyperspectral imagery and proved to be an advantageous method, for instance in identifying chemical components of different properties [19]. Its application can be standalone to extract features or can be used for pre-processing by reducing the dimensionality prior to other classification method and subsequently reduce the computational burden.

PCA is an often-cited tool for scaling down the computation as mentioned by Jia [24], Klerk [25] and Tyo [26]. The employment of PCA for hyperspectral imagery visualisation is also popular as demonstrated by Cai [27], Du [28], Minhayenud [29] and Tsagaris [30]. It is noted that the usual representation of PCA for hyperspectral imagery visualisation is to map the first three principal components of PCA to the RGB colour space [27, 31], with variations of research with different purposes. Cai [27] considers that noise-adjusted PCA may be a superior method than PCA because there might exist further object information in other PCs.

Several feature extraction models including PCA, Independent Component Analysis (ICA) and LDA have been studied by Du [32] with respect to class separability for colour visualisation of

hyperspectral imagery. Zhang [33] and Zhu [34] also investigated ICA for spectral image visualisation, where the former examined the mapping of PCs and ICs in different colour space whilst the later studied the performance of the first IC in different segmentation approaches.

It is noticeable that visualisation of hyperspectral imaging data has been considered by a number of researchers. Various mathematical models are applied in this field. However, the visualisation seems to be concentrating on the identification of different materials and structures of remote sensing imagery. Therefore, it is understandable that if the hyperspectral data of a painting is considered, the focus would be about pigment mapping.

Nevertheless, the quality of processed monochromatic images in terms of invisible information might also be interesting and very possibly provide further information not only for the scientific researchers but also for the restorers. Consequently, this research project looks at certain mathematical models in order to determine the best possible method regarding invisible **information**. The term “invisible information” will be elaborated in details in section 3.2.1.

## **2.8 Conclusion**

This chapter discussed different spectral imaging techniques and distinguishes spectral images from spectral curves as well as multispectral imaging from hyperspectral imaging; the principal difference between multispectral and hyperspectral imaging is the spectral resolution.

Including spectral imagery, other technologies such as SEM for invasive and Raman spectroscopy for non-destructive analyses are also implemented for conservation of paintings. Non-invasive techniques such as hyperspectral imaging are applauded for its ability to maintaining the state and preserving the value of the paintings.

A number of algorithms have been implemented in order to process hyperspectral imagery data for conservation of paintings. PCA is the most-cited method and has proved to be able to supply a sufficiently satisfactory result for various applications such as pigment mapping and colour visualisation. It is necessary to demonstrate the quality and differences of the monochromatic images processed by various mathematical techniques.

## 3 Methodology

The research fields of agriculture, forestry, surveillance and cultural heritage have been applying hyperspectral imagery with relatively good success. The research presented in this thesis falls within the cultural heritage application field and is focused in the conservation of paintings in particular. For this purpose one of the paintings by Norwegian artist Edvard Munch, *The Scream* held in The National Gallery, Oslo was studied. Hyperspectral data belonging to this painting were collected with two hyperspectral cameras. The data were pre-processed and passed onto the author for further processing and analysis. Several post-processing methods were considered in order to prepare images for comparison to find the most advantageous **technique in terms of “invisible” information defined in the project. Psychophysical evaluation** was conducted for the comparison and evaluation of the results. The invisible information subsequently was considered to be applied for image fusion between IR and VIS regions.

### 3.1 Object of Study

#### 3.1.1 Background

*The Scream* is the popular name given by the Norwegian expressionist artist Edvard Munch to each of his four versions of a composition. These are part of the series named *The Scream of Nature* (in Norwegian: *Skrik*; in German: *Der Schrei der Natur*). The artworks were created between 1893 and 1910, in both paintings and pastels. All of the works display a human figure with a disturbing expression at the forefront against the background of a landscape with a very turbulent and contrasting orange sky. The colours used seem to be very simple, but the concept appears abstract and the meaning conveyed is very striking. Aspden [35] describes that *The Scream* “depicts a moment of psychic calamity, of shattered nerves”, **and that the works are one of the most recognised pieces and disturbing images in modern art history. *The Scream* is considered as “an icon of modern art, a Mona Lisa for our time” [36].**

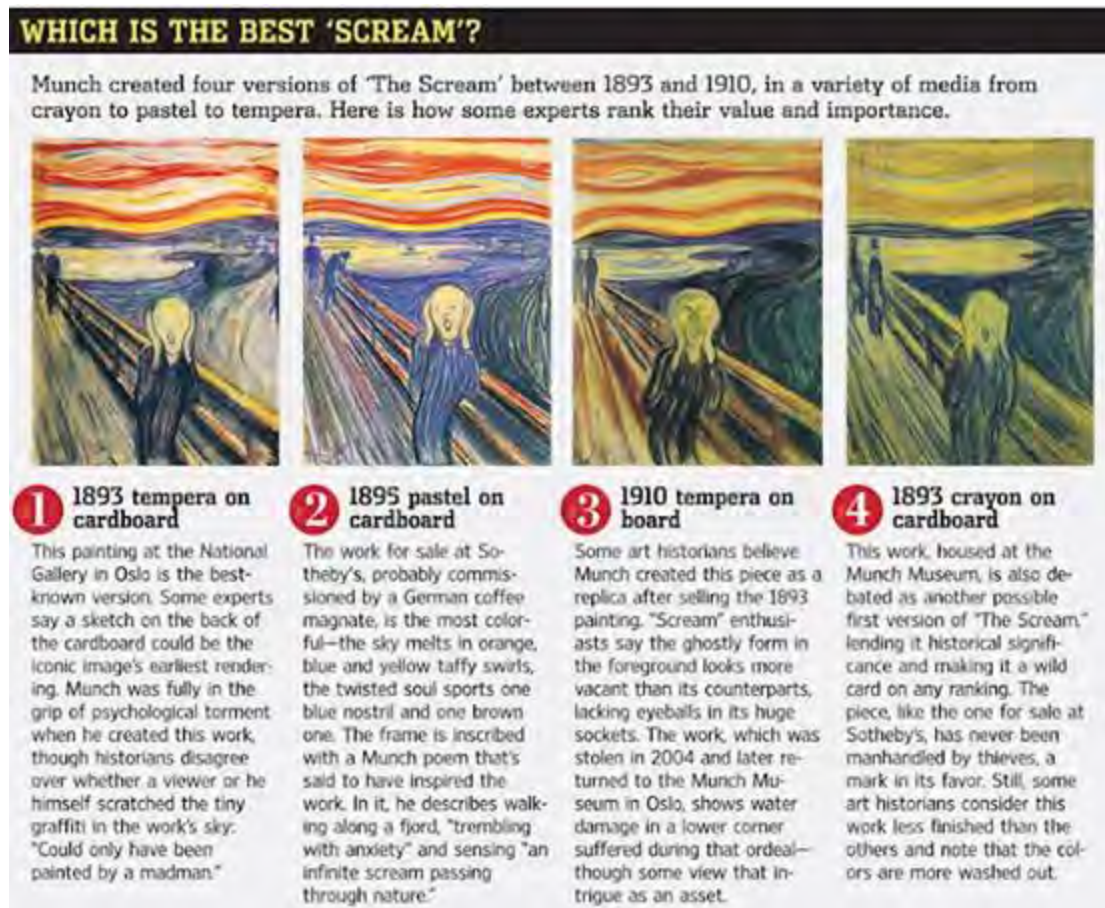
Four versions of *The Scream* were produced in various media by Edvard Munch as shown in Figure 3. One of the painted versions is held at the National Gallery in Oslo (Figure 3, 1). This version was created in 1893 and is the most well-known version of the four. The other painted version and a pastel version are held at the Munch Museum in Oslo (Figure 3, 3 and 4). The three versions have not travelled for years, but two of them have been the victims of several high-profile art thefts. The version in the National Gallery was stolen in 1994 on the same day as the opening of the 1994 Winter Olympics. It was recovered three months later after the collaboration of Norwegian police with the British police and the Getty Museum. The 1910 tempera on board version in the Munch Museum was stolen in 2004 along with another renowned Munch’s painting *Madonna*, and were recovered two years later.

The fourth version (Figure 3, 2) has been privately owned since 1937 until its auction during the Impressionist & Modern Art Evening Sale at Sotheby’s in New York. It was sold to financier Leon Black at the hammer price of \$119,922,600, which set the world record for any work of art sold at an auction [37]. The price surpassed another high profile auction price of \$106.5m for *Nude, Green Leaves and Bust* by Pablo Picasso. This version is considered to be the most colourful one and it has never been stolen or mishandled [38]. Aspden [35] argues that one of the reasons that make this version more compelling among the four is because of the **incorporated artist’s poem in its original frame about the visionary experience of how *The Scream* came to him:**

“I was walking along the road with two Friends / the Sun was setting – The Sky turned a bloody red / And I felt a whiff of Melancholy – I stood / Still, deathly tired – over the blue-black / Fjord and City hung Blood and Tongues of Fire / My Friends walked on – I remained behind / – shivering with Anxiety – I felt the great Scream in Nature – EM” [35].

The text is one of the alternatives written and dated in different dates by Munch for *The Scream* in Norwegian and German languages, as well as in French which accompanied the lithograph version of *The Scream*.

Though the text is not associated directly on the version in the National Gallery, the admirers of the artworks can draw a hint of insight on the artist’s tumultuous emotions during the creation of the first version of *The Scream*. It seems unknown which version of the two 1893 works was created first [38]. Esaak [38] believes that the 1893 crayon on cardboard version (Figure 3, 4) has not been the interest of theft was because it lacks vibrant colours and appears less finishes than the other versions.



**Figure 3: Four versions of *The Scream* [39].**

After all, the 1893 tempera on cardboard version (Figure 3, 1) is the most radical example of stylised Munch paintings [40]. It is presumed that Munch went through a number of stages in order to simplify it and make it in the way he wanted in a long process, and tried to convey “a panic attack, a feeling of despair” [40]. Jones [41] in particular located several parts of interest in

the painting and analysed the most intriguing details from the subjective and emotional point of view in order to interpret Munch's emotional experience during the creation of the artwork.

Various treatments of this painting in the past, for example, a second paint coat by the painter or retouch by the restorer as well as the damages from the theft and improper handling by the artist himself all make traces of the artefacts **identifiable on the painting**. The author's first visit to the National Gallery and discussion with the experienced museum artwork restorer Trond Aslaksby disclosed that the painting has been improperly handled due to a variety of reasons. Not to mention the notorious theft in 1994. Additionally, the artist himself also had been carelessly treating his own work.

Some of the mistreatment included, for example, subjecting the painting to outdoor conditions which resulted in a stripe of water mark on the left part of the painting. Several places were retouched by the previous restorers attempting to return the artwork to the previous state. A second coat of paint by the artist is also present, for example a small dark blue patch on the left part of the painting and a big dark blue patch on the right part of the painting. Mr Aslaksby mentioned that it is uncertain why the artist painted a layer of darker blue colour on the top. There also exist bird droppings and tallow droppings on the painting. Those features seem to be observable in the actual painting.

The other artefacts such as two lines of text possibly written by the artist, some scratches or cracks are not or barely perceivable by the human eye in the real painting. All those artefacts are of interest for this research and are examined from the scientific point of view.

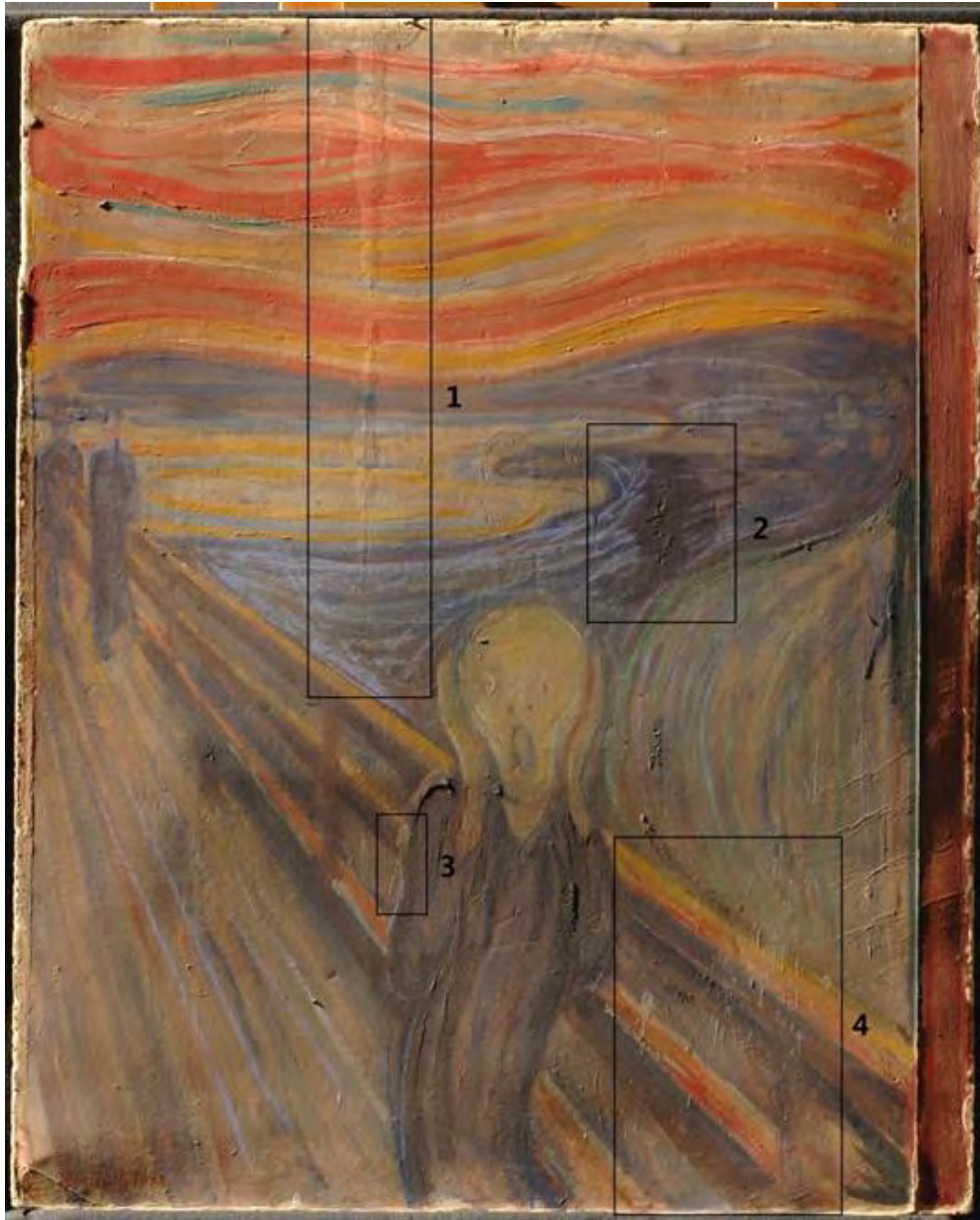
Figure 4 illustrates some examples of the artefacts. The image in this figure is a photographic RGB image taken under raking light obtained from the National Gallery. Detail 1 in Figure 4 is the water mark, detail 2 is the possible second coat paint by the artist, detail 3 is the bird dropping and detail 4 is the tallow dropping. Mr Aslaksby revealed that both the bird and tallow droppings have been attempted by previous restorers for restoration but it seemed not possible to remove the damage and restore the artwork to its original state.

### 3.1.2 Data Acquisition

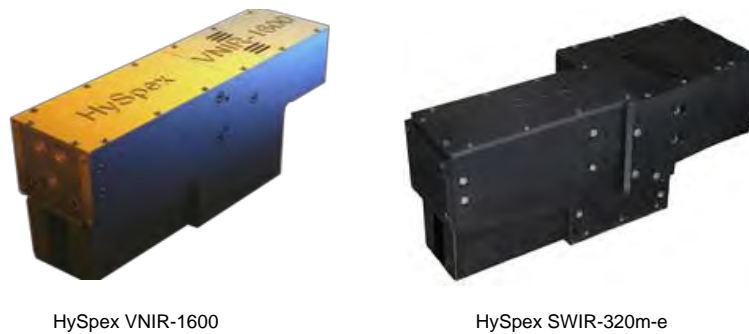
In hyperspectral imaging, spectral information is collected along with spatial data in order to create a three-dimensional hyperspectral data cube. Usually dimensions X and Y correspond to the spatial location of a pixel in a spectral band/plane and dimension Z describe the spectral signature of that pixel. Hyperspectral imaging can be implemented by high spectral resolution imaging monochromators which operate as band pass filters. Different technologies such as acousto-optic, liquid crystal tuneable filters (LCTF) and Fourier transformed interferometers are applied in imaging monochromators [19]. Hyperspectral cameras usually include the components of filters, imaging lenses, spectrographs and focal plan array sensors. In recent years, the two main methods used for acquiring hyperspectral images have been scanning and staring systems [42].

In this project, data were collected by two hyperspectral cameras, Hyperspectral Camera HySpex VNIR-1600 and Hyperspectral Camera HySpex SWIR-320m-e (Figure 5), which applies slit scanning system.



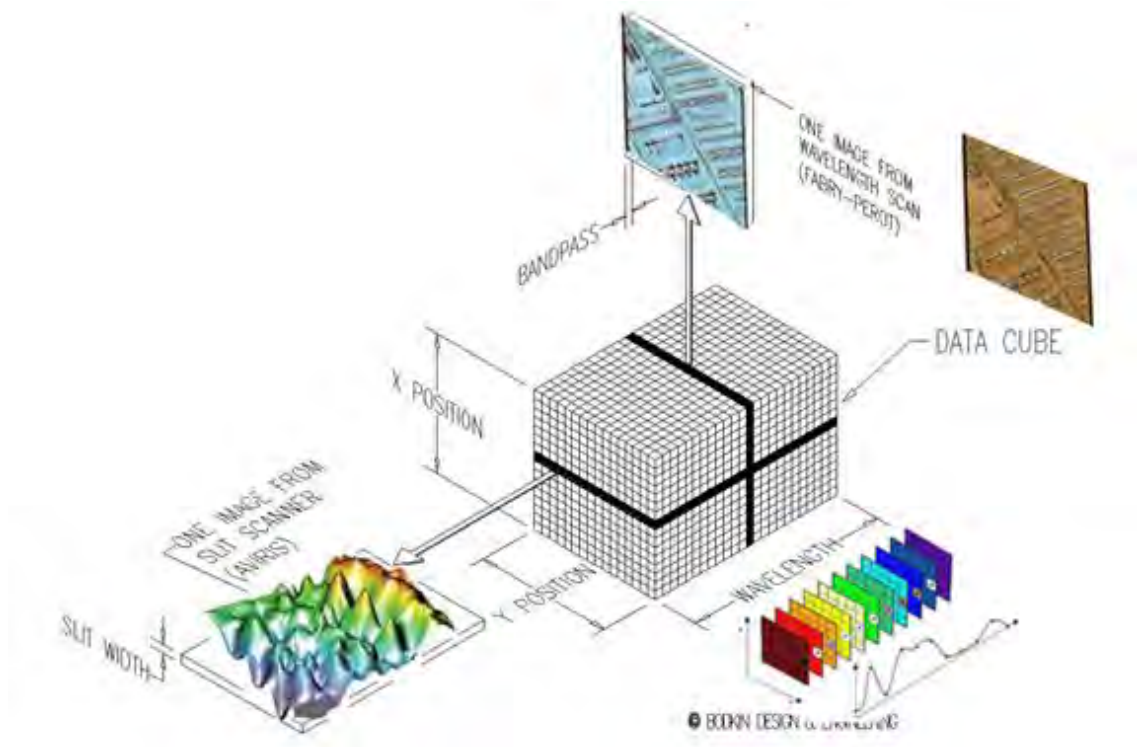


**Figure 4: Artefacts found in *The Scream* [43].**



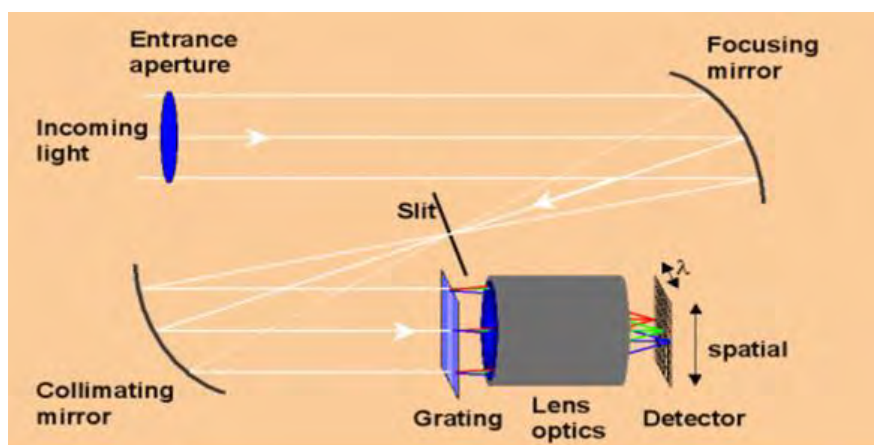
**Figure 5: Hyperspectral cameras used for data acquisition [44].**

This system obtains spectral data in slices at fixed positions and has the advantage of providing high resolution images and the disadvantage of unsuitability of high speed applications (Figure 6).



**Figure 6: Hyperspectral image acquisition [42].**

Figure 3.3 is the schematic of the optical illustration of the HySpex VNIR-1600 hyperspectral camera. Incoming light is reflected by an aspheric mirror (focusing mirror) onto a slit. After passing through the slit, a second aspheric mirror (collimating mirror) collimates the light onto a transmission grating in order to disperse the light. The light then is focused onto a two dimensional CCD detector array. HySpex SWIR-320m-e works in a similar manner.



**Figure 7: HySpex VNIR-1600 acquisition principle [45].**

The specifications of the two hyperspectral cameras used are detailed in Table 1.

<b>Detail</b>	<b>HySpex VNIR-1600</b>	<b>HySpex SWIR-320m-e</b>
Detector	SSI CCD 1600 x 1200	HgCdTe 320 x 256
Spectral range	400nm - 1000nm	1000nm - 2500nm
Spatial pixels	1600 (x1)	320 (x1)
FOV across track*	17°	13.5°
Pixel FOV across/along track*	0.18 mrad/0.36 mrad	0.75 mrad/0.75 mrad
Spectral sampling	3.7nm	6nm
Number of bands	160	256
Binning modes	2, 4, 8	-
Digitization	12 bit	14 bit
Max frame rate**	135 fps	100 fps
Sensor head weight	4.6 kg	7.5 kg
Sensor head dimension (lwh in cm)	31.5 x 8.4 x 13.8	36 x 14 x 15.2
Sensor head pwr. consumption	~6 W	~100 W
Camera interface	Camera Link	Camera Link

\* Can be doubled with field expander

\*\* At full resolution. Can be increased by binning/sub-windowing

**Table 1: Specifications of hyperspectral cameras used [44].**

The renowned Norwegian painter Edvard Munch's painting *The Scream* held in the National Gallery in Oslo, Norway was used in this research. The painting is of surface size 91cm x 73.5cm. Due to its limited size and resolution, the HySpex VNIR-1600 camera collected the spectral information of the painting in three main strips. The camera and the illumination source were controlled by a translator stage.

When the stage where the camera was attached remained fixed, the camera acquired data for each strip and the data of each strip was generated in slices from top of the painting to the bottom. In order not to lose information while generating data for each strip of the painting with the hyperspectral camera, the camera had to be placed in positions where the edges of the neighbouring strips overlapped. Subsequently, all the data collected had to be pre-processed before conducting further analysis. In terms of HySpex SWIR-320m-e, a similar data collection method was applied, but in eleven strips.

The camera parameters were set for optimal signal-to-noise ratio. In order to avoid specular reflections from the surface of the painting, lighting levels were controlled and polarising filters were employed accordingly.

Subsequently, data collected with both cameras include several sets: spatial resolution of 0.06mm obtained at focal length of 30cm and spatial resolution of ~0.2mm obtained at focal length of 100cm; one situation is to locate a polarizer in front of the illumination and in another situation in front of the camera.

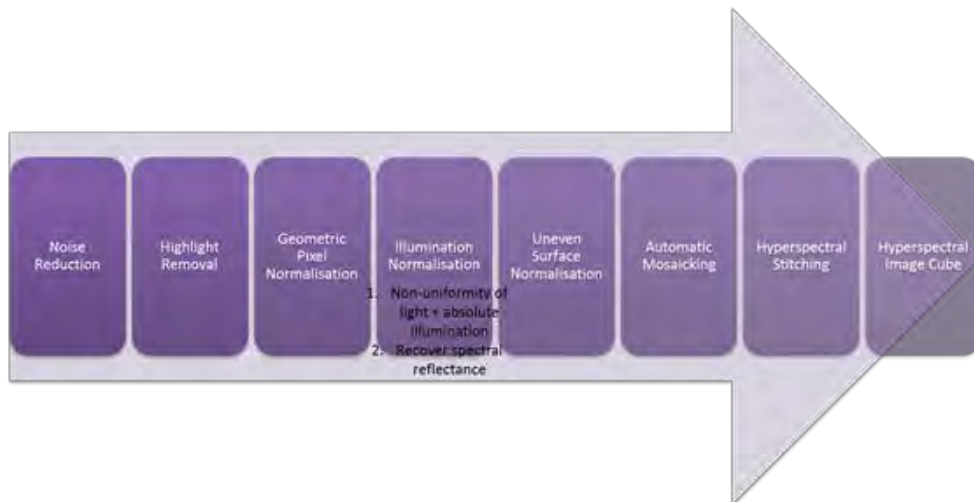
A calibrated grey patch and Macbeth Colour Checker were simultaneously captured as reference for normalization and conversion to spectral reflectance

### 3.1.3 Data Pre-Processing

Hyperspectral imagery contains much more information than the conventional imagery such as photographic RGB or IR images. In the meanwhile, hyperspectral data produce a large amount of redundancy since the neighbouring spectral bands usually have high correlation [31]. Subsequently, noise may exist in the bands that are not similar to their neighbours and the bands will have low SNR. Particularly, in remote sensing imageries, water absorption generates bad bands with low SNR. Furthermore, white spots coming from sensor saturation might also cause bad pixels [27]. Therefore, essential pre-processing steps are necessary to remove redundant and irrelevant bands and bad pixels.

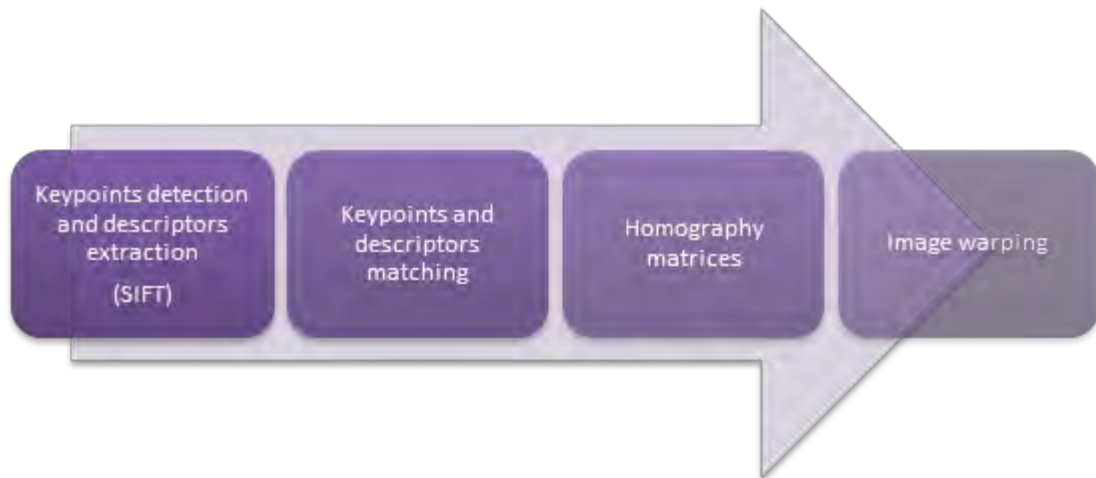
Various mathematical computations such as Correlation Coefficient (CC), entropy or Mutual Information (MI) can be used to remove bad bands. Sometimes an appropriate threshold is set for relevant algorithms. Cai [27] considers that noisy pixels can exist in two types: isolated pixels which are not correlated with their neighbours and the correlated pixels on stripping lines. Two sets of algorithms implementing recurring procedures and thresholding are applied to remove bad pixels.

For each set of hyperspectral data obtained from *The Scream*, similar steps should be carried out. Additionally, the acquired data has its particular property, for instance the VNIR-100cm data collected with spatial resolution of ~0.2mm and at focal length of 100cm are in three overlapping images instead of a full spectral image at each band. Furthermore, the illuminations might have changed also due to the lengthy acquisition of the three strips. Consequently, further processing such as illumination normalisation, mosaicking and stitching were performed. In this procedure, mosaicking denotes the process of arranging the pixels from the slices in appropriate orders so that the data for the aligned pixels can form a correct order of the painting in software for processing. Stitching signifies the process of matching the pixels on the overlapping edges of two strips so that two strips can be aligned together to cast a faithful appearance of the painting. Figure 8 illustrates the calibration and processing of the data.

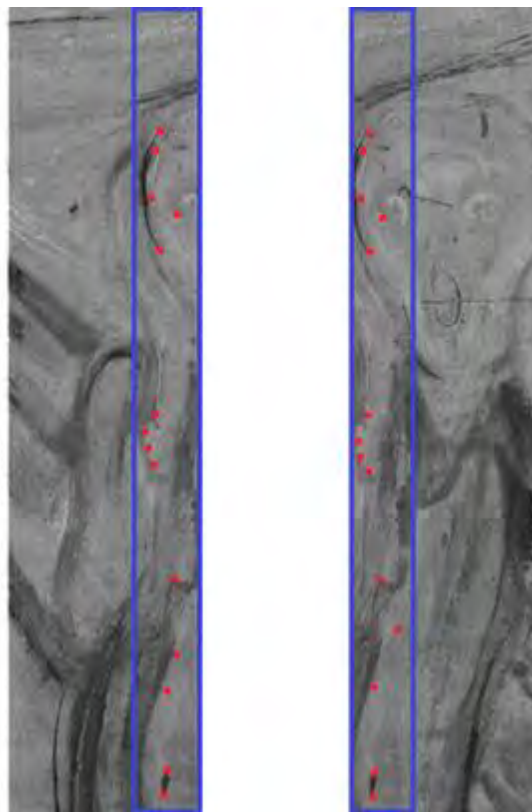


**Figure 8: Hyperspectral data processing flow [46].**

The exemplary schematic of the stitching process applying SIFT (Scale-Invariant Feature Transform) for two strips for one channel is depicted in Figure 9 and Figure 10.



**Figure 9: Image warping process [46].**



**Figure 10: Image stitching [46].**



### 3.1.4 Data After Pre-Processing

Several sets of data acquired by both cameras were processed in similar manners. After all the pre-processing procedures, the hyperspectral imagery can be represented in an image cube as in Figure 11.



**Figure 11: Hyperspectral data from *The Scream* [46].**

For instance, the final VNIR and SWIR data obtained with spatial resolution of ~0.2mm and at focal length of 100cm therefore have the characteristics shown in Table 2.

Detail	VNIR-100cm	SWIR-100cm
Dimension	2606 x 800 160	1060 x 1318 x256
Spectral Range	414.6nm – 992.5nm	967.3nm – 2498.9nm
Spectral Resolution	3.6nm	6.05nm

**Table 2: Characteristics of pre-processed data.**

## 3.2 Research Orientation

### 3.2.1 What is “Invisible” Information?

The spectral range of VNIR data used for this project envelopes not only the spectral range of VIS region from approximately 414.6nm to 778.1nm but also the IR region from approximately 781.7nm to 992.5nm. Depending on the VIS range defined by different literature, the range may vary slightly. The spectral range of SWIR data only covers short-wavelength IR range, and it is outside the VIS region that the human eye can perceive.

Figure 12 is an example of the situation when the object (the man) cannot be perceived by the human eye but can be captured by IR night vision equipment. Therefore, the author considers the “invisible” information as the information outside the VIS wavelength region since this region is invisible to the human eye.



**Figure 12: Active infrared night vision [47].**

Figure 13 displays a conventional photographic RGB image of the painting *The Scream*. Figure 14 is a mathematically processed image from SWIR data. It is observable that the marked details in Figure 14 are barely perceivable in Figure 13, especially details 1, 2, 3 and 4. According to the author, detail 1 is not visible at all in Figure 13, but it is distinguishable that it consists of written text in Figure 14. Details 2, 3 and 4 are hardly seen in Figure 13, but again very explicit in Figure 14.

Close examination of the original artwork in the National Gallery by the author has determined **that the details of interest 2, 3, 4 appear to be scratches or “depressions” as denoted by the expert of the National Gallery**, but they are still rather difficult to see even on the real artwork. Those details seem to be augmented in the processed image, and can be discovered effortlessly without even being pointed at. Subsequently, it is defined that the information is **also “invisible”** when it is implicit and barely perceivable by human eye in conventional photographs or original paintings but is augmented and explicit to the human eye applying different mathematical algorithms.



**Figure 13: RGB photograph of *The Scream*.**



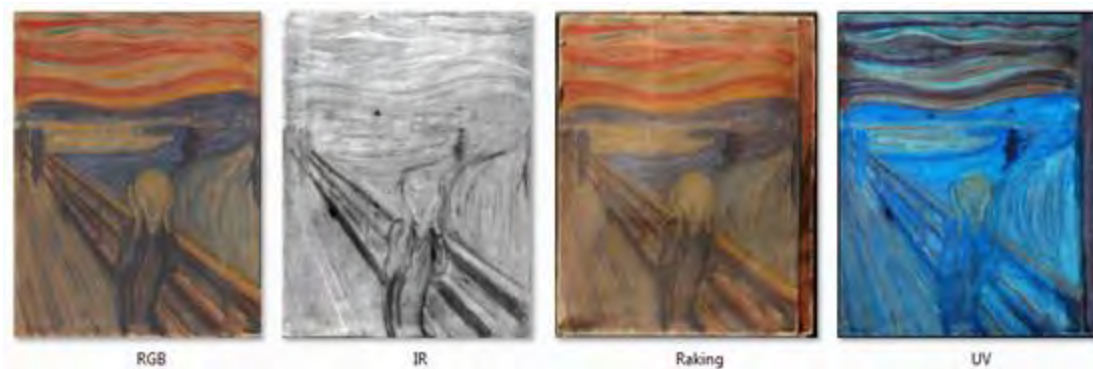


Figure 14: 4<sup>th</sup> IC processed with ICA of SWIR data .

### 3.2.2 Seeing the “Invisible” Information

The “invisible” information for this project is defined in section 3.2.1. The project intends to find the best method to see the “invisible” information as well as to study the possibility of embedding the “invisible” information into the VIS region.

There are a variety of methods that are considered to observe the invisible information. The cultural heritage team where the author is based at had the opportunity to obtain a series of valuable images from the National Gallery. Four of those images are taken into consideration for this project and they are: the photographic RGB image taken by a professional photographer from the National Gallery with digital camera Hasselblad H4D-200MS, a photographic RGB image taken under raking light placed at the top of the painting, a photographic RGB image taken under UV light and a photographic grayscale image taken with multispectral imaging camera with IR filter with its peak value at 1050nm between 1000nm and 1100nm. These images are all displayed in Figure 15 respectively.



**Figure 15: RGB, IR, Raking and UV versions of *The Scream* [43].**

As it has been mentioned previously in section 2.7, PCA has been a very promising and classical approach for statistical data analysis in order to extract features and data reduction. PCA thus is applied as one of the techniques to extract invisible information in this project. Other mathematical models such as ICA and MNF have also been applied in previous research although they are oftentimes thought to be similar to PCA. For instance, ICA is thought to be a generalisation of PCA [48] or an extension of PCA [49]. MNF is renowned for its property of two cascaded PCA. In the work published by ERDAS [50] it was noted that PCA and MNF are the two widely applied feature extraction techniques in remote sensing.

It is considered that there are not only similarities but also differences among the three mathematical models in terms of its mathematical principles. However, the comparison among the three seems to be rare in terms of the quality of the extracted features, especially in the field of hyperspectral imagery of paintings. The author thinks it is a new research direction and interesting to explore and compare the results to see which algorithm performs best in terms of perceiving invisible information.

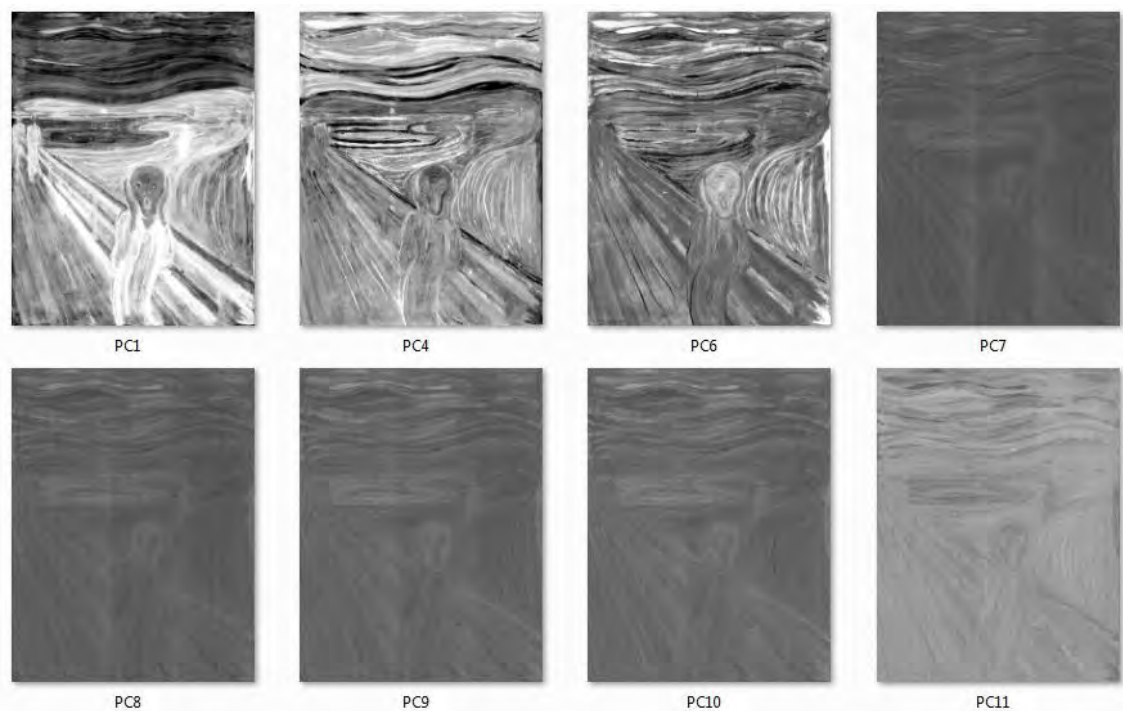
### 3.2.3 Principal Component Analysis

PCA is a typical mathematical procedure to transform a set of possibly correlated variables into a set of linearly uncorrelated variables of orthogonal principal components. The transformation is thus orthogonal and de-correlates the original set of observations. By translating and rotating

the original data into a new coordinating system, the purpose of maximising the information can be achieved, that is, the concentration of the available information on a single band thus can maximise the variance of the pixels and the features in this band [51].

Therefore, PCA constructs the ordering of the PCs based on their cumulative proportion of variance [51]. The first PC corresponds to the largest possible variance of the data and has as much of the variability in the data as possible. The succeeding second PC then accounts for the second largest possible variance of the data and so forth. The total number of PCs corresponds to the total number of channels of the hyperspectral data. As the index of the PC increases, the variability level tends to be lower.

As a result, the higher number the PC is, the more noise appears to be in the PC and the quality of the image decreases. Figure 16 illustrates an example of a series of PCA processed images on VNIR-1m data. The captions denote the indices of the PCs. It is observable that the quality of the image is deteriorating and the image tends to be noisier as the order of the PC becomes higher. Particularly, after the 6th PC and starting from the 7th PC, the quality of the processed image degrades so that the image is almost indiscernible and incoherent with the previous images.



**Figure 16: Images from *The Scream* using PCA.**

In most of the literature, the first six PCs are considered to perform the evaluation; usually merely the first three PCs are measured in some research. Consequently, in order to fully exploit the invisible information in the primary PCs as well as to reduce the computation burden, only the first six PCs are computed for this project. The constraint of the transformation is that it assumes the data have a Gaussian distribution and that can be independent only when the data is distributed normally. Subsequently, PCA is sensitive to relative scaling of the original data.

Statistically, PCA can be implemented with covariance method or singular value decomposition. The following steps briefly illustrate the implementation of PCA with covariance method for a hyperspectral entity with  $m \times n$  pixels per channel and  $p$  different channels:

1. Compute the covariance matrix  $C_x$  with the equation:

$$C_x = \frac{1}{m \times n} \sum_{i=1}^{m \times n} (x_i x_i^T - m_x m_x^T)$$

The PC therefore can be written as:

$$y_i = a_{1i}x_1 + a_{2i}x_2 + \dots + a_{pi}x_p$$

or:

$$Y_i = a_i^T X$$

Where  $x$  is the given N-dimensional variable  $[x_1, x_2, \dots, x_N]^T$ , i.e. each pixel of the hyperspectral data in a form of a vector whose components are the respective spectral responses of the hyperspectral channels.  $M$  is the mean vector  $[m_1, m_2, \dots, m_N]^T$  and  $m_x = E\{X\} = \frac{1}{m \times n} \sum_{i=1}^{m \times n} x_i$  is the coefficient of the transformation for each dimensional variable  $x_N$  in  $x$ .

The computed covariance matrix  $C_y$  is a diagonal matrix comprising of eigenvalues of  $C_x$   $\lambda_1, \lambda_2, \dots, \lambda_N$ :

$$C_y = \begin{bmatrix} \lambda_1 & 0 & 0 & \dots & 0 \\ 0 & \lambda_2 & 0 & \dots & 0 \\ 0 & 0 & \lambda_3 & \dots & 0 \\ \vdots & \vdots & \vdots & \ddots & \vdots \\ 0 & 0 & 0 & \dots & \lambda_N \end{bmatrix}$$

Where  $\lambda_1 > \lambda_2 > \dots > \lambda_N$ .

All components transformed can be denoted as  $y = A^T$  where  $y$  is the resulting N-dimensional variable  $[y_1, y_2, \dots, y_N]^T$  and  $A$  is the eigenvector matrix. The covariance matrix of  $y$  is obtained with  $C_y = AC_x A^T$ .

2. Project the original image onto the eigenvector. The images of PCs for each eigenvalue can be obtained by projecting the original images onto the corresponding eigenvectors. A new coordinating system is thus constructed from the transformation where the origin is at the centroid of the population, and the axes are in the direction of the eigenvectors of  $C_x$ .

The transformation aligns the data with the eigenvectors with the rotation and translation mechanisms and subsequently de-correlates the data.

### 3.2.4 Independent Component Analysis

ICA is a very powerful technique for array processing and data analysis and it is able to separate independent sources linearly mixed in several sensors by maximising the statistical independence of the estimated observations [52]. ICA performs a linear transformation to extract features where each component corresponds to a specific feature [50]. Those separated independent sources are called independent components or factors (latent variables).

The ability of separating the sources blindly by ICA has provided great potential in applications such as sound signals separation, telecommunication and medical signals treatment. However, it has not yet often been used by statisticians [48].

With ICA unobserved signals or sources are recovered from observed mixtures, the assumption of mutual independence among the signals thus can be explored. Therefore, this technique differs from PCA and assumes the data is non-Gaussian distributed in general. It signifies that ICA decomposes a set of mixed signals into a set of independent signals whilst PCA decomposes a set of signal mixtures into a set of uncorrelated signals [53].

Several ways can be applied to define independence for ICA algorithms, and the particular ICA algorithm is determined by the choice. The most often-cited definitions for independence of ICA algorithms are maximisation of non-Gaussianity as mentioned previously as well as minimisation of mutual information. Depending on the definitions, the algorithms vary; the most well-known algorithm for ICA is FastICA where a fixed-point iteration scheme is based and tends to maximise the non-Gaussianity.

An example where **ICA is employed is the famous “cocktail party problem”** where the aim is to distinguish a specific voice from the voice mixture captured with multiple sensors, usually with the same number of sensors as the number of the voices recorded. With ICA, the principle of FastICA can be explained as follows. When the sound sources are recorded, the same sound source appears to have different weights on different sensors, this algorithm works by finding the weights of each component. FastICA starts by guessing a random weight, followed by educated guesses in loops. After a certain number of guesses, the result will change less and less since the answer is getting closer. The algorithm stops when it finds weights with an error less than a user-specified bound. Before the FastICA algorithm is applied, the input data should be centred and whitened so that ICA estimation can be simpler and better conditioned. The process of de-correlating a set of observed variables and transform them into a set of new random uncorrelated variables whose variances equal unity is called whitening transformation.

Generally, it is not possible for ICA to identify the actual number of source signals, or a uniquely correct ordering or a proper scaling of the source signals [51, 54]. Since the ICs obtained from most ICA algorithms are arbitrary, it restrains the appropriate application of ICA in pattern discovery and dimension reduction [51].

Various researchers have worked on to determine specific ordering of ICs for ICA algorithms. For instance, Wu [51] proposed an optimal ordering solution of ICs according to the criterion of Minimum Square Error (MSE). Cross validation is also applied in order to select the number of dominant ICs. The method is proved to be promising. Shimizu [55] also developed a casual ordering method based on the non-normality of the observed variables in order to tackle problems like the inability of finding the casual direction between two variables. A topographic order is proposed by Hyvarinen [56] **making use of ICA’s higher-order** correlations. The dependence of two components is approximated by their residual dependence structure so that the proximity of the components can be estimated in the topographic representation.

However, Cheung [57] thinks that the existing methods do not consider the interactions among the individual components on the observed signals, and introduced a combinatorial optimisation problem and order the ICs based on their joint contributions in the reconstructed data. This approach was identified to have outperformed one of the existing methods.

PCA is well known for its application only on second order statistics information based on the information included in the covariance matrix of the data vectors so that it only de-correlates

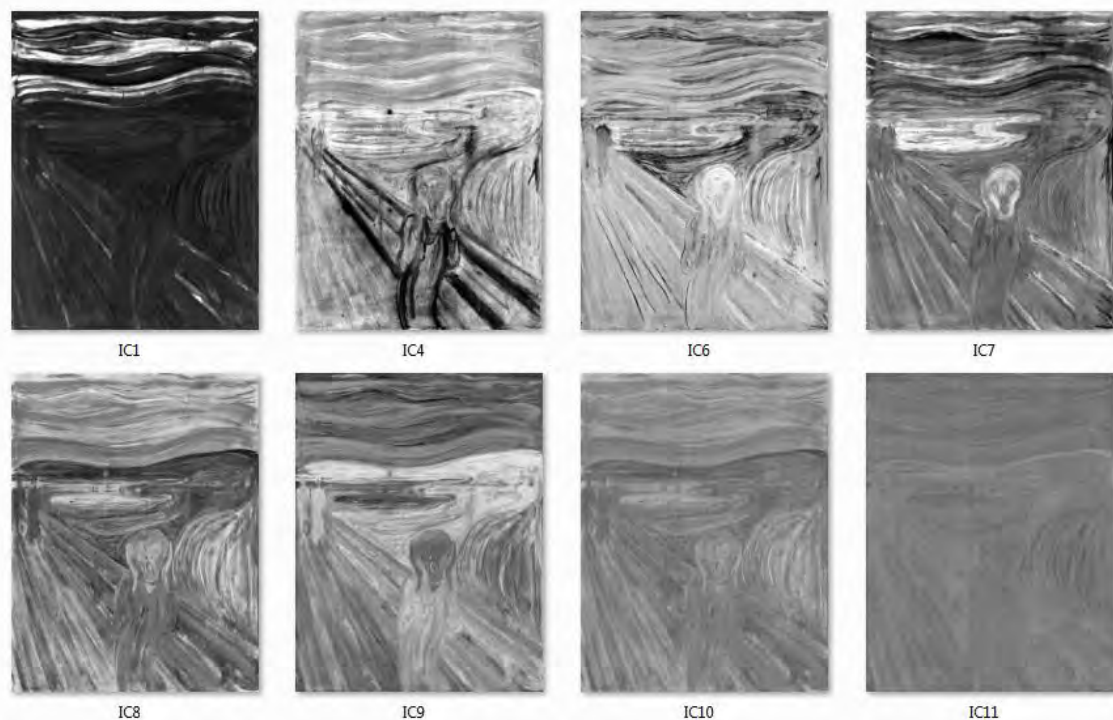


data but the resulting PCs are not independent [58]. On the other hand, higher order methods make use of the information not included in the covariance matrix of the data [58].

ICA accounts for higher order moments while performing extraction of ICs [59, 54, 57, 53]. ICs are considered to be able to reveal more interesting features and more useful information than PCs, especially in time-series evaluation [57, 60]. Bugli [48] concluded that a more useful data is represented by ICA than PCA in terms of electroencephalograms (EEG) analysis, especially for the representation of an EEG with a particular characteristic named event-related potential (ERP). However, PCA can be used as pre-processing step in some ICA algorithm.

The ordering mechanism applied for this project is to arrange the ICs according to 2D spatial coherence which takes the average of two correlation coefficients. The two correlation coefficients are computed between each spectral band and a version of itself, one is offset by one line, and another is offset by one sample. In this way, IC bands that contain more spatial structure and most of the information would appear first and IC bands that contain little spatial structure and more noise would appear last.

As a result, the higher number the IC is, the more noise appears to be in the ICs. Figure 17 illustrates the images processed on VNIR-1m data for an example. The captions denote the indices of the ICs. It is observable that the quality of the image is also deteriorating and the image tends to be noisier as the order of the IC becomes higher. However, the degree of degradation in of ICs from ICA tends to be slower than PCs from PCA since it appears that it is until 10th IC and starting from the 11th IC that the quality of the processed image becomes indiscernible and incoherent with the previous images.



**Figure 17: ICA processed versions of *The Scream*.**

Additionally, the PCs from PCA adopted for this research are the first six PCs. In order to compare the corresponding counterparts between PCs and ICs as well as reduce the computation burden, the first six ICs are also computed for this project only.

The non-linear ICA is a completely different case. It is not considered as yet for this project due to the time limitation, but it can be regarded as a research direction in the future work.

### **3.2.5 Minimum Noise Fraction**

MNF transform is a technique comprising of two consecutive data reduction operations. The first operation de-correlates and rescales the noise in the data based on the estimated noise **covariance or correlation matrix**. A **“shift difference” method applying local pixel variance** is implemented for noise statistics in order to estimate noise. By subtracting line-shifted and sample-shifted images from the raw data and averaging and scaling these two results, a virtual noise image can be created. This stage results in unit variances and no band-to-band correlations in the noise of the transformed data, therefore it does not involve the information between the band noise.

The second transformation performs as a standard principal component transformation on the noise-whitened data but corresponds to the original correlations [61, 62]. A set of variables containing weighted information about the variance across all bands from the raw data is created.

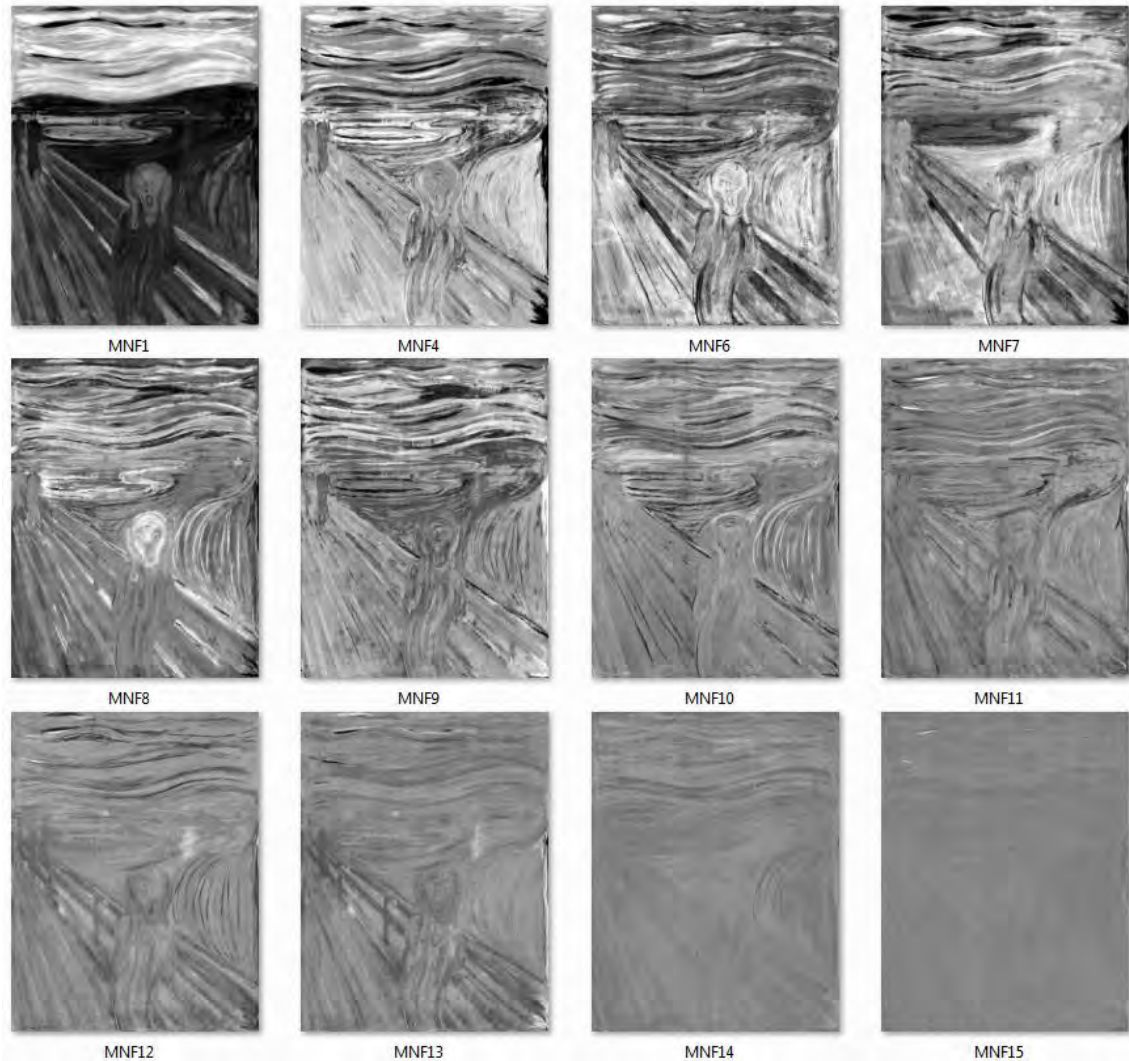
Similar to PCA, the subsequent result of the MNF transformed data is that, the first few bands contain the largest amount of variance; as the band number increases, the variance of the data decreases. After the first few dominant bands, the rest of the bands appear to be contributed only with noise and the images are not coherent any longer [61, 63]. The subsequent processing does not contain the bands with only noise.

In order to perform further spectral processing, the weighting levels of the transformed bands can be investigated based on examination of the final eigenvalues and the associated images. Two parts are formed from the transformed data space: one part is associated with large eigenvalues and coherent eigenimages and another part is associated with near-unity eigenvalues and noise-dominated images and it is complementary to the former part. With the application of the coherent components, the results of the spectral processing can be improved since the noise is separated from the data. The results can be associated with the raw bands whose contributions are the most to the information comprised in the dominant bands.

Consequently, the dominant bands can be used to conduct an inverse MNF transformation with the spectral subset with only the good bands or smoothed noisy bands, but result in the same number of transformed channels as the original data [61, 62, 64].

Green [64] noted that unlike the remote sensing data, the result of PCA in terms of aircraft scanner data does not order the image in the usual way where the image quality decreases as the PC number increases. However, MNF can always achieve the expected ranking result according to image quality. The transformation is considered to be equivalent to PCs when the noise variance is the same in all bands.

Subsequently, the higher number the component of MNF transformation is, the more noise appears to be in the component and the quality of the image decreases. Figure 18 illustrates examples of MNF processing on VNIR-1m data where the captions denote the indices of the components of the MNF transformation. It is observable that the quality of the image is deteriorating and the image tends to be noisier as the order of the component becomes higher.



**Figure 18: MNF processed versions of *The Scream*.**

Similarly, the degree of degradation in of components from MNF transformation tends to be slower than PCs from PCA, and even slower than ICs from ICA, since it appears that it is until 14th IC and starting from the 15th IC that the quality of the processed image becomes indiscernible and incoherent with the previous images.

The PCs from PCA adopted for this research are the first six PCs as well as the case for the number of ICs from ICA. In order to compare the corresponding counterparts with PCs as well as ICs, in the meanwhile reduce the computation burden, the first six components from MNF transformation are also computed for this project only.



### 3.2.6 Images for Comparison

As mentioned in section 3.2.2, four images were obtained from the National Gallery, Oslo. The first six components are to be calculated from the three algorithms, PCA, ICA and MNF. The hyperspectral data obtained to be processed for this project is VNIR-30cm and SWIR-1m. The choice of VNIR-30cm is because of its high resolution. The author thinks that there might contain more information in the hyperspectral data and the observers may be able to perceive additional invisible information from the processed images. Furthermore, since the VNIR data has less spectrum bands in the IR region comparing with the SWIR data, high resolution imagery of VNIR-30cm data may be able to compensate the disadvantage of fewer IR spectral channels. For each set of data, 6 images were generated respectively from the three methods mentioned above. A sum of 18 images is to be obtained for one set of hyperspectral data (Figure 19).

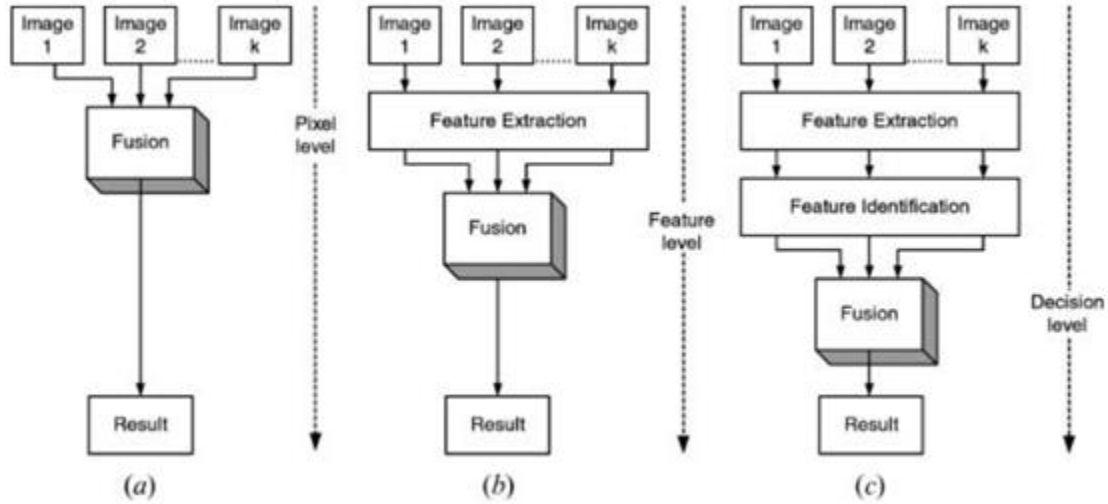


**Figure 19: SWIR and VNIR set of data.**

### 3.2.7 Embedding Invisible Information into the VIS Region

In the previous section, three computational techniques in terms of feature extraction and data reduction are introduced for this project to process the hyperspectral imagery of *The Scream* so that invisible information can be compared. On the other hand, if the invisible information is able to be extracted from the hyperspectral images, is it possible to embed this information to VIS region? If it is possible, how can this procedure be performed? This section therefore illustrates the possibility of embedding invisible information found from the infrared spectrum region into the VIS region.

The fusion method presented here and applied to the data is based on and adapted from Tsagaris' *Multispectral image fusion for improved RGB representation based on perceptual attributes* [30]. Enhanced visual interpretation can be achieved with fusion, where different spectral characteristics or image models are combined applying appropriate techniques. There are several ways of fusion as illustrated in Figure 20. It is observable that fusion at pixel level is when the raw data is processed directly; pixel-level fusion is considered to be able to improve the efficiency of classification and detection algorithms.



**Figure 20: Fusion Level [30].**

The primary concept of the technique is to produce an RGB colour image with maximum information from the original dataset and enhanced visual features in comparison with the source bands. The data used by Tsagaris is based on a four-band multispectral image with R, G, and B components as well one IR channel. In his research, Tsagaris converts the multispectral data into RGB space with a transformation, but preserves the correlation properties of RGB components existing in natural colour images. The properties of human vision perception as well as the attributes of natural colour images are explored. The covariance matrix obtained from PCA is adjusted according to the afore-mentioned properties in order to acquire the final colour image. Mutual information (MI) and Optimum Index Factor (OIF) are also considered to achieve maximum mutual information.

Since this transformation is based on the principle of the PCA, for the purposes of explaining this method, the same notation from section 3.2.3 is used. The transformation of PCA is always possible if  $C_x$  is real and symmetric; therefore locating a set of orthonormal eigenvalues is always possible. Say  $e_i$  and  $\lambda_i$  with  $i = 1, 2, 3, \dots, N$  are the eigenvectors and the corresponding eigenvalues of  $C_x$  ranked in descending order, and  $A$  is a matrix with rows constructed with the eigenvectors of  $C_x$ . The rows of eigenvectors are also ordered in the way that the first row of the eigenvector corresponds to the largest eigenvalue, and the last row of the eigenvector corresponds to the smallest eigenvalue. Matrix  $A$  thus is defined as the transformation matrix that projects  $x$  into vectors  $y$  and  $y = A(x - m_x)$ . The covariance matrix  $C_y$  of  $y$  is denoted as  $C_y = AC_xA^T$ . After the transformation, the mean of  $y$  is zero.

In the multispectral imagery used by Tsagaris, the transformation produced a grayscale image with the highest percentage of the total variance from the 1<sup>st</sup> PC. This is considered to be optimal since the image will have the highest contrast and bigger percentage of visual information. The 2<sup>nd</sup> PC held the second largest variance and contrast of total visual information and the 3<sup>rd</sup> PC the third largest counterparts.

However, if the first three PCs are constructed as colour image, where 1<sup>st</sup> PC as red, 2<sup>nd</sup> PC as green and 3<sup>rd</sup> PC as blue or the PCs are arranged with the primary colours in the other orders, the result is not optimal. It is because the three components are completely uncorrelated and it

does not correspond to the human visual system. Tsagaris thinks that a high degree of contrast will be displayed in the 1<sup>st</sup> PC if it is illustrated in red, a limited range of brightness will be displayed in the 2<sup>nd</sup> PC if it is illustrated in green, and even smaller range of brightness will be displayed in the 3<sup>rd</sup> PC if it is illustrated in blue.

Therefore, an alternative transformation is proposed by Tsagaris where the multispectral data is not completely de-correlated, instead the correlation between the components of the final colour image is controlled by moderating the covariance matrix. The correlation between the colour components of the final image is adjusted from the energy of the original data and to be related to the correlation of natural colour images.

This transformation is linear and denoted as  $\mathbf{y} = \mathbf{A}\mathbf{x}$  instead of  $\mathbf{y} = \mathbf{A}(\mathbf{x} - \mathbf{m}_x)$ , and the relation between the covariance matrices of  $\mathbf{x}$  and  $\mathbf{y}$  is  $\mathbf{C}_y = \mathbf{A}\mathbf{C}_x\mathbf{A}^T$ . However the covariance matrix  $\mathbf{C}_y$  of the resulting vector  $\mathbf{y}$  is constructed from a set of natural colour images defined by the Imagine Macmillan database provided in Tsagaris' research, in lieu of eigenvalues of  $\mathbf{C}_x$   $\lambda_1, \lambda_2, \dots, \lambda_N$  that are explained in section 3.2.3. The series of 100 images used by Tsagaris is considered to contain perceptually rich information content and pleasing sensation for the observers. They are subjectively categorised based on their variety of colours are grouped into four categories with 25 images each: the 1<sup>st</sup> category comprises of natural colour images considered with a great variety of rich colours and hues, the remaining three categories are dominated respectively by the images with one of the primary colours. For instance, when the blue colour is dominant in the group, an image with a jet ski in the sea can be considered. The statistical evaluation of the set of images is based on correlation coefficient  $r$  defined in the following equation:

$$r = \frac{\sum_m \sum_n (A_{mn} - \bar{A})(B_{mn} - \bar{B})}{\sqrt{\sum_m \sum_n (A_{mn} - \bar{A})^2 \sum_m \sum_n (B_{mn} - \bar{B})^2}}$$

where  $\bar{A}$  is the mean of  $\mathbf{A}$  and  $\bar{B}$  is the mean of  $\mathbf{B}$ .  $\mathbf{A}$  and  $\mathbf{B}$  can be any two components of a spectral entity. The values of the correlation coefficients are between -1 and 1 inclusive.

Correlation coefficient is a characteristic that describes the relations among the three components R, G and B in RGB space, where high correlation signifies the three components change also if the intensity changes. It is because of the overlapping sensitivity curves of the three types of cones in the human eye.

In terms of the set of 100 images, the correlation coefficients between each channel of R, G and B of the images are calculated and averaged, and the statistical mean values are displayed in Table 3.

Value	Corr(R, G) ( $r_{R,G}$ )	Corr(R, B) ( $r_{R,B}$ )	Corr(G, B) ( $r_{G,B}$ )
Mean	0.8487	0.7040	0.8849
Variance	0.0317	0.0990	0.0175

**Table 3: Statistical values resulting for the set of images studied.**

The level of correlation is generally higher than 0.6 for all pairs of components of all types of images, additionally, the variance of correlation coefficients is small, and therefore it is considered the averaged result is a sufficient estimator for the next processing.

The desired covariance matrix  $C_y$  of the transformed data is defined in the equation:

$$C_y = \Sigma R_y \Sigma^T$$

where:

$$\Sigma = \begin{bmatrix} \sigma_{y1} & 0 & 0 & \dots & 0 \\ 0 & \sigma_{y2} & 0 & \dots & 0 \\ 0 & 0 & \sigma_{y3} & \dots & 0 \\ \vdots & \vdots & \vdots & \ddots & \vdots \\ 0 & 0 & 0 & \dots & \sigma_{yN} \end{bmatrix}$$

and

$$R_y = \begin{bmatrix} 1 & r_{R,G} & r_{R,B} & \dots & 0 \\ r_{R,G} & 1 & r_{G,B} & \dots & 0 \\ r_{R,B} & r_{G,B} & 1 & \dots & 0 \\ \vdots & \vdots & \vdots & \ddots & \vdots \\ 0 & 0 & 0 & \dots & 1 \end{bmatrix}$$

The diagonal matrix  $\Sigma$  has the standard deviations of the transformed new vectors. The proposed transformation supposed to have high visual quality, it is intended that the energy of the original data is sustained and distributed equally in the final colour image. Therefore, the requirement  $\sum_{i=1}^N \sigma_{xi}^2 = \sum_{i=1}^3 \sigma_{yi}^2$  is necessary where  $\sigma_{y1} = \sigma_{y2} = \sigma_{y3}$  approximately. The energies of the remaining  $N - 3$  bands are set to be negligible. The values of their variance  $\sigma_{y4}^2, \sigma_{y5}^2, \dots, \sigma_{yN}^2$  are accommodated as  $\sigma_{yi} = 10^{-4} \sigma_{y1}$  ( $i = 4, 5, \dots, N$ ) so that the bands are small enough to be neglected.

In the case of 100 natural images:

$$R_y = \begin{bmatrix} 1 & 0.8487 & 0.7040 & 0 \\ 0.8487 & 1 & 0.8849 & 0 \\ 0.7040 & 0.8849 & 1 & 0 \\ 0 & 0 & 0 & 1 \end{bmatrix}$$

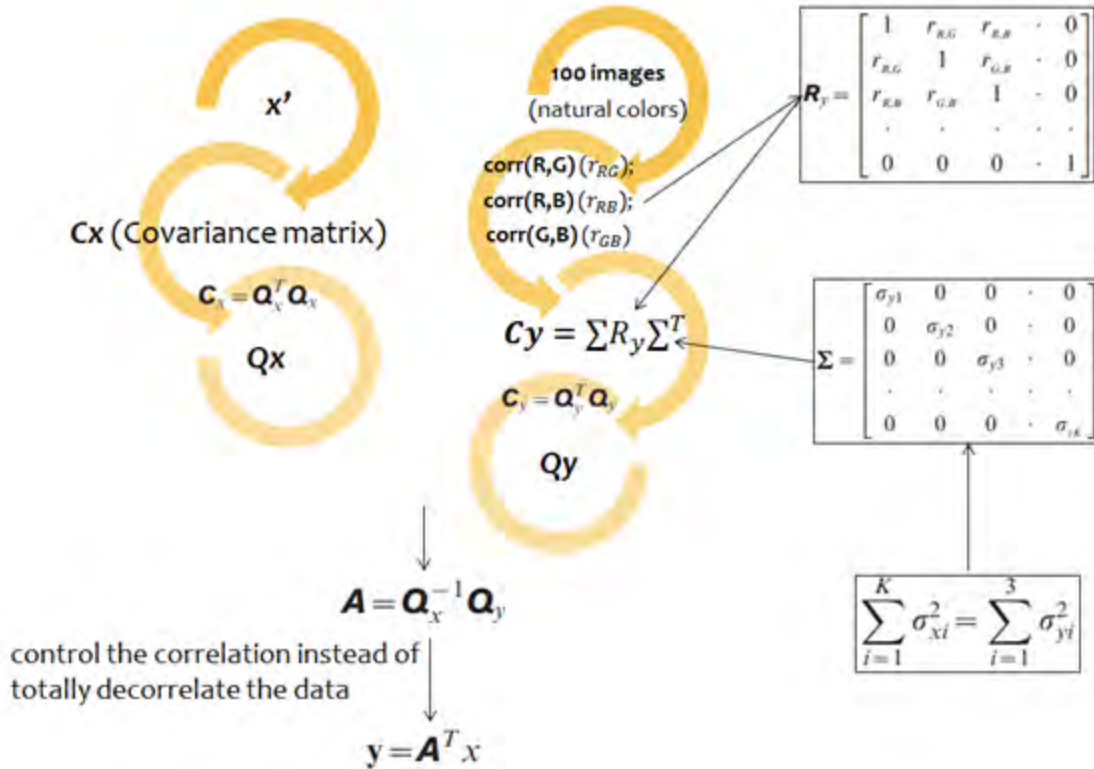
Currently, both  $C_x$  and  $C_y$  are known. Based on  $C_y = A C_x A^T$ , the problem is reduced to solving the transformation matrix  $A$  to be able to perform the transformation  $y = Ax$  and to acquire the final image.

Cholesky factorisation is able to decompose a symmetric positive definite matrix for example  $C$  in the form of an upper triangular matrix  $Q$  so that  $C = Q^T Q$ . Therefore  $C_x$  and  $C_y$  can be decomposed in the same way and thus  $C_x = Q_x^T Q_x$  and  $C_y = Q_y^T Q_y$ .

Consequently,  $C_y = A C_x A^T$  can be written as  $Q_y^T Q_y = A Q_x^T Q_x A^T = (Q_x A^T)^T (Q_x A^T)$  so that  $Q_y = Q_x A^T \Rightarrow Q_y A = Q_x \Rightarrow A = Q_x Q_y^{-1}$ .

The transformation matrix  $A$  implies that the linear transformation  $y = Ax$ , where  $A = Q_x Q_y^{-1}$  relates to the statistical properties of both the original data and the set of natural colour images.

Overall, the transformation proposed by Tsagaris can be performed in the steps illustrated in Figure 21: Transformation proposed by Tsagaris..



**Figure 21: Transformation proposed by Tsagaris.**

As mentioned previously the data applied in Tsagaris' research is based on a four-band multispectral image where R, G and B bands applied are from the spectral range of VIS regions R, G and B respectively, and one IR band from IR region. A total of four bands are implemented with the transformation in the article.

In contrast, the data conducted for this project are hyperspectral imagery which has 160 channels for VNIR data and 256 channels for SWIR data, data reduction has to be applied in order to perform the transformation.

Take for example, the 160-band VNIR data applied for this project; the following steps have to be conducted in order to combine the information from the IR region to the VIS region.

Firstly, regarding the hyperspectral data ranging from 414.6nm to 778.1nm in the VIS region, the tristimulus values X, Y, Z under the illuminant D65 are calculated based on the following equations:

$$X = k \int_{vis} R(\lambda)P(\lambda)\bar{x}(\lambda)d\lambda$$

$$Y = k \int_{vis} R(\lambda)P(\lambda)\bar{y}(\lambda)d\lambda$$

$$Z = k \int_{vis} R(\lambda)P(\lambda)\bar{z}(\lambda)d\lambda$$

with  $k = 100 / \int_{vis} P(\lambda)\bar{y}(\lambda)d\lambda$ .  $R(\lambda)$  is reflectance spectrum of the object and  $P(\lambda)$  is the Spectral Power Distribution (SPD) of the illuminant or light source. The 1931 Colour Matching Function (CMF- $\bar{x}(\lambda)$ ,  $\bar{y}(\lambda)$ ,  $\bar{z}(\lambda)$ ) is applied for the computation.

The resulting tristimulus values are then converted from XYZ space to RGB space with the linear transformation:

$$\begin{bmatrix} R \\ G \\ B \end{bmatrix} = M_{RGB} \begin{bmatrix} X \\ Y \\ Z \end{bmatrix}$$

where:

$$M_{RGB} = \begin{bmatrix} 3.240479 & -1.537150 & -0.498535 \\ -0.969256 & 1.875992 & 0.041556 \\ 0.055648 & -0.204043 & 1.057311 \end{bmatrix}$$

It is followed by the Gamma correction from RGB space to the Standard RGB (sRGB) space:

$$R' = f_\gamma(R), G' = f_\gamma(G), B' = f_\gamma(B)$$

where:

$$f_\gamma(c) = \begin{cases} 1.055 * c^{\frac{1}{2.4}} - 0.055, & \text{for } c > 0.0031308 \\ 12.92 * c, & \text{for } c \leq 0.0031308 \end{cases}$$

Standard RGB is a CIE-based conversion which allows sufficient transformation between sRGB and other colour spaces. This process can only be done in the VIS region since CMF is based on human vision. Though stretched CMF has been applied in previous research, this technique is not considered for this project.

The current data would have 3 bands, which can be considered as the counterpart of the R, G, B bands that Tsagaris applied in his research.

Secondly, regarding the hyperspectral data in the IR region, the best method obtained from the comparison of the 40 images presented in this research in terms of invisible information will be applied for the merging. For instance, if the best technique for the psychophysical experiment is concluded to be the 1st component of PCA from the VNIR data in the IR range (from approximately 781.7nm to 992.5nm), then this image will be used to substitute the

corresponding IR band applied in Tsagaris' original data. Therefore, a four-band image is produced from the hyperspectral data and can be applied for in the transformation.

In Figure 21,  $x'$  signifies the four-band vector to be processed to obtain the four-band output vector  $y$ . The process can also be found from the first part of Figure 22.



**Figure 22: Transformation to RGB.**

Let  $X'$  and  $Y$  denote the input and output four-band images respectively. However, the human vision is unable to perceive a four-band image unless it is processed further to a three-band image that can be presented as R, G and B channels. The post-processing can be the aforementioned mathematical models PCA, ICA or MNF. Alternatively, the bands can be selected manually or mathematically based on certain ordering techniques.

It has been noted before, that statistical methods like PCA de-correlate the data and the result does not pose an optimal solution for human perception basis. It is considered that the proposed transformation by Tsagaris takes into account of the initial bands that have the largest amount of energy, and that smallest amount of correlation is preferred between these bands and the remaining bands.

Tsagaris thus implemented two ordering approaches which satisfy the afore-mentioned requirements in order to rank the components of the four-band images so that the first three channels can be used to present RGB images. The techniques applied are OIF (Optimum Index Factor) and MEMC (Maximum Energy Minimum Correlation).

OIF is defined in the equation below:

$$OIF = \frac{\sigma_i + \sigma_j + \sigma_k}{|r_{i,j}| + |r_{j,k}| + |r_{i,k}|}$$

where  $\sigma_i$ ,  $\sigma_j$  and  $\sigma_k$  are standard deviation of band  $i, j, k$  respectively and  $r_{i,j}$ ,  $r_{j,k}$  and  $r_{i,k}$  are the correlation coefficient between bands  $i, j$ , between bands  $j, k$ , and between bands  $i, k$  respectively. The number of possible combinations of three bands is determined as:

$$\binom{N}{3} = \frac{N!}{(3! * (N - 3)!)}$$

Therefore, when the total number of the bands is 3, the number of possible OIF combinations is only 1; when the total number of the bands is 4, the number of OIF combinations is 4; when the total number of the bands is 5, the number of OIF combinations is 10 and so on. In the case of

the four-band image, all the 4 OIFs are calculated and ranked in descending order. The first three bands are thus chosen to represent R, G and B channels correspondingly.

MEMC is defined for each band, but related to the other bands as denoted in the equation below:

$$MEMC = \frac{\sigma_i}{\sum_{j=1, i \neq j}^N |r_{i,j}|}$$

where  $i = 1, 2, \dots, N$ ,  $\sigma_i$  is the standard deviation of the observed band  $i$  and  $r_{i,j}$  is the correlation coefficient between  $i$  and the rest of the bands. Similarly, all the MEMCs are calculated and ranked in descending order. The first three bands are selected to represent R, G and B channels correspondingly. MEMC is applied by Tsagaris before and after the transformation between the four-band images.

The framework of the whole process can be illustrated in Figure 22. The hypothesis proposed by the author therefore is that if the best processed image in terms of the invisible information found from the previous section can be fused into the VIS region, with the transformation containing the information from the 100 images with natural colours, the resulting image might be perceptually pleasing and in the meanwhile display the most invisible features.

### **3.3 Evaluation**

Currently, two research objectives are proposed. One is to see the invisible information. Different algorithms are applied to process the hyperspectral data; the resulting images are compared and evaluated in terms of the most identifiable invisible information in order to find the best processing method.

The other is to embed the most invisible information from IR region to VIS region applying a modified linear transformation based on a series of images with natural colours. The purpose is to produce a perceptually pleasant image as well as display maximum invisible information.

Therefore, two parts of the evaluations are considered; one for each objective respectively.

#### **3.3.1 Psychophysical Experiment**

In terms of the first objective, identifying the invisible information, a psychophysical experiment is considered to determine the best result.

#### **3.3.2 Experimental Criteria**

A psychophysical experiment is considered to be a quantitative method. It intends to examine and determine the relationship between physical stimuli and the sensations they evoke. **Psychophysics is described as** “the analysis of perceptual processes by studying the effect on a subject’s experience or behaviour of systematically varying the properties of a stimulus along one or more physical dimensions” [65].



Psychophysical experiment is a subjective assessment, which is associated with a scale of perception. The human observers are required to rank a series of images based on a provided criterion. The first psychophysical experiments were conducted by Ernst Weber in the 1830s where the Just Noticeable Difference (JND) is found to be proportional to the stimulus **magnitude, later identified as Weber’s law** [66].

The experimental method is considered to be related to design factors or general factors including script, task complexity, choice of subjects, terminology, control of variation, user interface, characterisation, accuracy and reporting of data. More precisely, the task given to the observers is better to be described as simple as possible without using terminology. It is desired that the task is easy enough for an average observer to be able to complete it and provide a sufficient answer. Choice of subjects describes the vision acuity of the observers. Control of variation relates to the environment where the experiment is conducted with the observers if the experimental environment is under the same controlled settings. Generally, the devices applied have to be characterised and calibrated before the experiment. User interface involves the stimuli presented for the observers [67].

Chong [68] presented three common psychophysical scaling experimental methods, category judgement, pair comparison and rank order. In category judgement, the observer is told to decide each of the images to a category, where each category indicates the level of the quality criterion is met. Pair comparison means that the observer is provided with an image pair and an evaluation criteria and s/he has to decide which image from the pair is the best in comparison with the original. Rank order is considered to be the equivalent of pair comparison to all images simultaneously, and the images are ranked from the worst to the best or from the best to the worst based on the criterion supplied in relation with the reference image.

Another psychophysical scaling method is Mean Opinion Score (MOS). This method was developed by the International Telecommunication Union (ITU) for the evaluation of audio quality, but it has since been used for image quality [66]. Usually MOS has a five point descriptive scale from Bad to Excellent (Bad, Poor, Fair, Good, and Excellent), the observer has to judge the quality from one to five where five is said to be the best quality. The object of the experiment should be chosen and placed in one of the scales considered by the observer. This method is easy to be understood and handled by naive observers due to its descriptive scale.

The type of scaling psychophysical experiment used for this project is category judgement. The observers are shown a set of 40 images at once, and they are required to place each image in a category according to the specified criterion. The scale values are 3, 2, 1, 0, -1, -2, -3. The category supplied for this psychophysical experiment is shown in Table 4.

3	2	1	0	-1	-2	-3
Extremely Good	Very Good	Good	Adequate	Poor	Very Poor	Extremely Poor

**Table 4: Categories used for the psychophysical experiment.**

For each set of images, the observer has to judge and decide the category of the quality of the image in terms of the extent of the invisible information presented in every specific detail. Extremely Good (3) signifies the described detail has excellent visibility, where the detail can be identified easily without explicitly point at it or prior knowledge of it, and Extremely Poor (-3)

denotes the described detail has very poor visibility, where the detail is not visible at all and there is only noise present. The detailed explanation can be found from Appendix 1.

### 3.3.3 Choice of Observations

The initial intention was to display all the 40 full images of the painting *The Scream* so that the observers are able to find the full image with the most perceivable invisible information. However, the extensive computation required to calculate ICs from the VNIR-30cm hyperspectral data and the limited hardware resources (memory) available at the laboratory where the author is based at meant that processing the data was not possible; the amount of memory required is at least 33GB. Furthermore, a total of 40 full images do not seem to be feasible for the observers to view and compare simultaneously and the result might be biased since there are too many images and the different sizes of the images also cause problems. An alternative approach has to be considered.

It has been mentioned previously that certain details from the painting are quite intriguing and are considered to be of interest for scientific examination in terms of invisible information. Excluding the possible second coat of paint by the artist as well as the retouch by the restorers in the past, some other artefacts are also observable on the real painting, and more distinguishable in the processed images. Additionally, it appears to be possible to display 40 images of one single detail to the observers at once, especially when arranged in the same folder, they can be adjusted to approximately the same physical size. A trial run of one detail cut off from all the processed images on one observer demonstrated this method is more feasible. Therefore, some of the details are picked out for analysis.

In order to make a better explanation for the areas of interest chosen for analysis and the already-processed image, the 4th component of ICA from SWIR-1m data is used to illustrate the details (Figure 23)

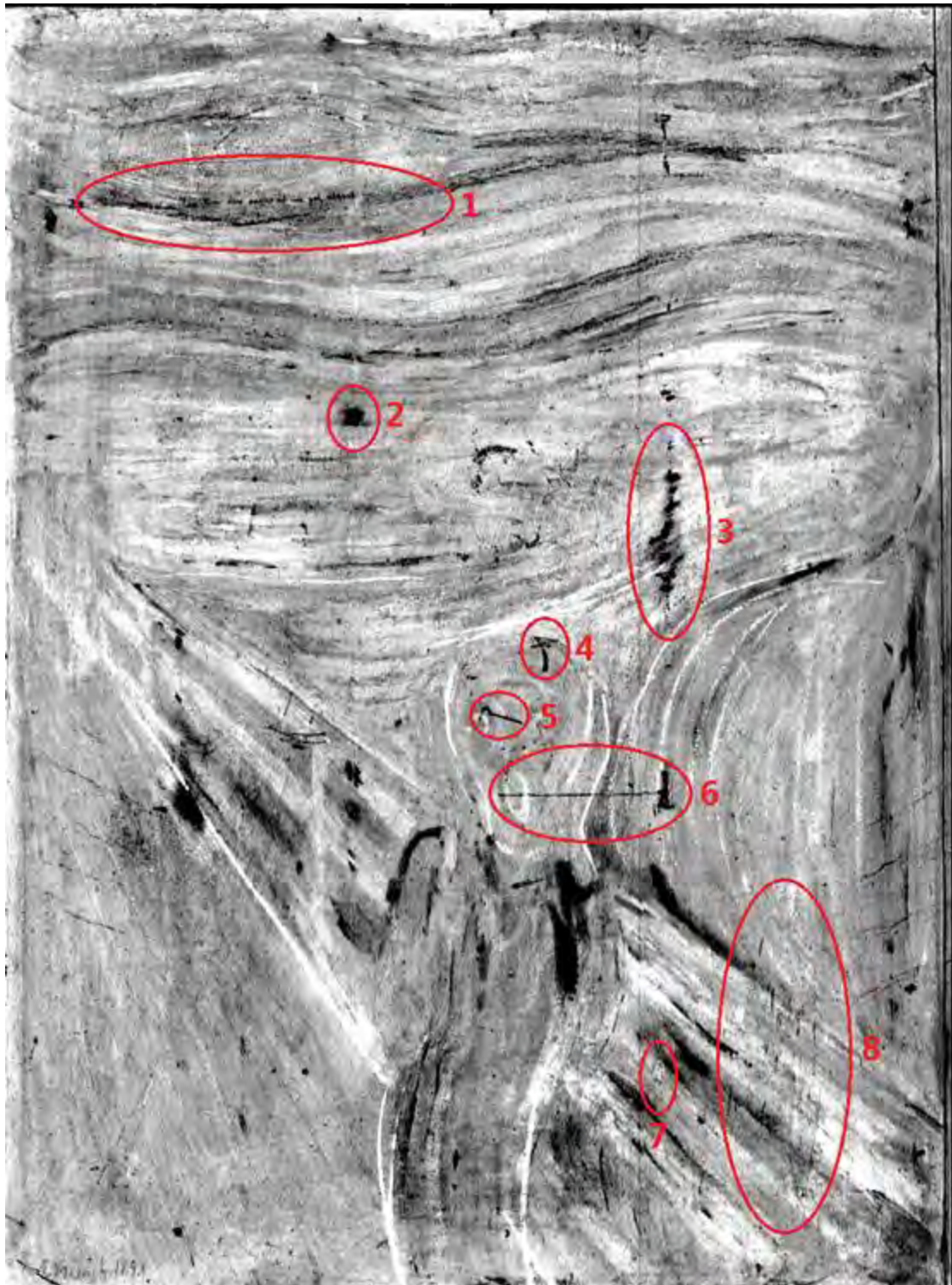
Detail 1 is the text written by the artist, detail 2 and 3 are the retouch or second paint possibly by the artist, detail 4, 5 and 6 seem to be scratches. However, the museum restorer Mr Aslaksby is **uncertain detail 4 and 5 are actually scratches and he named the two details as “depressions”**. Detail 7 and 8 are a tallow dropping and a cluster of tallow droppings respectively.

The author considers that detail 1 is identifiable as a series of text, but it is not distinguishable what is written exactly in the text unless further image processing tools such as sharpening are **implemented. Even with the most visible processed image from the author’s point of view, the text is still not distinct.** Furthermore, image processing is not the primary objective of this research. Therefore, detail 1 is not considered for the psychophysical experiment.

Both detail 2 and detail 3 are dark blue paint coat in the original painting. In most of the processed images, detail 2 seems to be more or less the same; the main difference is only a matter of size. Subsequently, detail 2 is also discarded, and detail 3 is chosen for the experiment.

As it has been briefly mentioned before, details 4, 5 and 6 appear to be scratches. They seem to be similar to the naked eye on the original painting, especially detail 4 and 5. The author believes it would be interesting to compare them from other observers’ **point of view to analyse** if the same result is obtained for the three details. The result may be able to provide a hint if

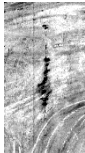

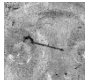
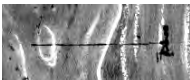

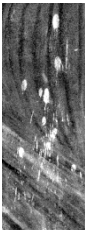
they are indeed the same kind of scratch or impression. Consequently, all the details are included for the psychophysical experiment.



**Figure 23: Details of interest.**

Both detail 7 and detail 8 are tallow droppings, one area is small and the other is big respectively. The author examined all the processed images on the two details and considers the image with the best quality in terms of invisible information for detail 7 is not necessarily the best for detail 8 and vice versa . The same situation occurs **for the worst image in the author's** opinion. Thus, both details are also added for the experiment.

As a summary, a total of 6 selected details are explained in the following manner in Table 5 and one of the best images is incorporated on the side in order to facilitate the comprehension. Those details are noted in an exemplary image in Figure 24.

Detail	Image
Detail 1: The blue colour was retouched with a darker blue; it is unknown if the artist intentionally painted it with darker blue or not.	
Detail 2: A tilted 4-shape scratch on the head of the figure, probably because of careless handling of the painting in the past.	
Detail 3: A hook-shape scratch on the eye of the figure, probably because of careless handling of the painting in the past.	
Detail 4: A horizontal line shaped scratch on the chine of the figure intersecting a vertical scratch to the right of the figure inflicted probably because of careless handling of the painting in the past.	
Detail 5: A bird dropping.	
Detail 6: A cluster of bird droppings with possible intentional restoration, but could not be removed without harming the painting.	

**Table 5: Selected details for the psychophysical experiment.**



**Figure 24: Details from Table 5.**

### **3.3.4 Observers and Setting**

The psychophysical experiment was implemented in a computer lab at Gjøvik University College. All the observers invited to perform the experiment in the lab were from the same



colour lab where the author is based at, therefore, they were not “naïve” observers, and may be considered in fact as expert observers.

The observers were asked to conduct the experiment on the same computer under the same setting of the environment. There were no other people at the time of the experiment except the author and the observer. Therefore, the environment was controlled and the observers were not disturbed at the time of observation. A total of 9 observers participated in the experiment in the lab.

The author accompanied the observers in case of confusions. The observers were asked to compare and evaluate the 40 images on the screen of the computer provided in the lab. They then notified the author the category they wish to place for each image based on the category criterion provided.

The author considers that the majority of the images are grayscale images, and only 3 out of 40 images are colour images, the intensity of the grey levels might affect the most in the result instead of colour. All of the details in the processed images differ mainly and greatly in the intensity of the grey scales. The detail appears more intense when the detail is neighboured with more contrasting surroundings. Furthermore, as mentioned above, all the participating observers from the colour lab have colour science background.

In order to test if those details in the processed images are affected by different settings and knowledge background, the author also requested some observers who have not studied colour science before to perform the experiment. They can thus be considered as naïve observers. This set of observers was in completely different locations. Thus, each was sent an electronic copy of the psychophysical experiment comparison sheet and images so that the experiment could be conducted at their own locations and at their own paces. Therefore, all the settings of the experiment from this group and the background knowledge of individuals in this group are different. A total of 6 observers joined in the experiment.

### **3.3.5 Comparison Between Natural Colour Images and Munch’s Image**

With regard to the second objective, it is known that 100 images with natural colours were associated in the transformation in order to generate a perceptually pleasing image. With the possibility of merging the best invisible information from the IR region with the VIR region, maximum invisible information may be perceived from the final image at the same time.

**It is demonstrated in Tsagaris’ research that the information applied in the fusion from the IR region is not the image with maximum invisible information, but only the image acquired with a simple IR camera, however the resulting image indeed displayed a perceptually more natural and more attractive effect. Based on this concept and the application of the 100 images used by Tsagaris containing natural colours, the author considers that it might be possible to also apply 100 images with only Edvard Munch’s paintings with his specific style in the image fusion process in order to compare and evaluate the quality of the images obtained from both fusions.**

**The author analysed many of Edvard Munch’s paintings, though almost all of them display dark emotions and pain, the colours applied in different paintings of his are still very different. As a matter of fact, the author believes that *The Scream* from the National Gallery, Oslo is one of his**

paintings implemented the most vibrant and turbulent colours. It might not be sensible to apply the same concept in the image fusion.

However, there exist photographic RGB versions of the painting which resemble the most to how the human eye observes the real painting. It might be reasonable to try to use a good photographic version of the painting in order to produce the transformation matrix  $A$  applying **the same algorithm proposed in Tsagaris' work**. Problems usually exist during the acquisition stage of hyperspectral data (with VIR range), when the hyperspectral data is converted to an RGB image with CMF and Gamma correction; the RGB image obtained might differ greatly from the photographic RGB version of the actual image perceived by the human eye. Therefore, they hypothesis is that, by performing the transformation associated with the photographic RGB version of the painting, the resulting image transformed from the hyperspectral imagery might resemble more to the photographic version of the painting. The algorithm might be used to correct the data errors generated in the hyperspectral data acquisition stage.

Consequently, the photographic RGB version obtained by a professional photographer from the National Gallery with digital camera Hasselblad H4D-200MS is considered to obtain the transformation matrix  $A$ .

Basically, the calculations introduced in section 3.2.7 remain unchanged for this conversion, only the 100 images used by Tsagaris are changed to one single RGB image in order to obtain matrix  $A$  as shown in Figure 25. The image obtained with regard to 100 images with natural colours and the image acquired associated with the Hasselblad RGB image are thus compared.

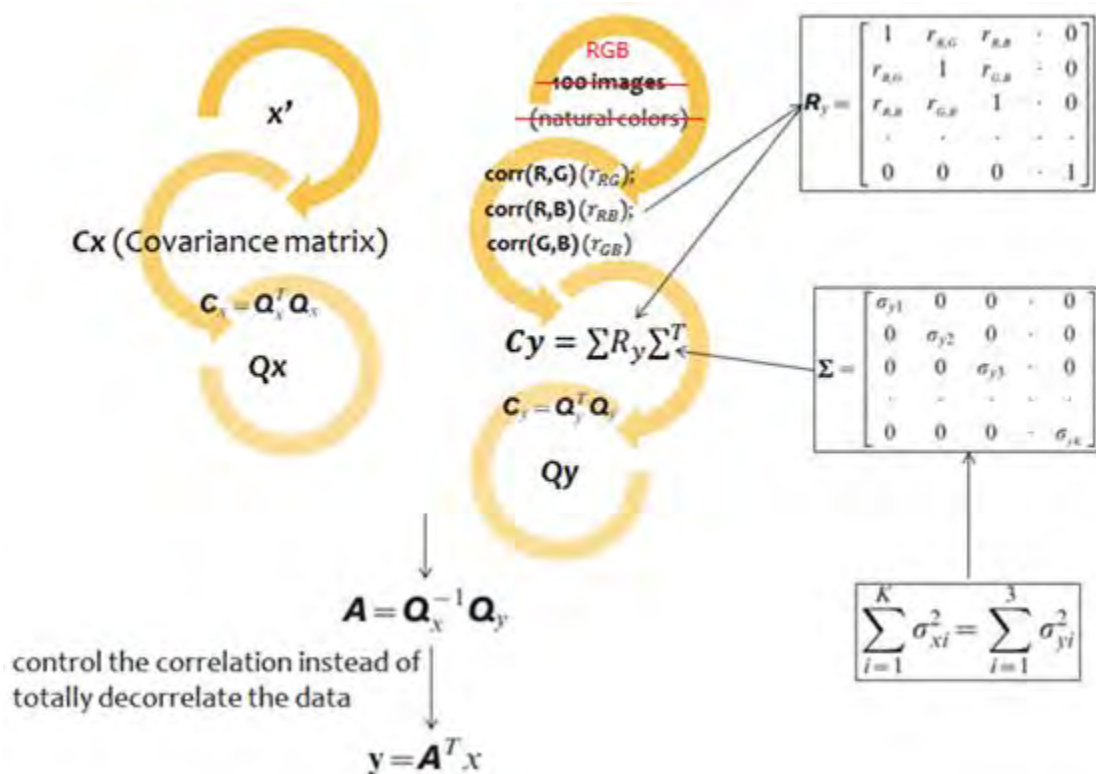


Figure 25: Modified process proposed.

### 3.4 Conclusion

The series of artwork *The Scream* are considered as one of the most sensational work in modern art history. The painting version in the National Gallery, Oslo is regarded as the research subject to obtain hyperspectral imaging data. The painting has gone through extensive history in the past. Because of careless handling of the painting as well as the theft incident in 1994, some damage appears in the painting. The hyperspectral imagery intends to identify the invisible information, possibly as a direct result from those events, in order to facilitate vital information to the restorers for restoration purposes as well as to benefit the spectators for educational purposes.

The research fields of agriculture, forestry, surveillance and cultural heritage have been applying hyperspectral imagery with this research project belonging to cultural heritage area. The hyperspectral data used was collected with two hyperspectral cameras. The data were pre-processed and passed onto the author so that further implementation could be done. Several post-processing methods are considered in order to prepare images for comparison.

The definition of invisible information in terms of hyperspectral imagery for this project is defined in this chapter. The post-processing techniques thus are mainly applied to obtain the images for the psychophysical experiment in order to identify the image possessing the most invisible information. When the processed image with the best quality from IR region is selected based on the subjective evaluation, the image is proposed to be combined with the VIS region data.

The fusion between IR and VIS regions is based on but adapted from the principal of PCA as the proposed transformation does not decorrelate the data completely but controls the correlation between the channels. A series of 100 images with natural colours are used in order to control the correlation between the bands.

Two evaluations are considered for the two objectives mentioned above. One is a psychophysical experiment with a total of 15 observers. Approximately half of the participants were expert observers and conducted the experiment under the same setting. The other half consisted of naive observers and performed the experiment under completely different settings. The intention of the two groups is to identify the possible effect of the environment and the background knowledge of the individuals for this experiment.

Another evaluation is with respect to the fusion. Two images obtained applying the same procedure. The difference is that the correlation between bands is controlled according to different set of images. The first set of images are 100 images with natural colours, another set is only one RGB photographic version of the painting. A linear transformation matrix is calculated based on the two sets of images in order to produce the final images. The two images are to be compared and evaluated.



## 4 Results and Discussion

Chapter 3 introduced the proposed methods for the processing of the hyperspectral data as well as the evaluation techniques for the processed data. Chapter 4 analyses the obtained results based on the experimental evaluation conducted.

### 4.1 Results

#### 4.1.1 Psychophysical Experiment

The observers were shown six sets of processed image details in order to identify which image has the most invisible information. Each set of images was designed to consist of 40 images in total based on the method proposed in Chapter 3.

Since VNIR data has less spectrum bands that are outside the visible region in comparison with SWIR data, it is expected that VNIR data will have less invisible information. In order to take the advantage of the high resolution feature so that more invisible information might be identified, subsequently the VNIR-30cm data was considered by the author for processing. However, the available VNIR-30cm hyperspectral data only contains a cut off of the painting instead of the full image of the painting as shown with an exemplary image in Figure 26. Some of the selected details (detail 1 and detail 6 noted in Figure 24) for comparison are therefore not included in Figure 26. Consequently, in terms of detail 1 and detail 6, a total of 22 images are only comprised.

The six sets of image details are shown in Figure 27, Figure 29, Figure 31, Figure 33, Figure 35 and Figure 37. The associated results from the psychophysical experiment are illustrated in Figure 28, Figure 30, Figure 32, Figure 34, Figure 36 and Figure 38 respectively. The results are the average scores for each image in terms of individual details from the total of 15 observers.

Due to the different number of the images contained in one folder and different sizes of individual details cut off from the processed full images, images shown below are for illustration purposes only. The actual experimental images have to be consulted in the psychophysical experiment folder provided by the author.

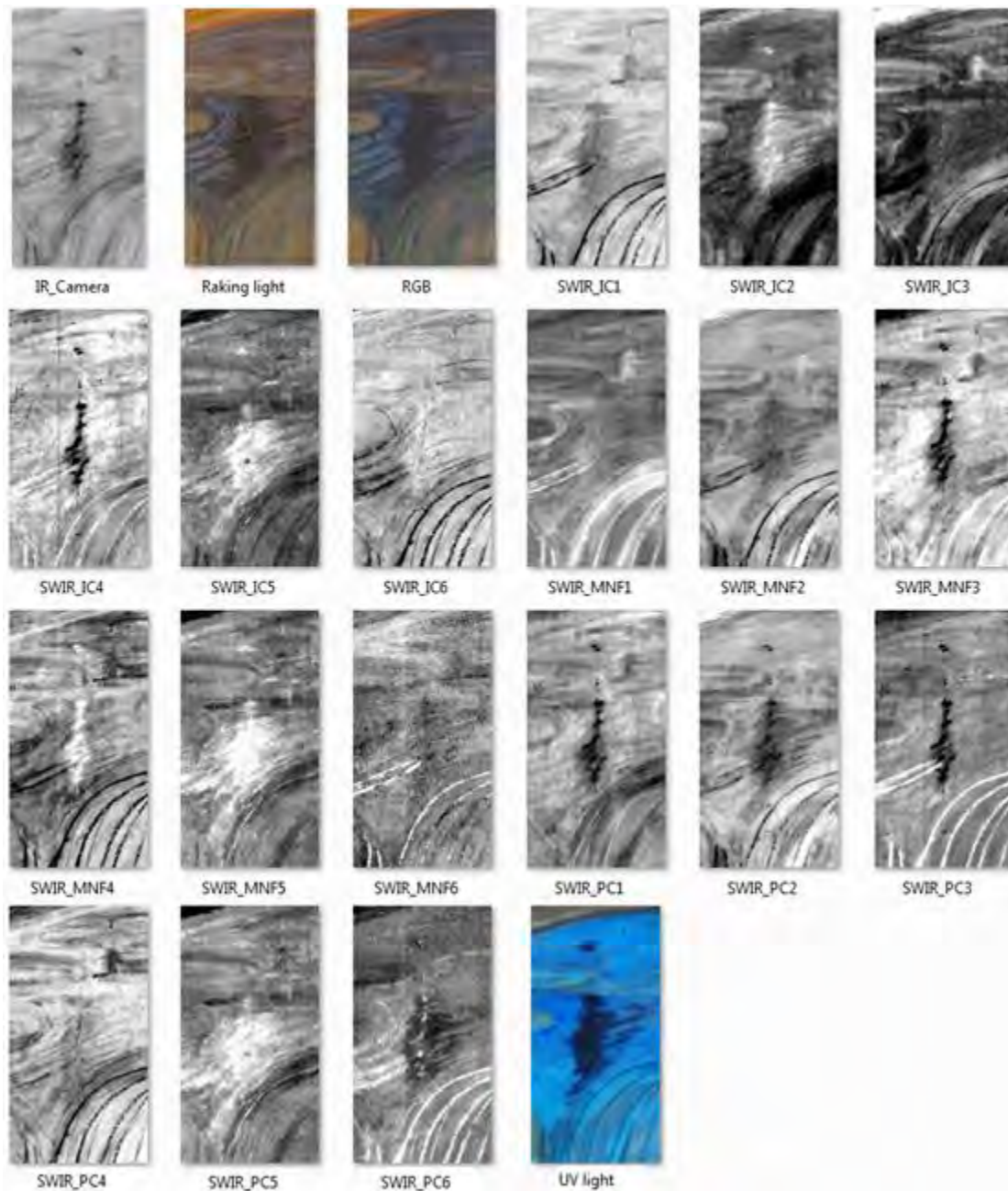
In order to facilitate the explanation of the methods, the notation from Table 6 is applied. All images are discussed regarding the quality in terms of invisible information.



**Figure 26: VNIR-30cm data from *The Scream*.**

<b>Notation</b>	<b>Description</b>
RGB	The photographic RGB image taken by a professional photographer from the National Gallery with digital camera Hasselblad H4D-200MS
Raking light	The photographic RGB image taken under raking light placed at the top of the painting
UV	The photographic RGB image taken under UV light
IR	The photographic grayscale image taken with multispectral imaging camera with IR filter with its peak value at 1050nm between 1000nm and 1100nm.
SWIR_IC1	1 <sup>st</sup> component obtained applying ICA with SWIR data
SWIR_IC2	2 <sup>nd</sup> component obtained applying ICA with SWIR data
SWIR_IC3	3 <sup>rd</sup> component obtained applying ICA with SWIR data
SWIR_MNF1	1 <sup>st</sup> component obtained applying MNF with SWIR data
SWIR_MNF2	2 <sup>nd</sup> component obtained applying MNF with SWIR data
SWIR_MNF3	3 <sup>rd</sup> component obtained applying MNF with SWIR data
SWIR_PC1	1 <sup>st</sup> component obtained applying PCA with SWIR data
SWIR_PC2	2 <sup>nd</sup> component obtained applying PCA with SWIR data
SWIR_PC3	3 <sup>rd</sup> component obtained applying PCA with SWIR data
VNIR_IC1	1 <sup>st</sup> component obtained applying ICA with VNIR data
VNIR_IC2	2 <sup>nd</sup> component obtained applying ICA with VNIR data
VNIR_IC3	3 <sup>rd</sup> component obtained applying ICA with VNIR data
VNIR_MNF1	1 <sup>st</sup> component obtained applying MNF with VNIR data
VNIR_MNF2	2 <sup>nd</sup> component obtained applying MNF with VNIR data
VNIR_MNF3	3 <sup>rd</sup> component obtained applying MNF with VNIR data
VNIR_PC1	1 <sup>st</sup> component obtained applying PCA with VNIR data
VNIR_PC2	2 <sup>nd</sup> component obtained applying PCA with VNIR data
VNIR_PC3	3 <sup>rd</sup> component obtained applying PCA with VNIR data

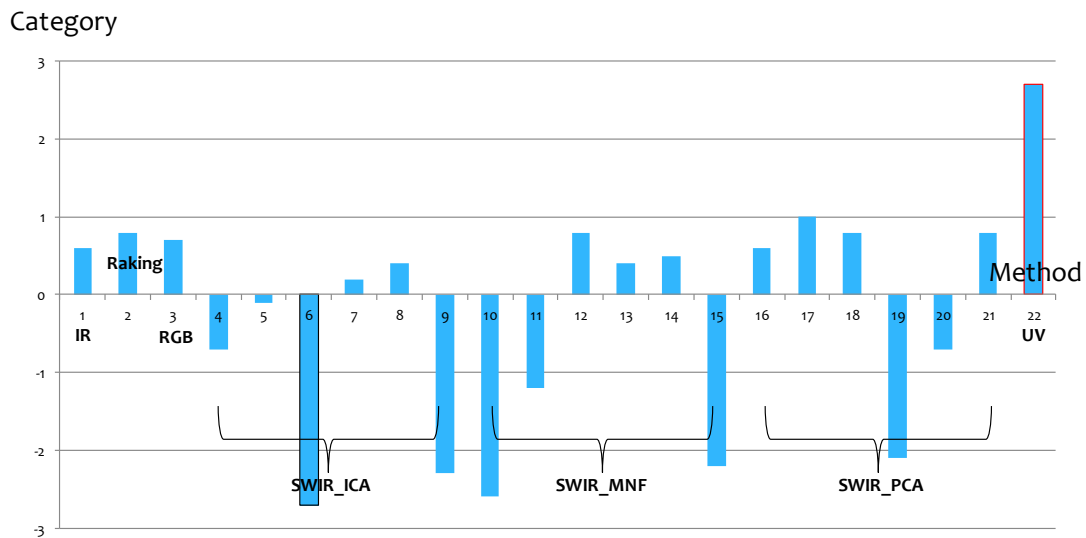
**Table 6: Notation to describe processed images from details of interest.**



**Figure 27: Detail 1: Second coat of paint by the artist.**

Detail 1 (Figure 27) is a second coat of paint possibly conducted by the artist himself. This detail seems quite visible in the original painting, but the patch where the dark blue coat is appears more like a damaged spot in the painting. Mr Aslaksby revealed that Munch painted a layer of dark blue on the top; it is unknown whether the artist intentionally painted the layer with darker blue colour than the surroundings. Since VNIR-30cm does not include this detail, a sum of 22 images is displayed to the observers. The result (Figure 28) shows the average scores for each of the 22 images from the total of 15 observers. It is observable that in terms of detail 1, the observers think the image taking under UV light has the best quality in terms of invisible information, whilst SWIR\_IC3 shows the least invisible information. The other processed

images do not seem to have a particular pattern according to the perceptual quality of invisible information by the observers.



**Figure 28: Psychophysical results for Detail 1.**

Detail 2 (Figure 29) is a tilted 4-shape scratch on the head of the human figure; this detail is **barely visible in the original painting in the author’s view. This detail is named by Mr Aslaksby as “depression” but the specific reason for the artefact is unknown.** It is likely because of careless handling of the painting in the past. Both VNIR-30cm and SWIR-1m data have this detail; a total of 40 images thus are displayed to the observers. The result shows the average scores for each of the 40 images from the total of 15 observers.

It is observable that in terms of detail 2, the average result shows that the SWIR\_IC4 displays the most invisible information whilst UV, VNIR\_IC5 and VNIR\_IC6 show the least invisible information. The other processed images do not seem to have a particular pattern according to the perceptual quality of invisible information by the observers also. It appears that a majority of the methods do not produce a good result in terms of invisible information, particularly the images processed with ICA from VNIR data that 5 out of 6 images have negative scores.

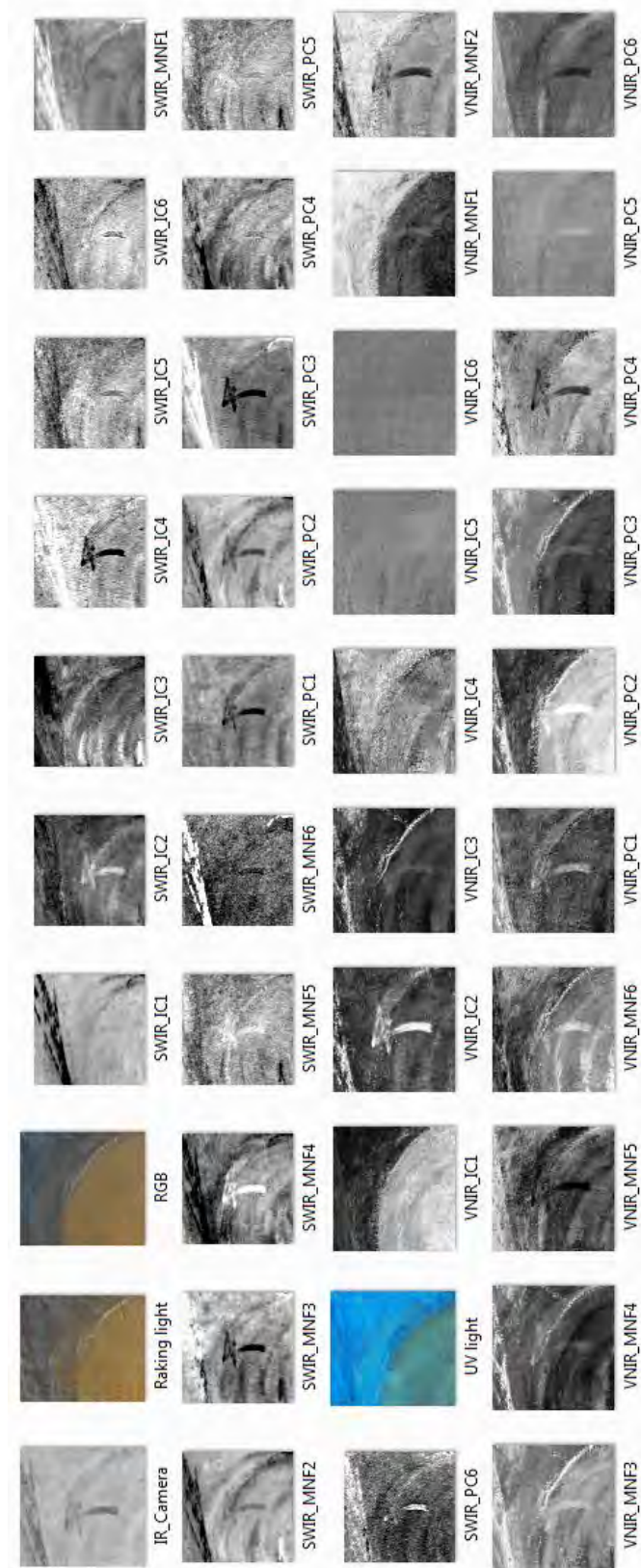
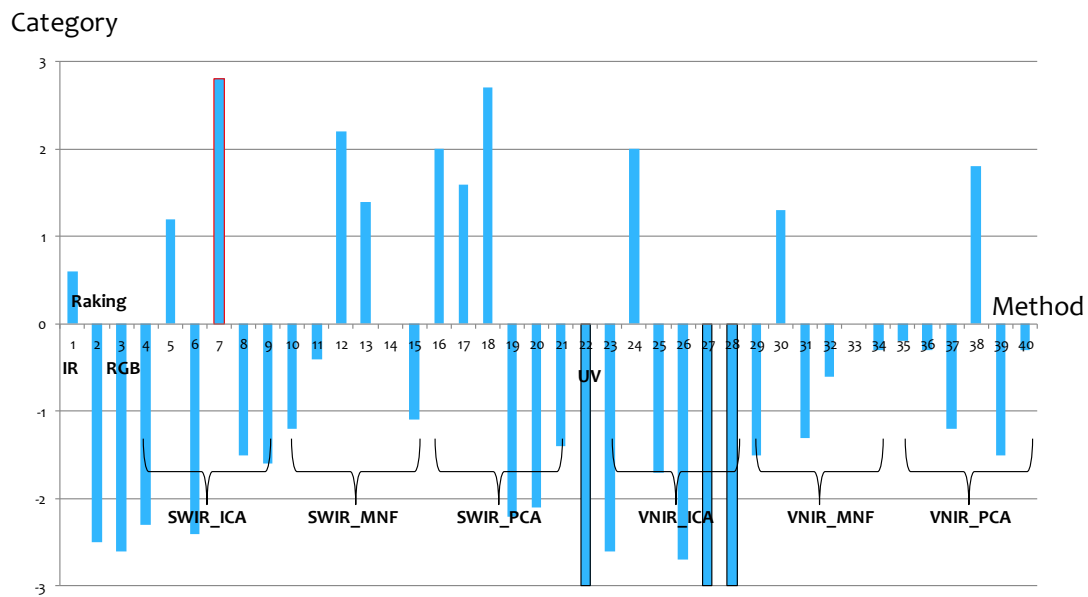


Figure 29: Detail 2: Tilted 4-shaped “scratch”.



**Figure 30: Psychophysical results for Detail 2.**

Detail 3 (Figure 31) is a hook-shape scratch on the eye of the human figure of the painting, this detail does not seem quite visible in the original painting to the author’s observation. This detail is also dubbed by Mr Aslaksby as “depression” but the specific reason for the scratch is unknown also. It is possibly because of careless handling of the painting in the past. Both VNIR-30cm and SWIR-1m data have this detail; a total of 40 images thus are displayed to the observers. The result shows the average scores for each of the 40 images from the total of 15 observers.

It is observable that in terms of detail 3, the average result shows that the SWIR\_PC3 displays the most invisible information whilst VNIR\_IC6 shows the least invisible information. The other processed images do not seem to have a particular pattern according to the perceptual quality of invisible information by the observers also. Similarly, a majority of the methods do not produce a good result in terms of invisible information, and like detail 2 the particular case happens to the images processed with ICA from VNIR data that 5 out of 6 images have negative scores.



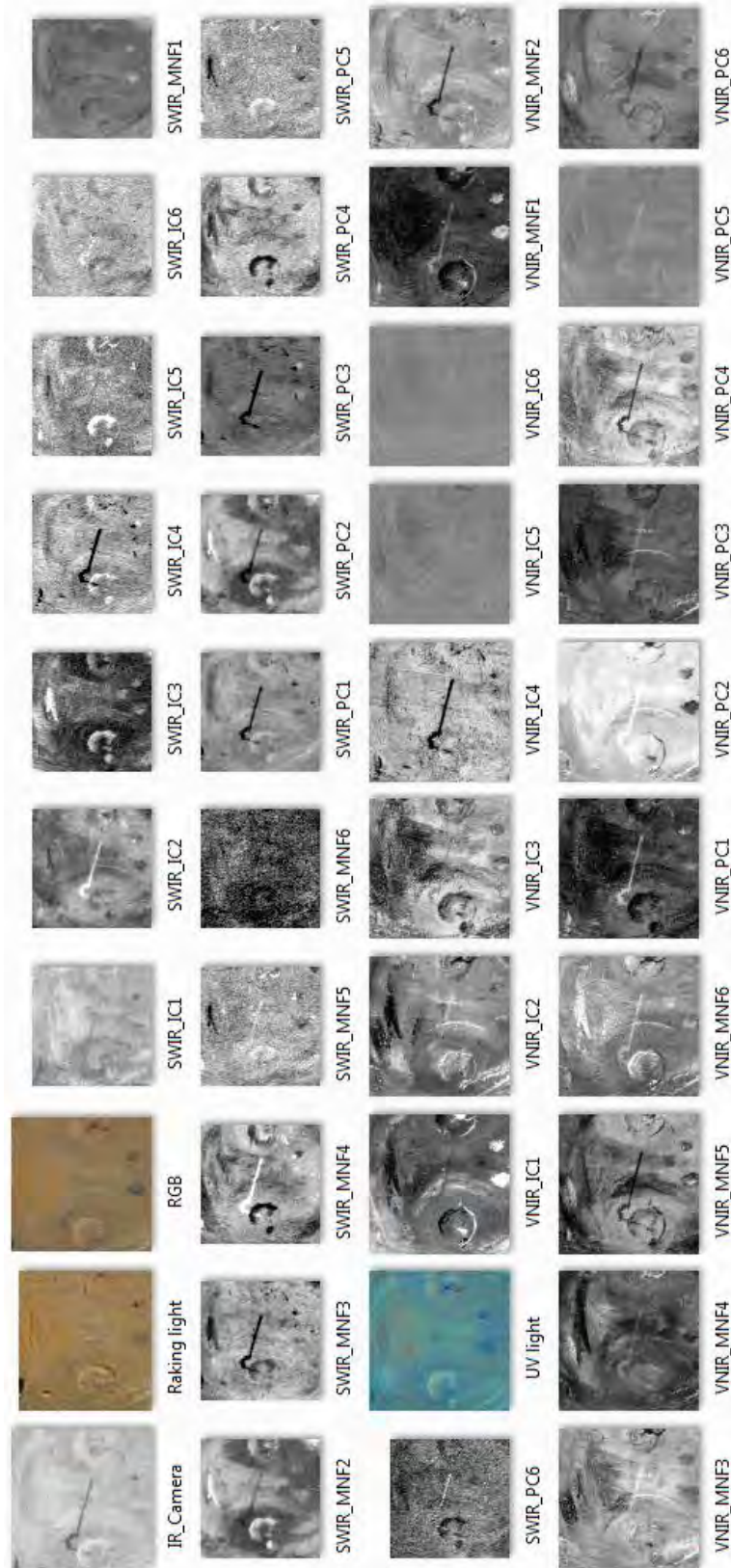
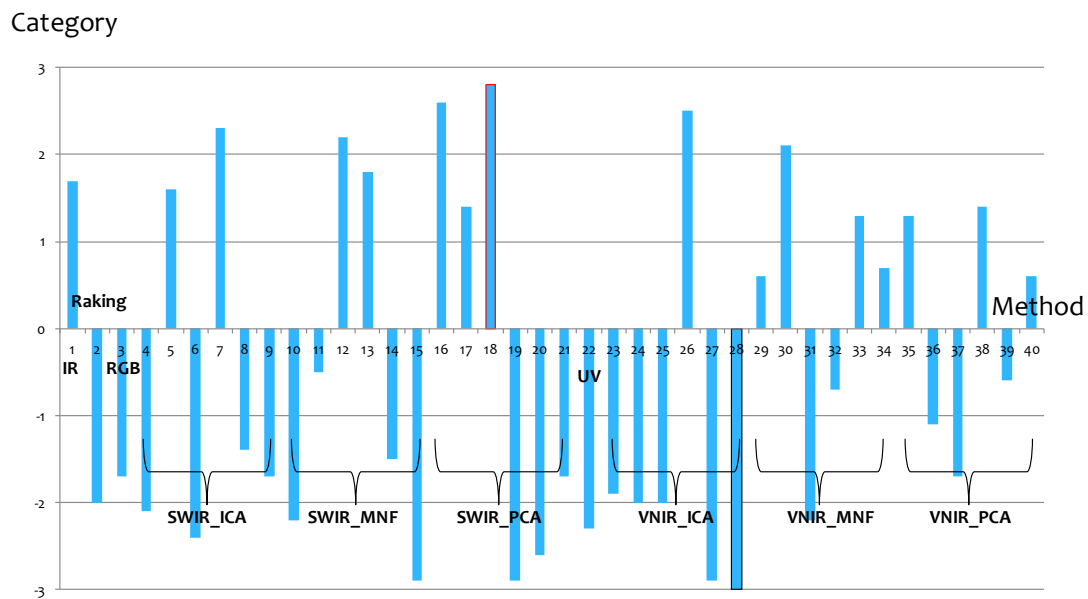


Figure 31: Detail 3: Hook shaped “scratch”.





**Figure 32: Psychophysical results for Detail 3.**

Detail 4 (Figure 33) is a horizontal line shaped scratch on the chin of the human figure intersecting a vertical scratch to the right of the figure. The horizontal line is visible in the **original painting in the author’s standpoint if observed closely to the painting, but the vertical scratch is not.** The specific reason for the scratches is unknown, but it is very likely because of careless handling of the painting in the past. Both VNIR-30cm and SWIR-1m data have this detail; a total of 40 images thus are displayed to the observers. The result shows the average scores for each of the 40 images from the total of 15 observers.

It is observable that in terms of detail 4, the average result shows that SWIR\_IC4 displays the most invisible information whilst SWIR\_PC5 shows the least invisible information. In terms of the other processed images, it appears that several processed SWIR images have better results than the others. However in general it does not seem to have a particular pattern according to the perceptual quality of invisible information by the observers; however it appears that a majority of the methods do not produce a good result in terms of invisible information.

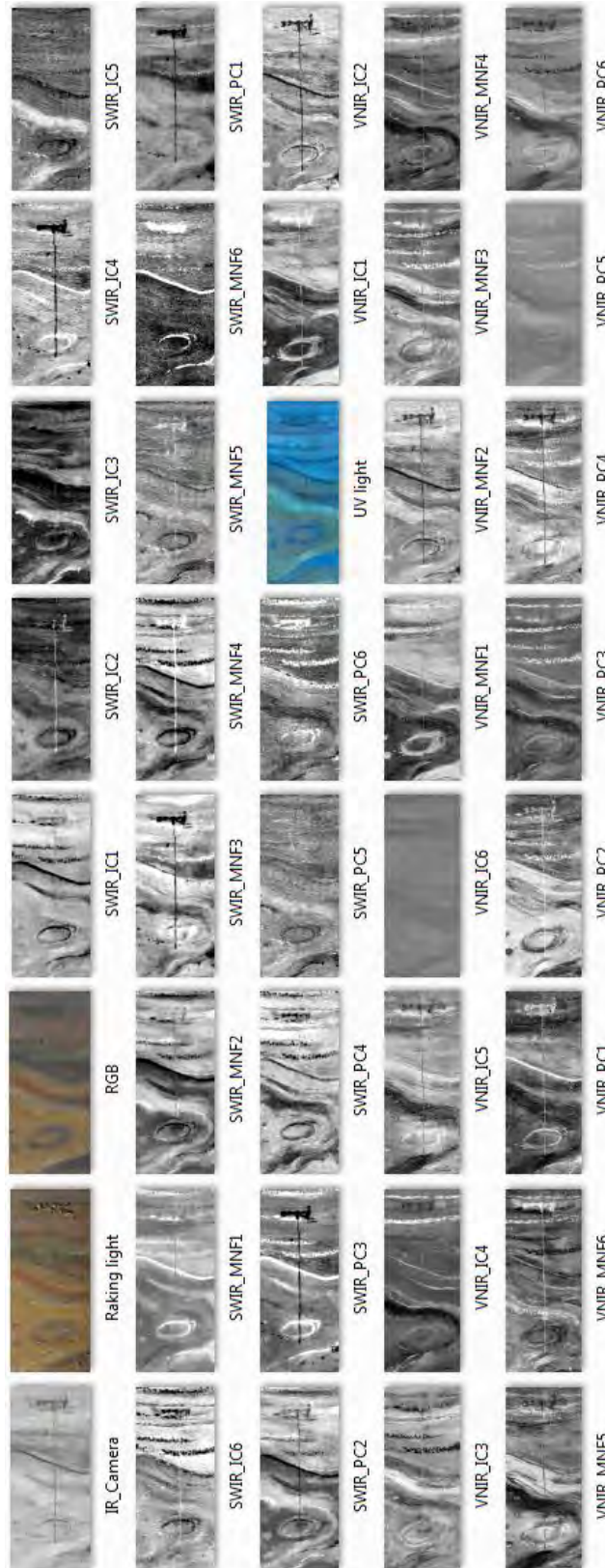
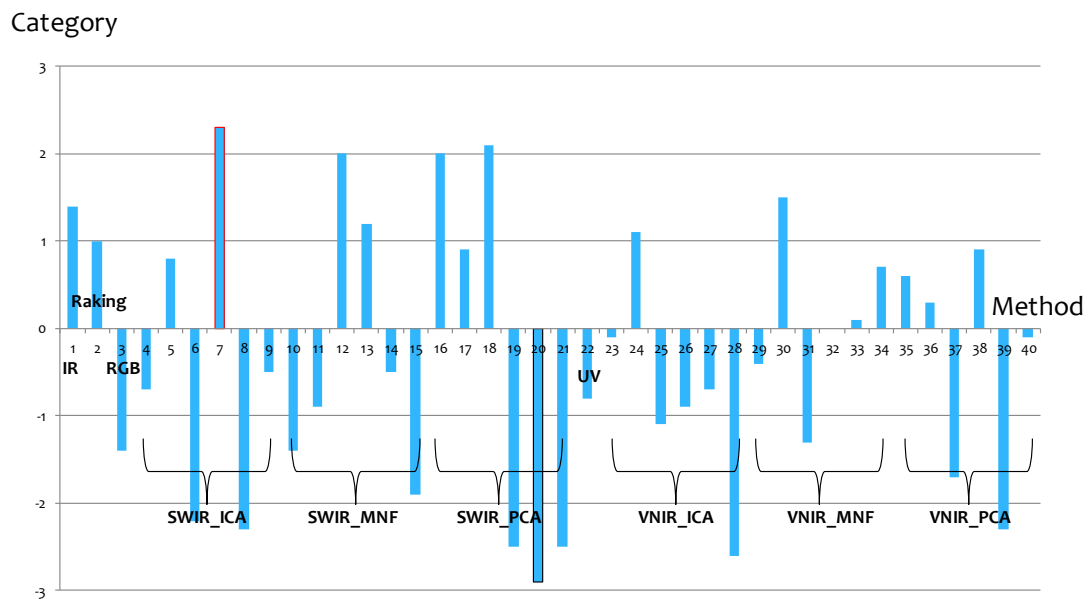


Figure 33: Detail 4: Horizontal “scratch”.



**Figure 34: Psychophysical results for Detail 4.**

Detail 5 (Figure 35) is a tallow dropping. Mr Aslaksby disclosed that the restorers have intentionally tried to remove the layer of damage and restore the work to its original state, but it had been unsuccessful. The restoration was not possible without harming the painting. Both VNIR-30cm and SWIR-1m data have this detail; a total of 40 images thus are displayed to the observers. The result shows the average scores for each of the 40 images from the total of 15 observers.

It is observable that in terms of detail 5, the average result shows that VNIR\_IC2 displays the most invisible information whilst VNIR\_IC6 show the least invisible information.

The other processed images do not seem to have a particular pattern according to the perceptual quality of invisible information by the observers also, and that a majority of the methods do not produce a good result in terms of invisible information. It seems that most of the processed images with MNF and PCA methods for VNIR data have positive scores. Interestingly, most processed images for SWIR data have negative scores.

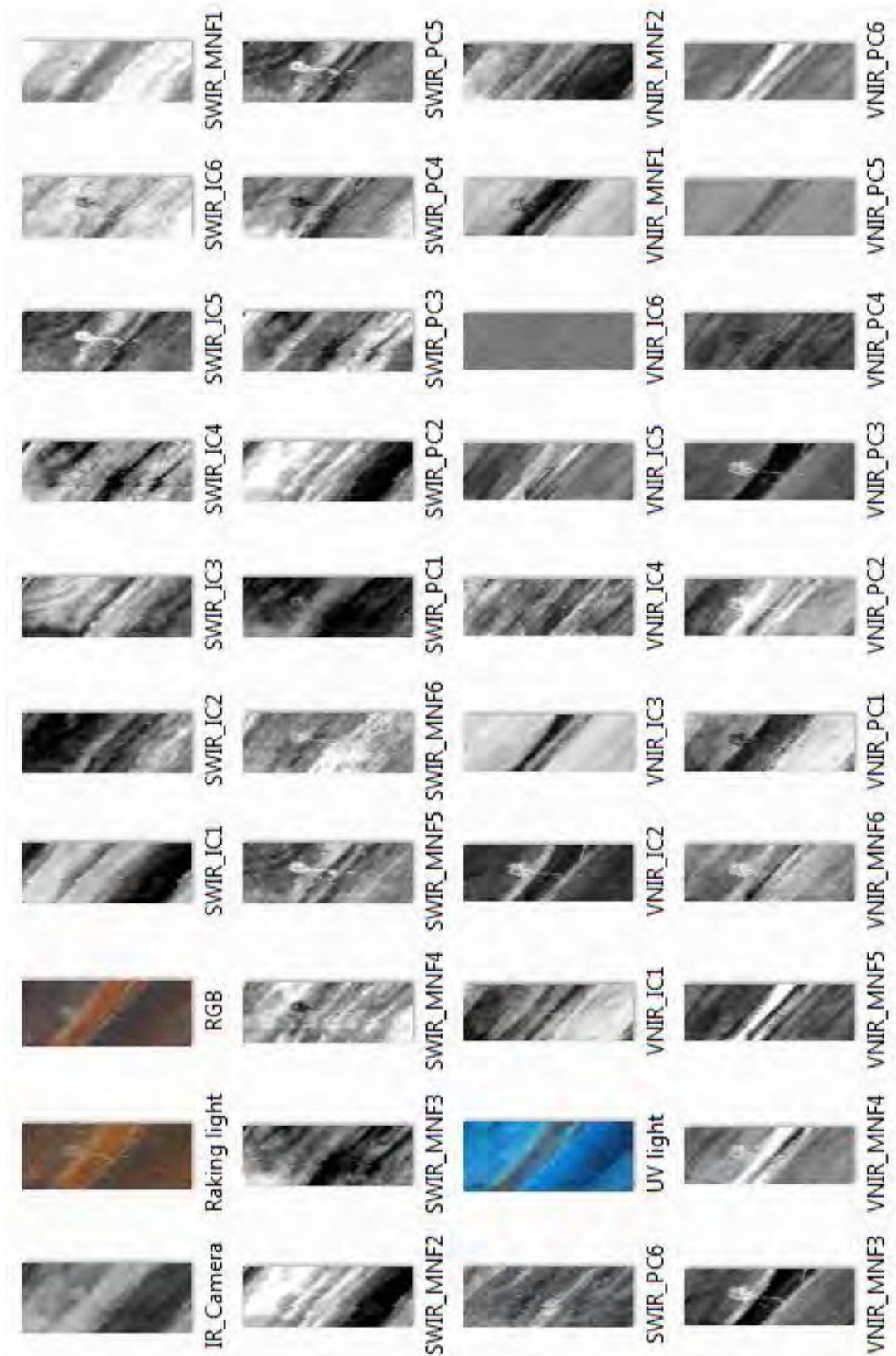
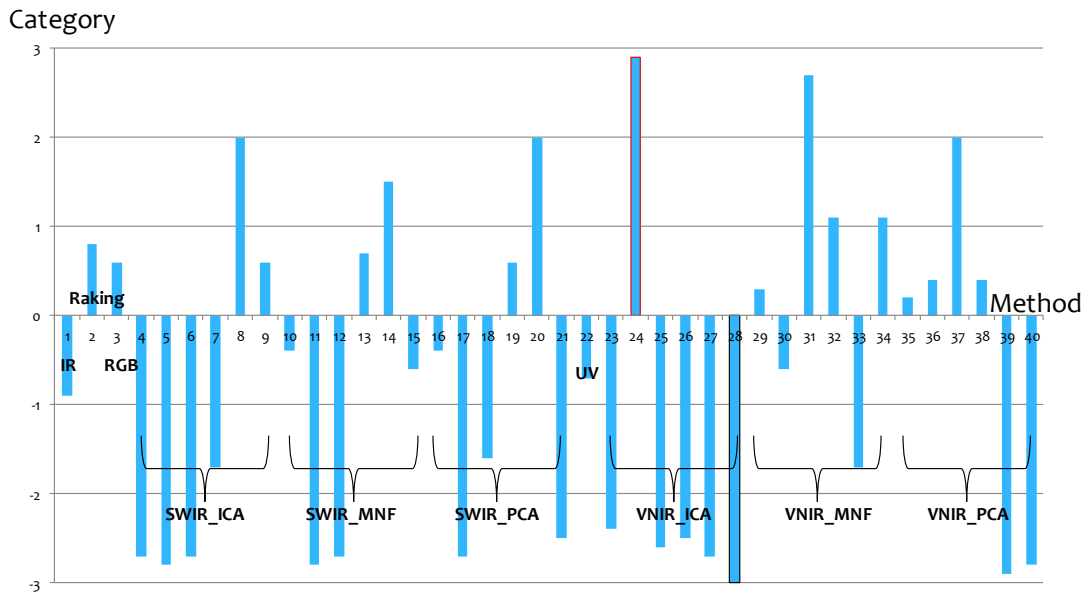


Figure 35: Detail 5: A tallow dropping.



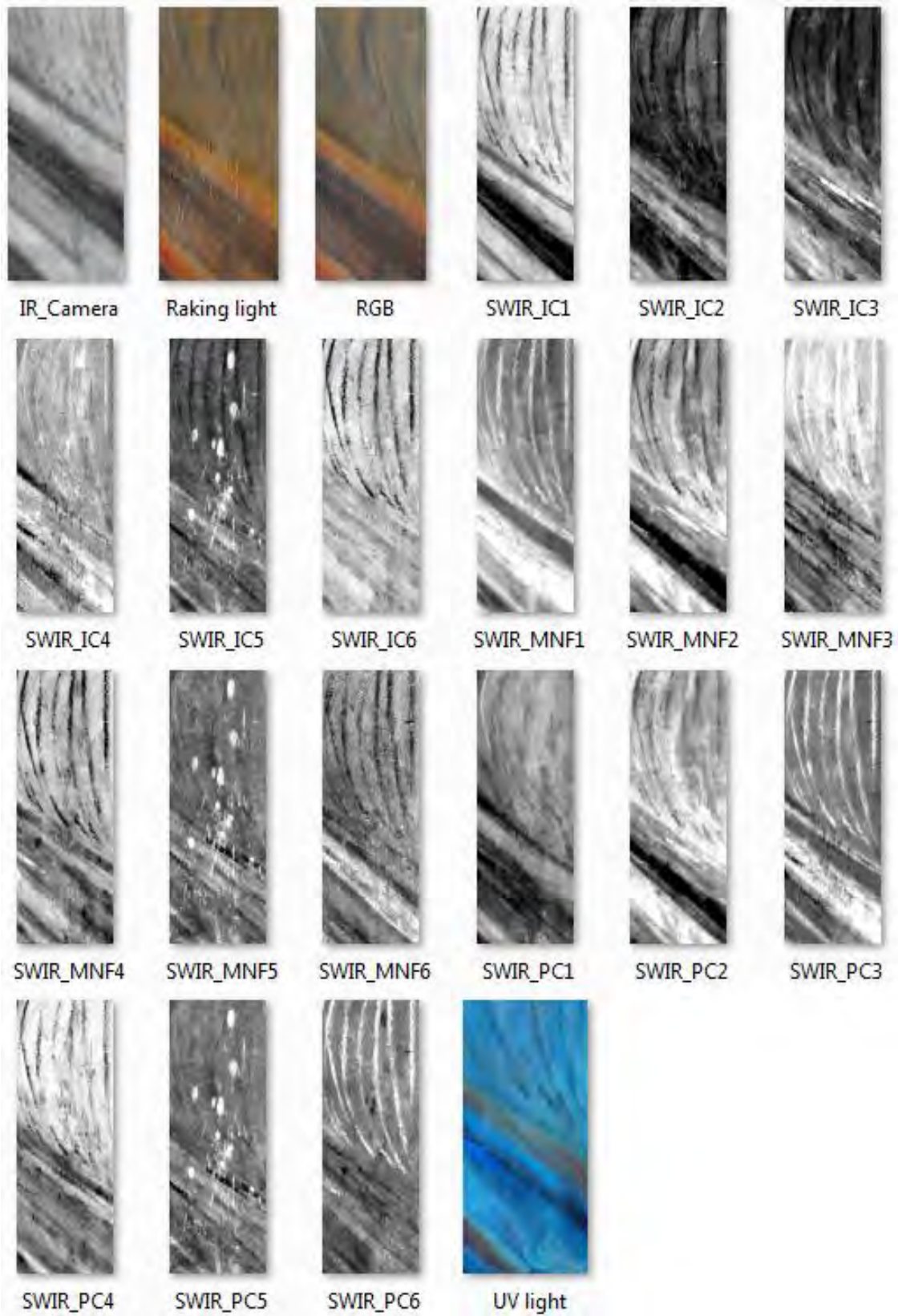
**Figure 36: Psychophysical results for Detail 5.**

Detail 6 (Figure 37) is a cluster of tallow droppings. Like detail 5, the restorers have intentionally tried to remove the layer of damage and restore the work to its original state, but it had been unsuccessful. Similarly, VNIR-30cm does not include this detail; a sum of 22 images is also displayed to the observers. The result shows the average scores for each of the 22 images from the total of 15 observers.

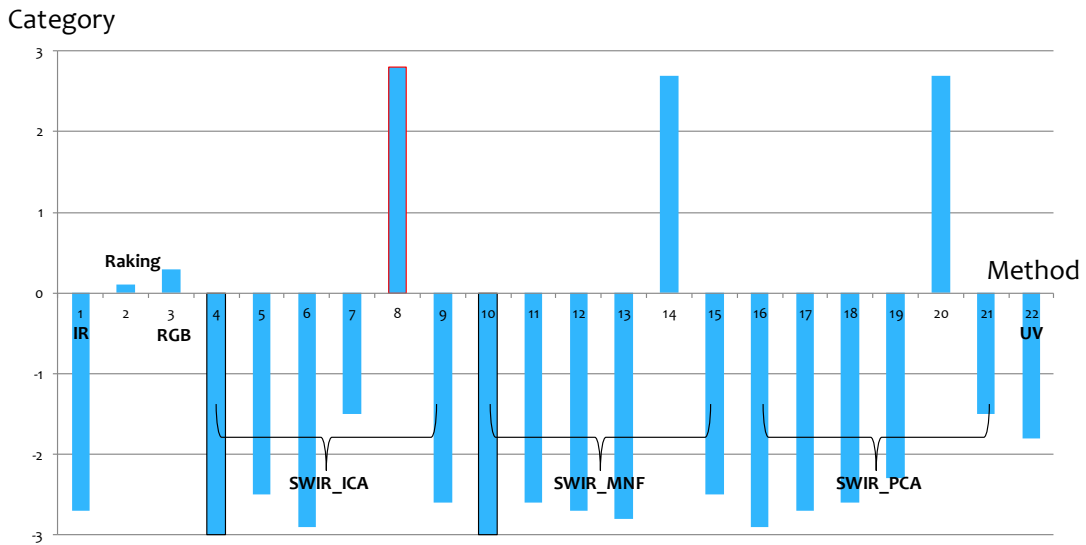
It is observable that in terms of detail 6, the average result shows that SWIR\_IC5 displays the most invisible information whilst SWIR\_IC1 and SWIR\_MNF1 show the least invisible information. Unlike detail 5 which is also a tallow dropping, it is rather interesting that it seems almost all methods have bad result except the 5th components from all the three mathematical processing methods with the 5th component of ICA outperforming the other two.

Furthermore, the best result obtained for detail 5 does not correspond to the best result acquired for detail 6 even both of them are the same artefacts on the painting. Though all the 5th components from the three mathematical models with SWIR data have very good result for detail 5, but VNIR\_IC2 outperformed all the processed images. The reason for the occurrence of the phenomenon might be related to the surroundings as well as the size of the described details from the subjective point of view. The described detail 5 is much smaller than the cluster of tallow droppings in detail 6, yet the surrounding of detail 5 appear to be complicated with regard to its size. However, the VNIR hyperspectral data per se may be the primary reason for carrying extra invisible information for specific features. Hypothetically, SWIR data supposed to possess more invisible information, but detail 5 has displayed an intriguing result for VNIR data. It would be interesting for further analysis if detail 6 is available in VNIR data also.





**Figure 37: Detail 6: Cluster of tallow droppings.**



**Figure 38: Psychophysical results for Detail 6.**

The best and worst results are grouped together as a summary in Figure 39. It is identifiable that in general, the ICA algorithm in terms of SWIR data has provided the best result and the 6th components applying ICA with VNIR data has generated the worst result overall. Furthermore, most of the best results are obtained with SWIR (four out of six situations). It is noted before that detail 1 and detail 6 does not include the processed images with VNIR data. If only details 2, 3, 4 and 5 are considered for a conclusion, SWIR data still outperformed the VNIR data (three out of four situations). It might be expected since SWIR data are all outside the visible range of human vision.

	Details					
	Second Coat	Scratches			Tallow Dropping	
<b>Best</b>	With UV light	SWIR_ICA4	SWIR_PCA3	SWIR_ICA4	VNIR_ICA2	SWIR_ICA5
<b>Worst</b>	SWIR_ICA3	UV VNIR_ICA5 VNIR_ICA6	VNIR_ICA6	SWIR_PCA5	VNIR_ICA6	SWIR_ICA1 SWIR_MNF1

**Figure 39: Summary of best and worst results.**

The second coat of painting appears to be a special case since it is the only detail that has a photographic RGB image as the best result. The image with the best quality in terms of invisible information is not obtained by further processing of the hyperspectral data. The reason might be that the second coat of the painting per se is not actual hidden or invisible detail since it is actually perceivable in the conventional photographic version of the RGB images or the real painting.

With regard to the scratches considered in the experiment, SWIR\_IC4 appears to be the best algorithm since two (details 2 and 4) out of three scratches (details 2, 3 and 4) are quite visible

applying this algorithm. On the other hand, VNIR\_IC6 performed the worst not only for the scratch-like features but also in the general case as two (details 2 and 3) out of three scratches (details 2, 3 and 4), and three (details 2, 3 and 5) out of six details have the least visibility in terms of invisible information.

In relation to the tallow droppings, the ICA algorithm seems to have produced the best results for both details. However, the data applied to generate the best result differ as the image with best quality with regard to invisible information for the small tallow dropping is obtained with VNIR data whilst for the big chunk of tallow dropping are obtained with SWIR data.

The MNF algorithms do not seem to be performing moderately well in general since neither best nor worst images were obtained with this set of algorithms.

It seems that there is no universal the most advantageous technique for all the details. Individual detail necessitates specific method to display more invisible information. Nevertheless, ICA algorithm seems to be a favourable model for almost all the details and this technique can be exploited further in the hyperspectral imaging of the painting in the future. Especially the 4th component of ICA from SWIR data might be beneficial for the restoration scientists to explore details related to scratches.

#### **4.1.2 Comparison between Natural Colour Images and Munch's Image**

In the previous chapter, a linear transformation was introduced by Tsagaris [30] based on the principle of PCA. It makes use of the perceptual attributes of 100 images with natural colours to control the correlation of the bands. The concept is to find the image with the best quality from the hyperspectral data, most likely from the IR region of the hyperspectral data, and merge this image into the VIS region so that the final image can be perceptually pleasant, and at the same time, display more invisible information.

The result displayed from the previous section shows that a majority of the good results are obtained from SWIR data. However, the VIS region is included in the VNIR data. Problems thus merge. It is mentioned previously that not only the spectral sizes of SWIR and VNIR data are completely different, but also the spatial sizes of both. Particularly the spatial size subsequently yields a problem as if an image processed from SWIR data is to be merged into an RGB image transformed from VNIR data, **and then the pixels won't be corresponding to each other. A pixel registration problem occurs and has to be solved.** This research is currently out of the knowledge and research area of the author, therefore an illustration with an exemplary data will be applied for this objective instead of directly applying the result from the first objective to the transformation in the second objective.

The data applied for this section is the VNIR-1m data instead the VNIR-30cm and SWIR-1m data. Because of the availability of the VNIR-1m data given to the author by the time the author applied this algorithm as well as for the sake of avoiding heavy computation, the middle strip of the data is applied instead of the full image of the painting is used. The 1st component applying PCA in the IR region of the VNIR-1m data is computed and assumed to be the best result obtained from the first objective in the previous section.

The computed results applying the 100 images as well as a Hasselblad photographic RGB version of the painting are displayed on the right of Figure 40 and Figure 41 respectively.



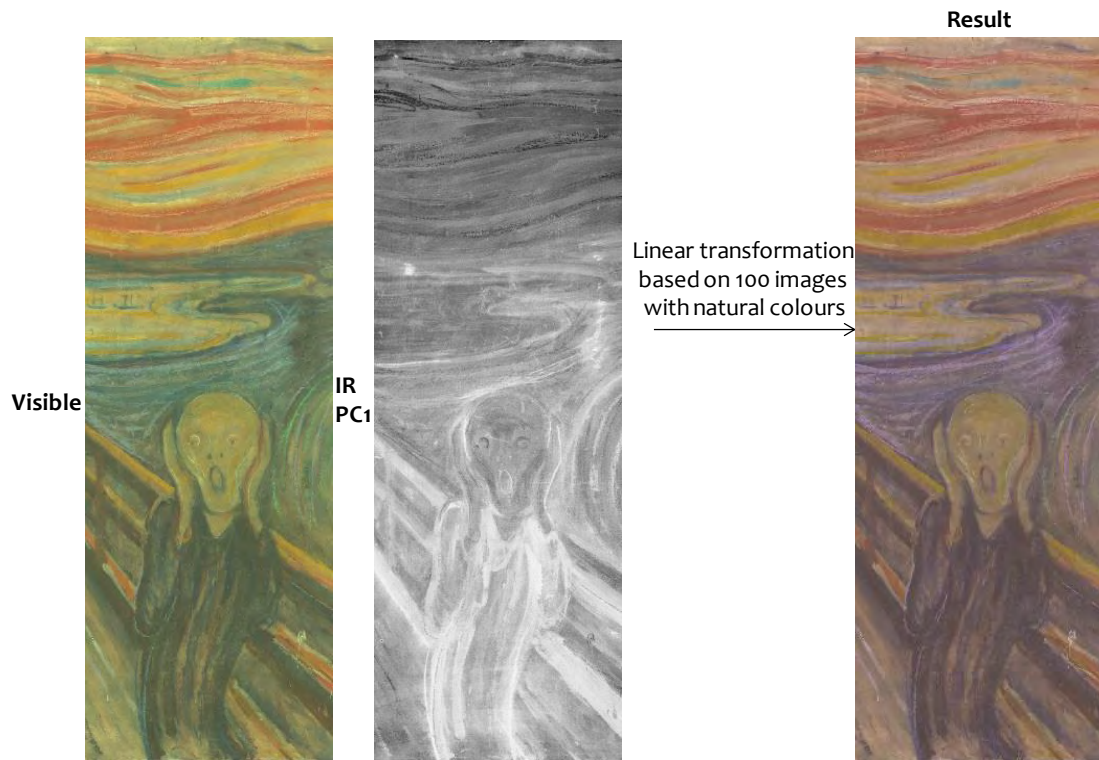


Figure 40: Linear transformation using 100 images with natural colours.

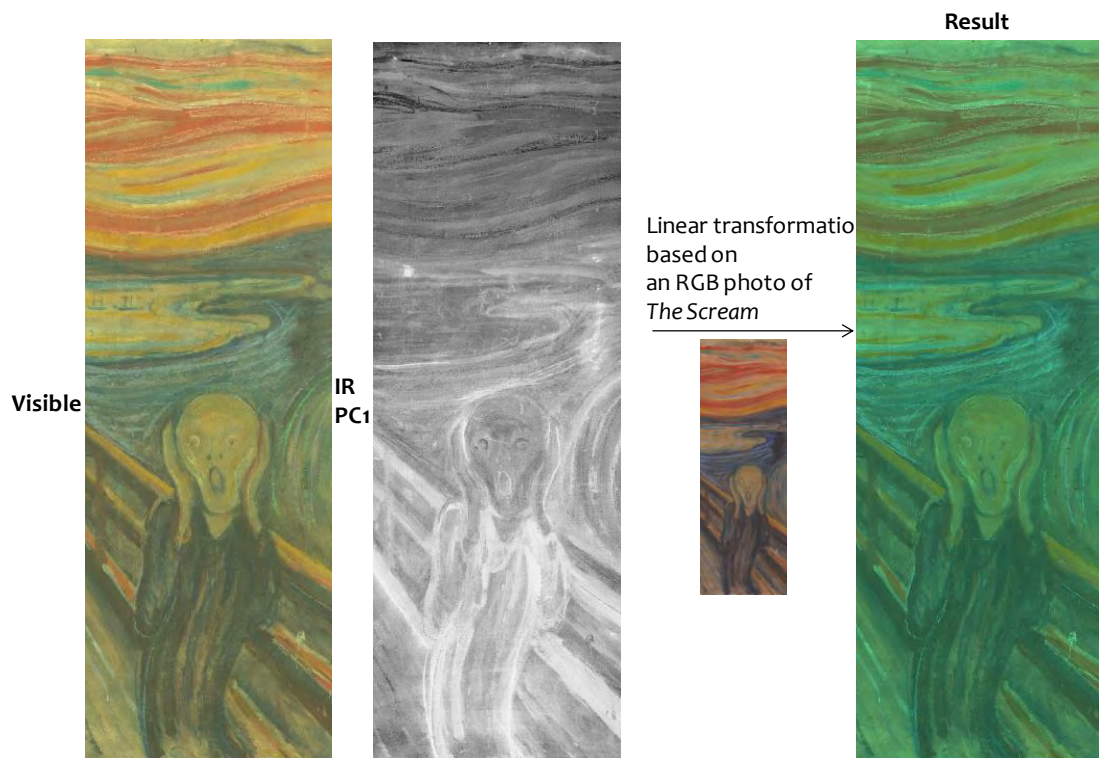


Figure 41: Linear transformation based on an RGB photo.

It was noted previously that the main difference between the two implementations is that the correlation coefficient matrix is altered. Therefore, the images on the left in both figures are the same and are the RGB images obtained from the VNIR-1m data applying 1931 CMF function under illuminant D65, followed by Gamma correction. The images in the middle in both figures are also the same; they are the 1st component of PCA from the IR region of the VNIR-1m data. The difference appears in the transformation. The resulting images can be found on the right of both figures.

It appears that the transformed RGB image from the hyperspectral data does not resemble the actual painting. Several investigation and recalculations confirmed there were no mistakes in the computation or the algorithms in the coding. Instead, there have been some problems with the acquired data during the acquisition stage. However the final image generated from the transformation based on 100 images with natural colours in Figure 40 actually renovated the RGB image on the left to a better looking image or an image with more pleasing colour to the **author's point of view. On the other hand, the resulting image obtained from the transformation** based on the Hasselblad photographic RGB version of *The Scream* in Figure 41 seems to possess more astonishing greenish colours as a matter of fact.

The first result might be expected because of the properties of the 100 images; the resulting image appears soothing even in comparison with the Hasselblad photographic RGB image. The colours in the image seem to be closer to the original photographic version of the RGB image than the RGB image transformed from the hyperspectral VNIR-1m data. However, subjectively speaking, the colours of Hasselblad the photographic version of the RGB image are slightly altered in this image to certain extent.

In terms of the second resulting image, the figure is unexpected. The colours of the image neither do not resemble the Hasselblad photographic version of the RGB image, nor do not resemble the RGB image converted from the hyperspectral data. It also does not seem to have **any aesthetic characteristics of Edvard Munch's paintings. It seems that this method might not** be applicable for the proposition proposed by the author.

## 4.2 Discussion

### 4.2.1 Success

Regarding the psychophysical experiment, the results might have been positive in general. As it has been noted before the psychophysical experiment was conducted among 15 observers. 9 out of the 15 observers were expert observers who are specialised in colour science and performed the experiment under the same setting and surroundings. The rest were naïve observers without any prior knowledge of colour science whatsoever, each individual participated the experiment in completely different environment and setting. For example, all their computers are having different characteristics without calibration among the devices. Furthermore, the images placed in individual detail folders for the psychophysical experiment provided for the six observers were rearranged so that the orders are differential in each folder to avoid the observers get used to the orders.

The analyses were carried out separately initially in order to identify if there indeed exist some inconsistencies in the results between the two sets of observers. The computed results from the two series of data discovered that the best and the worst results are the same, even for the intermediate results. The differences only exist in the decimal points of the averaged scores. It is

believed that the insignificant differences in the results from the psychophysical experiment might be because almost all the images included for experiment are only greyscale images, particularly the images with the best qualities. The intensities of the grey levels are the major influential factors instead of colours which involve more complicated factors.

The author considered that those discrepancies did not affect the final results; subsequently they were merged together for examination. On the one hand, the approach is positive in terms of total number of observers; on the other hand, it might not be scientific from the experimental point of view. It is believed that it might be more advantageous to conduct the same experiment under the same setting.

Two more visits were made by the author along with the Cultural Heritage Team where the author is based at to the National Gallery in Oslo after completing the data processing and obtaining the final results. The first visit was to present the final result to the museum restorers. Feedback by the restorers suggested that it was desired that a full image with the best quality regarding the invisible information be supplied in lieu of individual details. Further interesting details were revealed in the meeting which are detailed in the following paragraphs. One mistake found by the restorer was that the author may have mistaken the tallow dropping as bird dropping which was located in the other part of the painting. After all, the mistake did not affect the final examination.

The second time of the two visits was to conduct an interview with Mr Aslaksby in terms of invisible information revealed from the processed images. The interview discovered extra information not only for the author, but also for the restorer. However, the circumstance was changed slightly in comparison with the psychophysical experiment due to extra data provided for processing. The author was provided with a set of VNIR-1m data which covers the full painting instead of a cut off of the full painting. Subsequently, 36 full images obtained from both VNIR-1m and SWIR-1m data can be processed this time with all the details noted in the psychophysical experiment present. The advantage of applying a new set of data with all the **details available on the full image is that it satisfied the requirement from the restorers'** feedback; the disadvantage is that part of the data thus is not consistent with the data applied in the psychophysical experiment. The algorithms applied for the details and for the full images may have been altered, thus the result of the interview may not be consistent with the result of the psychophysical experiment.

The 36 processed images were printed out with high spatial resolution. Mr Aslaksby was asked to observe the 36 images in order to determine the details in the images the most interesting for him, and select the images that display the maximum invisible information for any details he found intriguing.

The images Mr Aslaksby chose to be appealing were identified either in terms of single details, or with regard to the total invisible information identified. The images selected are: SWIR\_IC1, SWIR\_IC3, SWIR\_IC4, SWIR\_MNF5, SWIR\_MNF6, SWIR\_PC1, SWIR\_PC2, SWIR\_PC3, SWIR\_PC5, VNIR\_IC3, VNIR\_MNF1, VNIR\_MNF3 and VNIR\_PC5.

It is observable that a total of 13 images were selected. 9 out of 13 images are processed from SWIR data. It once again proved that SWIR data may contain more invisible information than the VNIR data despite different data have been used for this set of images. Furthermore, Mr

Aslaksby thought that SWIR\_IC4 was the image that gives the most invisible information in comparison with all the rest images. Interestingly, this coincides with the result obtained from the psychophysical experiment. Particularly, Mr Aslaksby considered that the details marked in red in the following figures are very intriguing for him while they were compared with the photographic Hasselblad RGB image at the same time.

Figure 42 shows SWIR\_IC1 where Mr Aslaksby found it was difficult to associate it with the original painting if it was related to a specific pigment or paint and said it was an interesting feature visible in that area.

Figure 43 displays SWIR\_IC3 where the town at the right hand side of the painting is very discernible for Mr Aslaksby, and he could not find it so distinguishable in the other processed images. For the author, it was also a new finding since the town at the far right of the scene in the painting had never been noticed until it was pointed out by Mr Aslaksby in the image.

In terms of Figure 44 which illustrates SWIR\_IC4, Mr Aslaksby not only thought that it was the best image in terms of invisible information and indicated several features that were barely visible in the conventional viewing condition, but also noticed some stroke-like features from the far left end of the painting extending to the right of the painting. The detail is marked in red **in the image and shaped like the character “L”**. It was considered that they might be something underneath of the painting and directly on the support, possibly glue resolution made by white brush or sponge for practical reason. However, Mr Aslaksby was uncertain about the cause of these features but thought they were interesting.

Figure 45 is SWIR\_MNF5. Mr Aslaksby thought it has very strong contrast, particularly the tallow droppings. Though it is a soft image, but it seems to contain more information than the components that are also able to display the tallow droppings. The white spot on the bottom left of the painting seemed to be new for Mr Aslaksby and he also expressed the interest to research it further.

Figure 46 is SWIR\_MNF6. Mr Aslaksby considered the white curve on the shoulder was very visible and different from the other images.

Figure 47 is SWIR\_PC1. Mr Aslaksby particularly identified those parts circled in red appeared be text, but he was uncertain about it.

Figure 48 is SWIR\_PC2. The face of the human **figure especially caught Mr Aslaksby’s attention** and thought to be interesting since different layers seem to be present on the face.

SWIR\_PC3 was noted to present similar stroke-like features in the figure as in SWIR\_IC4. SWIR\_PC5 also displays strong contrast as SWIR\_MNF5 as well as the white spot that appears in SWIR\_MNF5, but Mr Aslaksby considered that SWIR\_MNF5 looks like containing more information than SWIR\_PC5. Due to the similarities between the figures, these images are not shown.

Figure 49 is VNIR\_IC3. Mr Aslaksby found this white detail marked in red might be wax or crayon while it was compared with the RGB image. He revealed that they thought this part was

initially red pigment, but the colour has fallen off currently, and probably that was the reason this detail is popped out in this image.

Figure 50 is VNIR\_MNF1. This circled part was mainly blue colour and this part might be related to chromatic rendering.

In terms of VNIR\_PC5, it displays similar feature as SWIR\_IC3, whilst VNIR\_MNF3 has the **similar characteristics as SWIR\_IC4 and SWIR\_PC3 in terms of the “L” shaped brush strokes.**

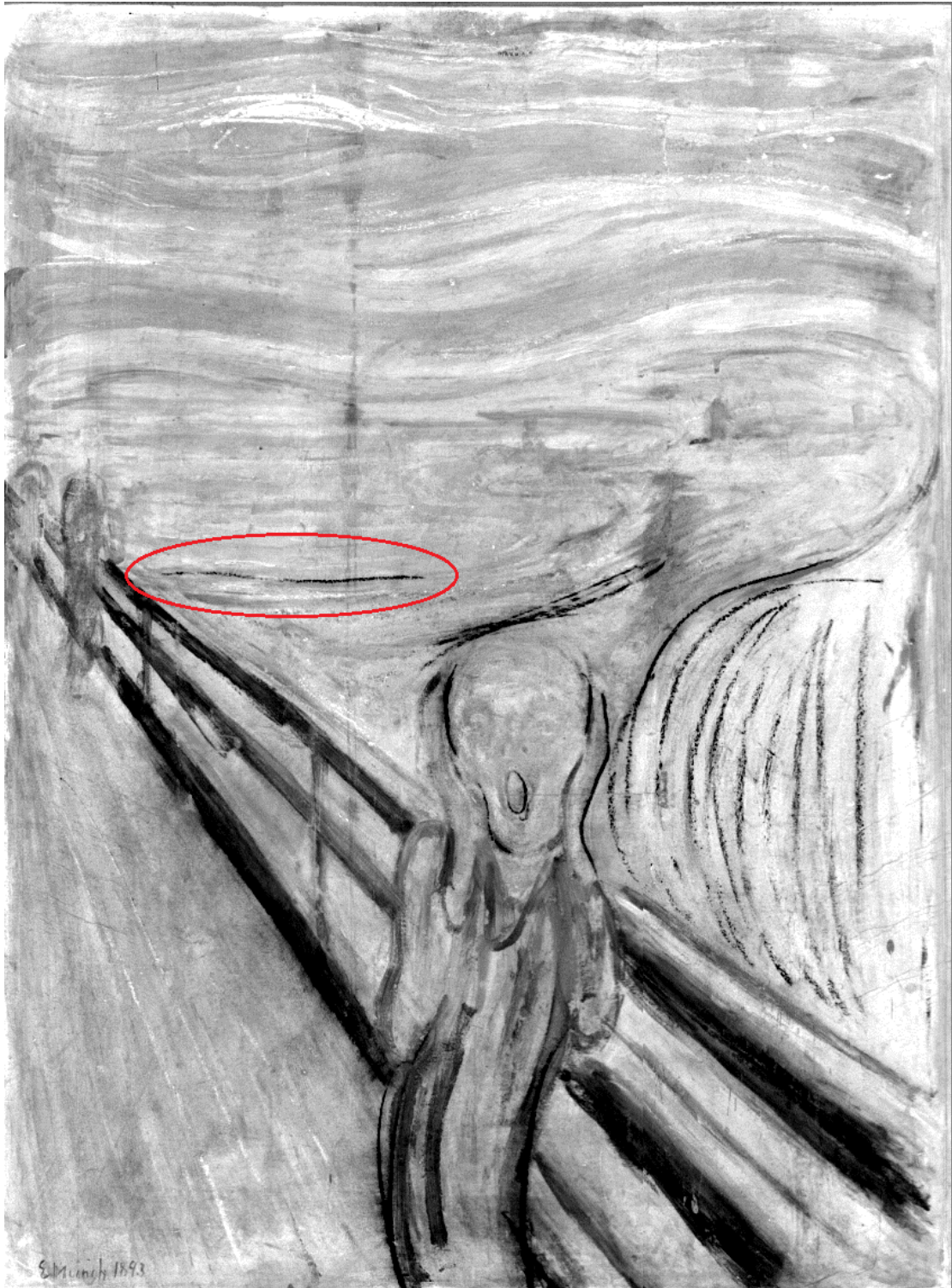
Overall, Mr Aslaksby noticed and agreed that there was no single image that can display all of the invisible information as desired even though SWIR\_IC4 was considered to be the best image among all.

However, the author considers that it might still be possible to combine all the images with the best qualities in terms of invisible information applying false colour technique.

A false colour image differs from true colour image that is based on natural colour rendition. Natural colour rendition means how the colours of an object viewed by the human observer directly, how the colours of the object will appear in in the image. On the other hand, the purpose of false colour image is to detect features that are usually indiscernible by the human eye. It thus does not satisfy natural colour rendition. The afore-mentioned representation of R, G and B channels with the first three components of PCA is an example of false colour imaging.

Excluding the photographic RGB image under UV light, the best methods found from the psychophysical experiment include SWIR\_IC4, SWIR\_PC3, SWIR\_IC5 and VNIR\_IC2. It has been mentioned previously that there exist a pixel registration problem between VNIR and SWIR data, thus VNIR\_IC2 is not included for forming the false colour image. The other three methods are combined to construct a false colour image in an attempt to view all the invisible details in one image. There are several possibilities of combinations of the three components. After multiple trials on different combinations, the author thinks the image shown in Figure 51 might be of interest. The second coat of paint, the tallow droppings and the scratches are visible in the image since the chosen algorithms are based on the best images showing the aforementioned details. It appears to the author that some of the features may have been enhanced, but others may have been diminished. **However it is only based on the author’s sole point of view**, in order to determine if false colour is indeed useful for presenting invisible information, further research should be conducted.





**Figure 42: SWIR\_IC1 image of *The Scream* selected by the restorer.**





**Figure 43: SWIR\_IC3 image of *The Scream* selected by the restorer.**





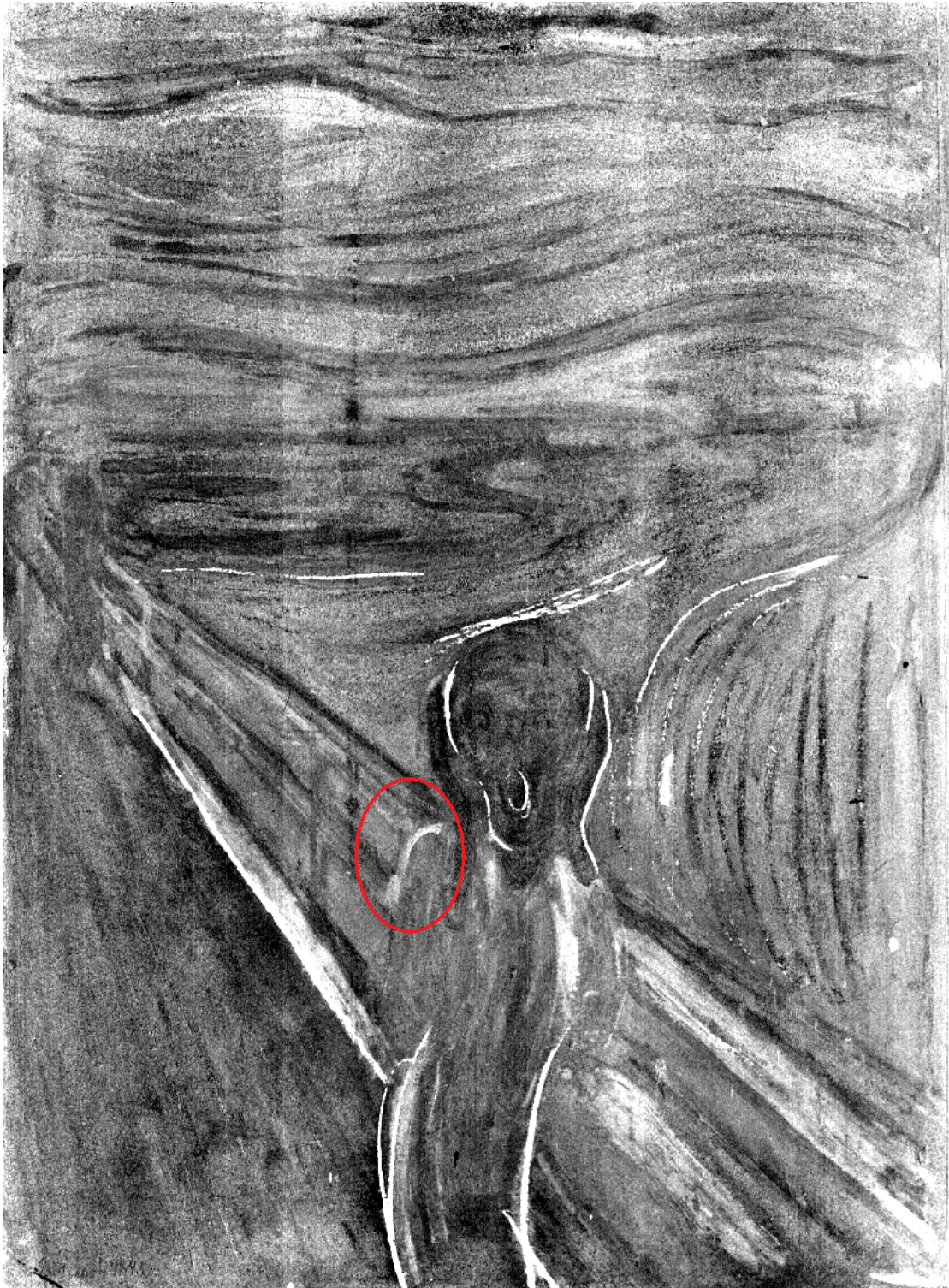
**Figure 44: SWIR\_IC4 image of *The Scream* selected by the restorer.**





**Figure 45: SWIR\_MNF5 image of *The Scream* selected by the restorer.**





**Figure 46: SWIR\_MNF6 image of *The Scream* selected by the restorer.**



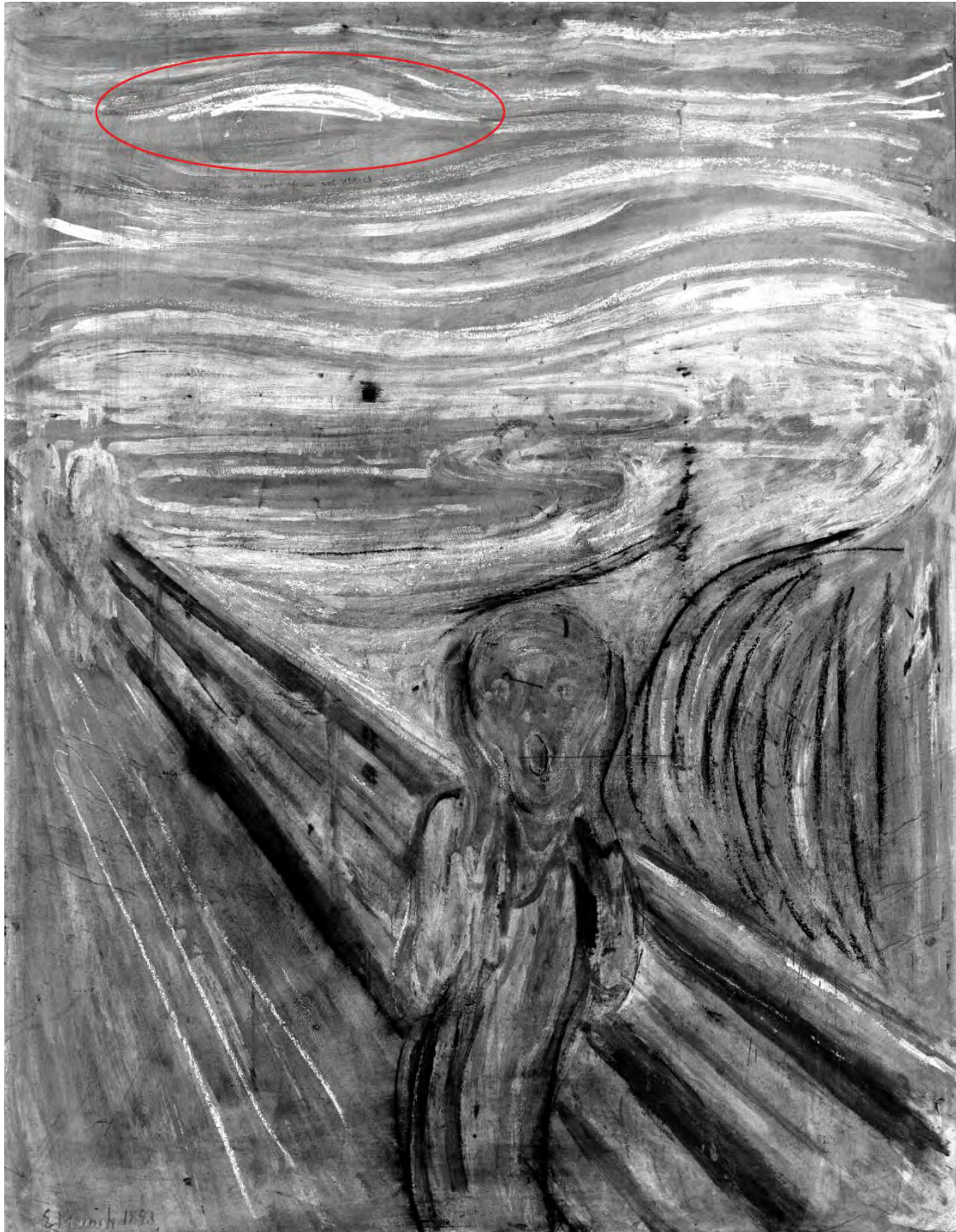


**Figure 47:** SWIR\_PC1 image of *The Scream* selected by the restorer.

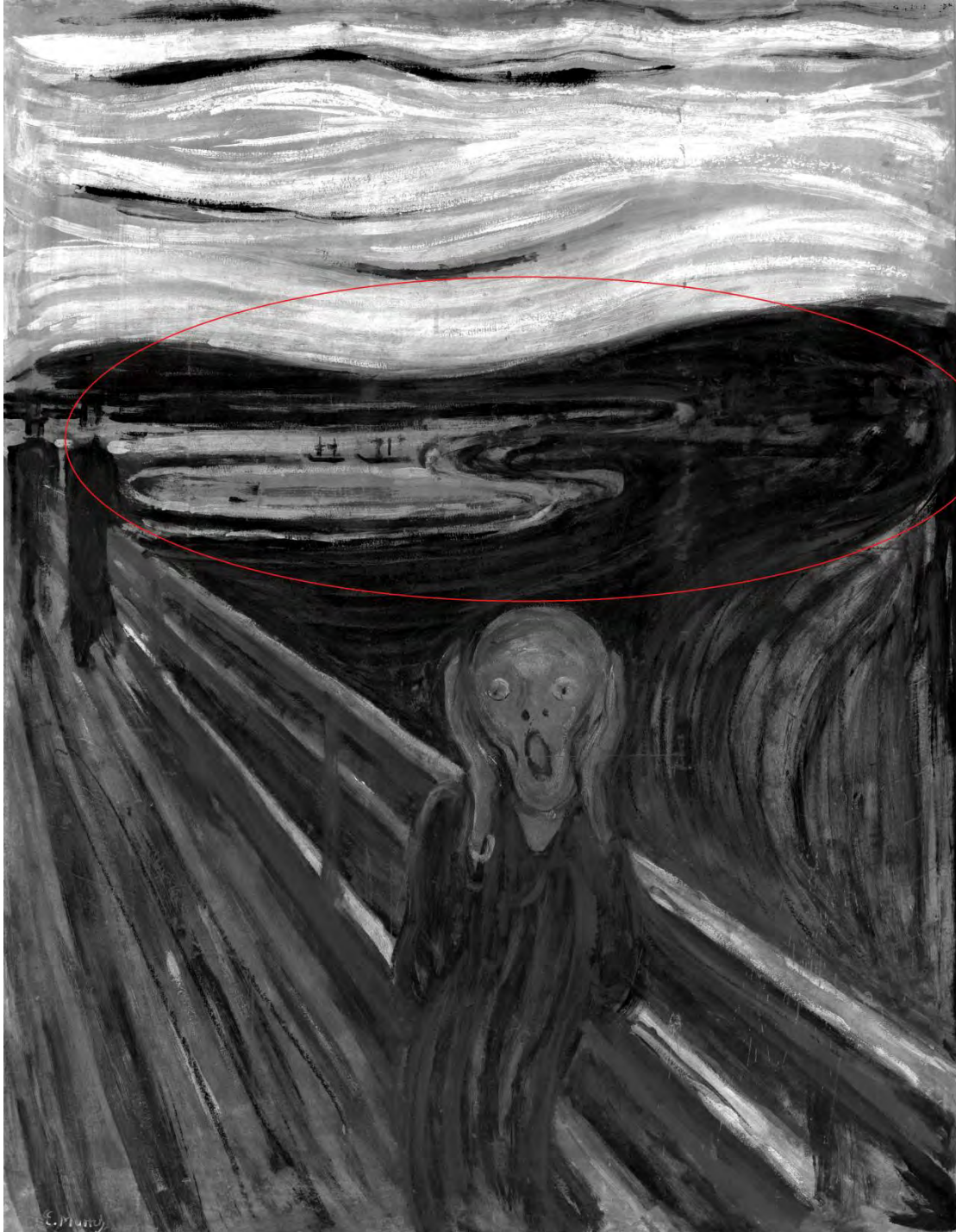


**Figure 48: SWIR\_PC2 image of *The Scream* selected by the restorer.**



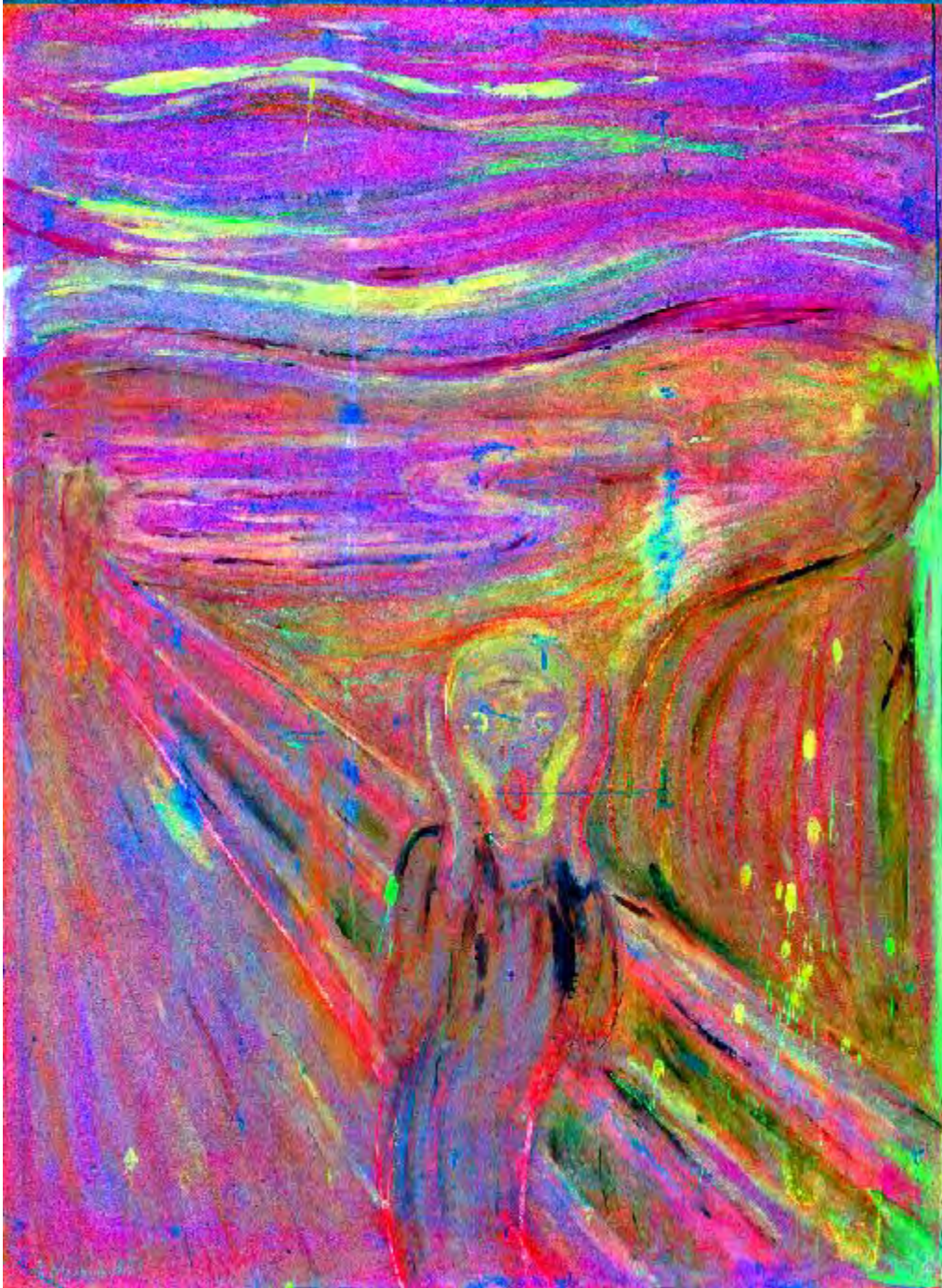


**Figure 49: VNIR\_IC3 image of *The Scream* selected by the restorer.**



**Figure 50: VNIR\_MNF1 image of *The Scream* selected by the restorer.**





**Figure 51: False colour image generated with the best images from psychophysical experiment.**

Furthermore, a piece of software inspired by the work from the previous researchers was developed. The purpose of this application is to display differences visually between two chosen images for the museum visitors. Two images can be selected. For example, a conventional RGB image can be chosen as the base image and a mathematically processed image is chosen as the overlay. By controlling the level of the transparency of the two images with a slider, the viewer can see clear changes during the transition of between the images, particularly between the

conventional RGB images and the processed images that have clear hidden features. It is rather interesting for the museum visitors to be able to see the details that they cannot see in the real paintings with naked eye; even to be able to envisage the history of the painting to certain extent. This feature is considered to be very educational for the museum spectators or art lovers in general

#### **4.2.2 Failure**

This research so far seems to have achieved encouraging results. However it seems there exist some problems in the process also due to various issues like high computation demand, different dimensions of the data and the unavailability of the data.

First of all, it was noted previously that the author considered the VNIR-30cm data for processing for the first objective in order to benefit from its high resolution so that its lack of spectral bands in the IR region could be compensated. However, the VNIR-30cm data only has a cut off of the full painting. A VNIR-30cm of the full painting is unavailable. Therefore 2 out of the 6 observed details could not be included in the psychophysical experiment.

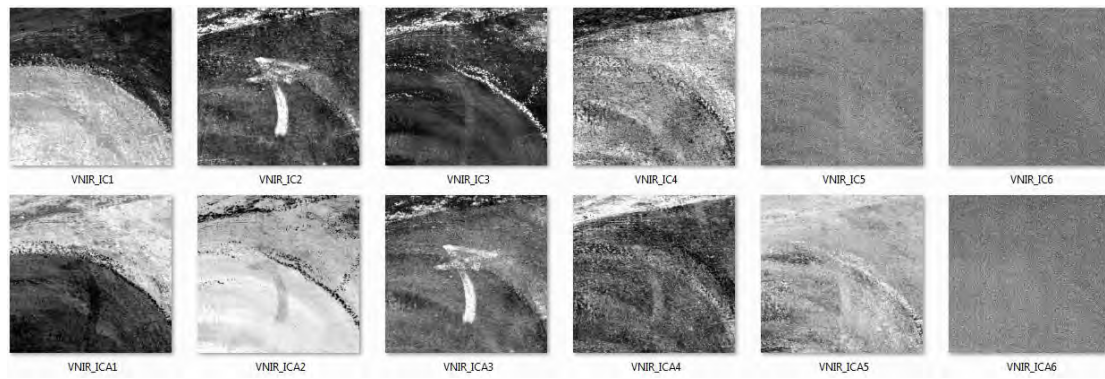
Furthermore, the computation of the ICA algorithm for VNIR-30cm has been a big concern since the amount of computational resources required for the calculation exceeded 32GB of memory and none of the available workstations was able to implement the calculation. Subsequently, the VNIR-30cm had to be sub-sampled for ICA calculation in order to reduce the computation.

Two approaches were applied for the subsampling. One was to cut off individual details directly from the raw data for computation of the ICA algorithm; another was to reduce the size of the raw data to half so that a processed full image could be obtained firstly and then the details from the processed images would be cut off for comparison. The images used for psychophysical experiment were obtained from the first approach.

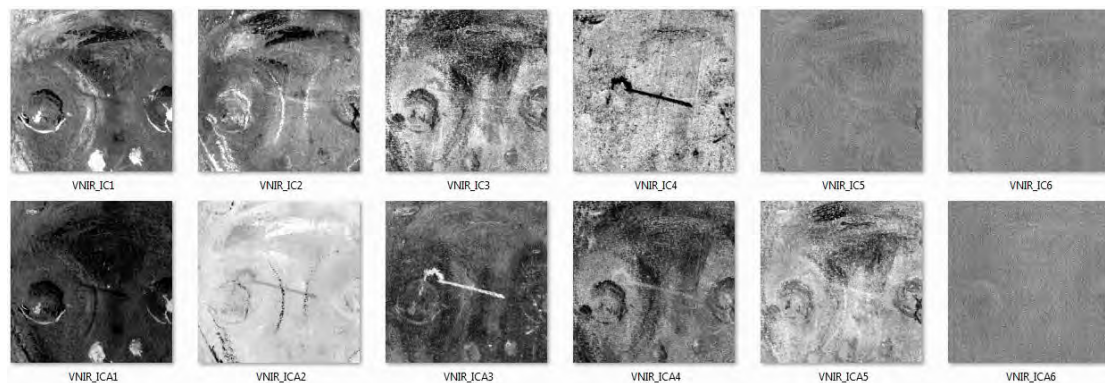
For all the other calculations, including the computations for PCs and MNFs of VNIR-30cm data as well as ICs, PCs and MNFs of SWIR-1m data, sub-sampling of the details were conducted after the processed images were obtained. As a result, the algorithms applied for all the 36 images differ.

Consequently, the algorithm applied with ICA on VNIR-30cm data and the rest of the algorithms may be different and not comparable. Figure 52 displays an example of the images. The images are of detail 2 as described in the previous sections and processed with the ICA algorithm. The top row shows the images acquired with the first approach whilst the bottom row shows the images obtained with the second approach. Conceptually, it appears to the author that the images obtained applying the second approach do not display a significant improvement in comparison with the images obtained implementing the first approach. Figure 53 is another example of the processed images. The images are detail 3 described previously and processed with ICA algorithm also. Similarly, the quality of the images seems to be worse in the bottom row than the top row in general. The other details are observed to have shown a similar phenomenon. Therefore, it is considered that the result of the psychophysical experiment might have not been affected significantly.





**Figure 52: ICA output of detail 2.**



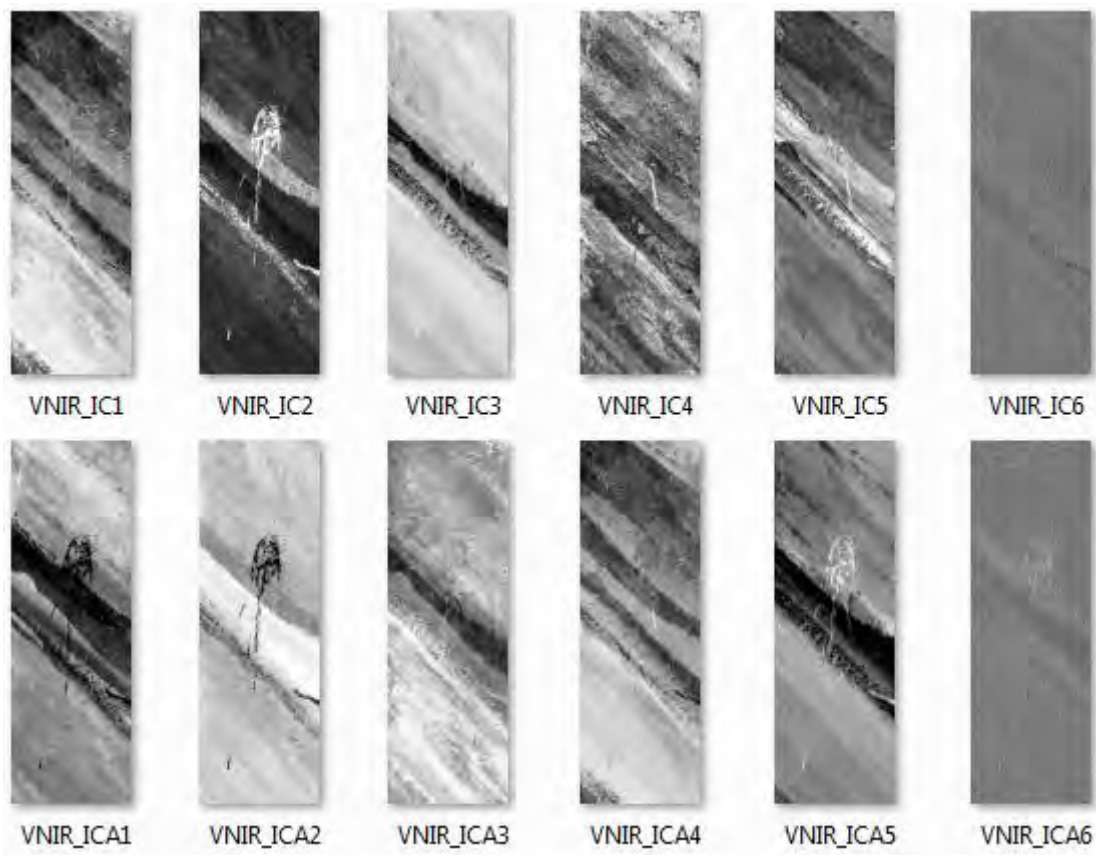
**Figure 53: ICA output of detail 3.**

With regard to detail 5, VNIR\_IC2 has produced the best result in the psychophysical experiment. In order to validate if the choice of the approach affect the result, a comparison between the images applying the two sub-sampling approaches is implemented as shown in Figure 54. As a matter of fact, it appears that VNIR\_ICA2 has better visual quality than VNIR\_IC2 which implies that even the second approach of sub-sampling is applied; the best result in the psychophysical experiment for this detail might still be the 2<sup>nd</sup> component of VNIR data.

A similar problem occurred while producing the processed full images with VNIR-1m data for the interview with Mr Aslaksby. Several attempts were made in order to generate ICs from ICA with VNIR-1m data; however they had all been unsuccessful. Data reduction thus was performed. This time, the second approach mentioned above was applied. The data was firstly reduced in half in X and Y dimensions, then the full images instead of sub-sampled details were processed. Since the purpose of applying the VNIR-1m data was to display all the full images to Mr Aslaksby, thus details were not cut off for the illustration in the interview.

Secondly, the evaluations have been conducted mainly based on human visual perception. Though quantitative examination applying psychophysical experiment was conducted, the examination was rather subjective. The author has considered the possibility of analysing the data in a more objective manner such as applying Root Mean Square Error (RMSE); nevertheless it seems unfeasible since the comparison is always between VNIR and SWIR data which have completely different spectral and spatial resolutions. As it has mentioned previously

that the differential dimensions, particularly the spatial resolution causes the pixel registration problem if they are to be compared in the same quantitative and mathematical way when they supposed to have the same spatial resolution.



**Figure 54: ICA output of detail 5.**

Furthermore, a ground truth image has always been a problem since a suitable image has not been able to be determined to perform the role. Spatial resolution can also be a problem if the Hasselblad photographic RGB image is considered to be the ground truth. Consequently, the evaluations are not measured in any objective mathematical models. However, if the spatial resolutions of both VNIR and SWIR data can match, more objective evaluation may be performed.

Additionally, there exist setting and knowledge discrepancies for the observers. Though the computed result does not seem affect substantially for the final extreme results, it is recommended to perform all the observations under the same environmental and technical setting so that the experiment can be more scientific.

Thirdly, it was recommended that ICA, PCA and MNF mathematical techniques can also have non-linear forms. Due to the time limit, the research direction of non-linear models for those algorithms is not considered in this research. Nevertheless, this research approach can be regarded in the future.

Lastly, the concept of the second objective was considered by the author to be interesting in terms of human visual perception. The produced final image based on the perceptual attributes **of the 100 images with natural colours does certainly appear more pleasing from the author's** point of view. The colours in the image seem to resemble more to the photographic RGB version of The Scream than the RGB image transformed from the hyperspectral data which is a plus in terms of the transformation.. Nevertheless, it does not seem to be applicable for the museum restorers. Additionally, the final image generated based on the perceptual attributes of a photographic RGB version of The Scream has produced shocking greenish colours, which agree neither with the photographic RGB version of The Scream nor with the RGB image converted from the hyperspectral data. Perceptually, the resulting image does not seem to be pleasant either. Therefore this research direction should be reconsidered or modified to make it more sensible.

### 4.3 Conclusion

This chapter applied the methodologies discussed in Chapter 3. A series of algorithms have been implemented. The evaluations are conducted for two objectives. Both evaluations are based on subjective opinions.

A psychophysical experiment was applied for the first objective. 15 observers were invited in the experiment. Due to the discrepancies in the spatial coverage of the painting, two details were analysed among 22 images whilst four details were examined among 40 images. The overall outcome displays the advantages of SWIR data in terms of disclosing invisible information. The result might be expected since SWIR data contain only the information outside the human vision. ICA algorithm seems to have good performance in general, especially for SWIR data. Furthermore, the 4th component obtained with ICA from SWIR data has displayed the best result for the scratch like features. On the other hand, the 6th component of ICA from VNIR is the worst algorithm in terms of invisible information.

The interview and discussion with the museum restorer Mr Aslaksby has revealed several interesting features not only for himself but also for the author. For example, Mr Aslaksby found a spot from two of the processed images that he has never noticed in the original painting at the same location. Mr Aslaksby agrees that there is no single processed image can reveal all the invisible features however concluded that SWIR\_IC4 is also the best image for him in terms of invisible information. It coincides with the result of the psychophysical experiment even though the data applied for performing those algorithms were altered.

In terms of the second objective, the transformation based on the images with natural colours has generated an expected image which appears perceptually more pleasing in terms of the **author's standpoint. However the image obtained based on the perceptual attributes of the** photographic version of the RGB image seems to have unexpected colours. The algorithm is considered to be interesting however does not seem **to be associated with restorer's work.**

Both failure and success of the project are also discussed. Some problems may be able to be amended in the future such as the issues with the observers and the implementation of the algorithms. Some may not be able to be changed due to the existing infrastructure. If the available data and condition allow, improvement in the research should be made not only on the corresponding data processed but also on the algorithms applied.

## 5 Conclusions

The research encompasses two primary objectives: to perceive the invisible information from hyperspectral data and to combine the invisible information, most likely from the IR region into the VIS region. The hyperspectral data were acquired with two hyperspectral cameras. The **object of interest for this research is Edvard Munch's renowned painting *The Scream*** located at the National Gallery in Oslo.

The definition of invisible information applied for this project, as defined in Chapter 3, is the information outside the visible range according to human vision and the information that is barely visible for human eye in conventional photographs or real paintings. This information however can be augmented applying different mathematical techniques.

Three main mathematical models are applied in this project to obtain processed images in order to view some of otherwise invisible features. These models are PCA, ICA and MNF. Including four images supplied by the National Gallery in Oslo a total of 40 images were generated and used for evaluation. A psychophysical experiment was conducted to examine those images in order to find the image that according to a group of observers can display the most invisible information.

The set of data applied for this objective are VNIR-30cm and SWIR-1m. There are both cons and pros when applying VNIR-30cm data. VNIR-30cm data was obtained at the focal distance of approximately 30cm therefore the image is only a cut off of the full painting. Subsequently, two of the details chosen for examination are not included in the data. On the other hand, the data are considered to possess a great amount of information since the spatial resolution is higher than the VNIR-1m data. However, this factor produces another problem: computation burden. This factor was of particular importance as none of the available workstations where the author is based at was able to perform ICA algorithm on the VNIR-30cm data. Subsequently, sub-sampling sets of the details were produced directly from the raw data followed by the application of the ICA method. All the computations for the rest of the images were done in the way the mathematical models were applied originally on the complete set of data followed by sub-sampling of the processed images. These included PCA and MNF processing of VNIR-30cm data and ICA, PCA and MNF processing of SWIR-1m data since none of the computations required more memory resources than those from the workstations available. The algorithms applied for the images thus might be considered as different.

In order to justify the images obtained from the subsampling of the details on the raw data before computation of ICs on VNIR-30cm data used for the psychophysical experiment, another calculation approach was applied. The VNIR-30cm was subsampled first spatially to half the size of the original image. The result is therefore a smaller size of a full image which was used to compute ICs. The details were thus obtained from the cut off of the processed full-size images.

The images obtained from the second approach do not appear to be better than the images **obtained from the first approach. As a matter of fact, they seem to be worse to the author's point of view.** The reason might be that the area covered for processing ICA algorithm is bigger than the previous situation; this might result in a greater chance of including irrelevant information in the data used for processing. Subsequently, the quality of the images obtained applying the

second approach might be as not good as the images obtained applying the first approach. After all, the images used for the psychophysical experiment might still be considered acceptable.

A total of 22 images for details 1 and 6 and a total of 40 images for details 2, 3, 4 and 5 were used for the psychophysical experiment. 9 out of 15 participants can be considered as expert observers, 6 out of 15 participants are naïve observers. The computed results from both groups however do not seem to vary significantly. The possible reason is that almost all the images are greyscale images instead of colour images; the factors influencing the human observation might be slightly simpler than the situation of comparison among colour images. As a result, the scores from the 15 observers were combined for analysis. However, it is suggested that a more scientific approach should be considered with regard to the observers.

The result of the psychophysical experiment seems to be reasonable since the average scores from the observers revealed that SWIR data has proven to be able to supply images with more invisible information. Thus is not surprising as SWIR data contain only the spectral information outside the human visual range. In particular, the ICA method outperformed all the other algorithms, especially based on SWIR data. The 4th component applying ICA on SWIR data was identified to be the best method for the scratch like features on the painting. With regard to the worst algorithm, the 6th component of ICA processed on VNIR data appears to show least hidden information not only for the scratches, but also in general.

In order to verify the result from the psychophysical experiment, the set of 18 images were also computed on the VNIR-1m data so that full images could be obtained. The images were gathered along with the full processed images from SWIR-1m data and were provided to the museum restorer Mr Aslaksby for comparison and evaluation.

An interview and discussion was conducted with Mr Aslaksby by the author during the third visit. The outcome of the interview was quite positive even though one set of data applied was altered in comparison with the data applied in the psychophysical experiment. The processed image with the best invisible quality considered by Mr Aslaksby coincides with the best result obtained from the psychophysical experiment: SWIR\_IC4 image.

However, Mr Aslaksby accepted the fact that there is no universal best image for all the details since some of the details such as the tallow dropping were not visible even on SWIR\_IC4, but on the other processed images. It can be concluded that for certain type of details, a specific algorithm might be applied. Consequently, based on the result obtained previously, it might also be concluded that scratch-like artefacts might be identified with SWIR\_IC4 algorithm and tallow dropping artefact might be identified with SWIR\_IC5 or VNIR\_IC2. The second coat of painting on the other hand might be identified with UV image. However, these conclusions should be researched further to determine if they can be applied universally. Furthermore, Mr Aslaksby identified a few image sections that he considered intriguing and novel to him on the painting based on the processed images and expressed a keen interest to research it further.

A piece of software was developed based on previous work so that the differences appearing during the transition between images could be observed by the museum spectators for educational purposes. The images used can be, for instance, a photographic RGB version of a painting and processed image with the best quality in terms of invisible information.

When the image with the most identifiable invisible features is located according to the psychophysical experiment, this image can be combined into the RGB image acquired from VIS region. Since the hyperspectral data is applied for this project, the RGB image was attained implementing CMF under illuminant D65 followed by Gamma correction. An image fusion method proposed by Tsagaris based on perceptual attributes was applied to fuse the image obtained from IR region to the RGB image. 100 images with natural colours were applied as the attributes.

The proposal by the author was to fuse the best result obtained from the first objective, most likely a processed image from IR region, to the RGB image acquired from the hyperspectral data. With the transformation taking advantage of perceptual attributes based on the images with natural colours, it was possible to display an image with perceptually more pleasing colours while revealing invisible information.

Different spatial and spectral dimensions on the available VNIR and SWIR data caused pixel registration problems; pixels could not be matched correspondingly for the afore-mentioned transformation. Subsequently, an example was applied for this objective instead of applying the actual result obtained from the objective number one. The first principal component from PCA in the IR region of VNIR-1m data was used as the IR region image. In order to compare the fused image, a photographic RGB version of *The Scream* substituted the 100 images with natural colours to obtain the correlation coefficient between the bands.

The colours of the image obtained based on perceptual attributes of the 100 images indeed seem to have been improved in comparison with the RGB image converted from the hyperspectral data. The author considers the image to appear perceptually more pleasant. The image obtained based on the photographic RGB version of *The Scream* instead produced unexpected colours. This image does not resemble the photographic RGB image or the RGB transformation from the hyperspectral data. Furthermore, the result does not seem to be applicable for museum restorers. The transformation proposed by Tsagaris and adapted by the author may seem to be novel and interesting; the actual application of the transformation however should be researched further.

## 6 Future Work

The proposed questions and hypotheses have been tackled to a certain extent. Particularly, regarding the first objective of observing invisible information some interesting results have been found at the time of the research. Nevertheless, problems also occurred during the process. Considering the intrinsic problems such as the existing infrastructure, the data supplied and the algorithms applied in order to obtain the processed images some concerns have been raised.

As mentioned previously, several sets of data contain different spectral and spatial resolutions in order to implement the proposed approaches for the research; different data with the same spatial resolution are desirable. Consequently, the pixel registration problem should be solved so that the algorithms proposed in this project can be applied accordingly and appropriately.

Furthermore, the images processed for the psychophysical experiment were not obtained according to the exact same framework. Though the implemented calculation for the research did not seem to affect significantly the final result, it is preferable that all the images acquired for the experiment are based on the same computation algorithms. A calculation and psychophysical experiment applying the same structure could then be conducted.

In addition, both evaluations were conducted based on subjective and perceptual opinions, objective calculation such as RMSE seemed not feasible due to the distinguishing sizes of the data. It would be interesting to analyse the images based on objective mathematical models.

The mathematical models for feature extraction and data reduction applied in this project are only concerned with linear transformations. Non-linear models were not considered since they are completely different cases from the linear model, for example ICA. It might also be a direction of interest for this project by alternating the linear models to non-linear models.

Hyperspectral data acquired from different paintings might be applied to substitute the current data in order to verify if the results for both objectives mentioned in the research remain the same for other cases.

## Bibliography

- [1] **Think Spectrally**, “What is spectral imaging?,” 2007. [Online]. Available: <http://www.vision.uji.es/~essys/what.html>. [Accessed 3 July 2013].
- [2] **Applied Spectral Imaging**, “What Is Spectral Imaging?,” 2013. [Online]. Available: <http://www.spectral-imaging.com/sales/what-is-spectral-imaging>. [Accessed 3 July 2013].
- [3] A. Plaza, J. A. Benediktsson, J. Boardman, J. Brazile, L. Bruzzone, G. Camps-Valls, J. Chanussot, M. Fauvel, P. A. Gualtieri, J. A. Gualtieri, M. Marconcini, J. C. Tilton and G. Trianni, “Recent Advances in Techniques for Hyperspectral Image Processing,” *Remote Sensing of Environment*, vol. 113, no. 1, pp. 110-122, 2009.
- [4] International Council of Museums - **Committee for Conservation**, “The Conservator-Restorer: a Definition of the Profession,” 1984. [Online]. Available: [http://www.icom-cc.org/47/#.Udls\\_22LebE](http://www.icom-cc.org/47/#.Udls_22LebE). [Accessed 3 July 2013].
- [5] **A. A. Gooch and J. Tumblin**, “Visualizing pentimenti : revealing the hidden history of paintings,” *Journal of Mathematics and the Arts*, vol. 0, no. 0, pp. 1-11, 2007.
- [6] N. Ohta and A. Robertson, *Colorimetry: Fundamentals and Applications.*, Chichester, UK: John Wiley & Sons, 2005.
- [7] T. Moseley and G. Zabierek, *AURPO Guidance on the Safe Use of Lasers in Research and Education*, Association of University Radiation Protection Officers, 2006.
- [8] J. Byrnes, *Unexploded Ordnance Detection and Mitigation*, Il Ciocco, Italy: Springer, 2008.
- [9] **9-4fordham**, “Electro Magnetic Spectrum and light,” [Online]. Available: <http://9-4fordham.wikispaces.com/Electro+Magnetic+Spectrum+and+light>. [Accessed 3 July 2013].
- [10] **C. Fischer and I. Kakoulli**, “Multispectral and hyperspectral imaging technologies in conservation: current research and potential applications,” *Reviews in Conservation*, vol. 7, pp. 1-16, 2006.
- [11] **The Full Spectral Imaging Project**, “Full Spectral Imaging - Description,” 6 April 2012. [Online]. Available: <http://fullspectralimaging.net/FULL%20SPECTRAL%20IMAGING.htm>. [Accessed 6 July 2013].



- [12] L. Ferrato and K. W. Forsythe, "Comparing Hyperspectral and Multispectral Imagery for Land Classification of the Lower Don River," *Journal of Geography and Geology*, vol. 5, no. 1, pp. 92-107, 2013.
- [13] Wikipedia, "Hyperspectral imaging," 19 June 2013. [Online]. Available: [http://en.wikipedia.org/wiki/Hyperspectral\\_imaging](http://en.wikipedia.org/wiki/Hyperspectral_imaging). [Accessed 6 July 2013].
- [14] R. Shrestha, A. Mansouri and J. Y. Harderberg, "Multispectral imaging using a stereo camera : concept, design and assessment," *EURASIP Journal on Advances in Signal Processing*, p. 57, 2011.
- [15] P. Barry, C. Sejal and S. Carman, "EO - 1 Hyperion science Data User's Guide," *TRW Space, Defense and Information Systems*, vol. 1, pp. 1-65, 2001.
- [16] P. Shippert, "Introduction to Hyperspectral Image Analysis," *Research Systems, Inc.*, Undated.
- [17] National Museum Liverpool, "Scanning Electron Microscopy," 2013. [Online]. Available: <http://www.liverpoolmuseums.org.uk/conservation/departments/science/scanning-electron-microscopy.aspx>. [Accessed 6 July 2013].
- [18] The British Museum, "Scanning Electron Microscopy (SEM)," 2013. [Online]. Available: [http://www.britishmuseum.org/about\\_us/departments/conservation\\_and\\_science/research/scientific\\_techniques/scanning\\_electron\\_microscopy.aspx](http://www.britishmuseum.org/about_us/departments/conservation_and_science/research/scientific_techniques/scanning_electron_microscopy.aspx). [Accessed 6 July 2013].
- [19] G. Epitropou, "Hyperspectral imaging and spectral classification algorithms for the non-destructive analysis of El Greco's paintings," *Technical University of Crete, Kounoupidiana, Chania*.
- [20] The Field Museum, "Portable X-Ray Fluorescence (PXRF)," 2013. [Online]. Available: <http://fieldmuseum.org/portable-x-ray-fluorescence-pxrf>. [Accessed 6 July 2013].
- [21] M. Perez-Alonso, K. Castro and J. M. Madariaga, "Investigation of degradation mechanisms by portable Raman spectroscopy and thermodynamic speciation: The wall painting of Santa Maria de Lemoniz (Basque Country, North of Spain)," *Analytica Chimica Acta*, vol. 571, pp. 121-128, 2006.
- [22] P. Vandenberghe and L. Moens, "The application of Raman Spectroscopy for the Non-destructive Analysis of Art Objects," *Roma 2000 15th WCNDT, 2013*. [Online]. Available: <http://www.ndt.net/article/wcndt00/papers/idn163/idn163.htm>. [Accessed 6 July 2013].
- [23] R. Mukhopadhyay, "The art of Raman," *Chemistry World*, pp. 44-47, January 2010.
- [24] X. Jia and J. Richards, "Segmented principal components transformation for efficient hyperspectral remote-sensing image display and classification," *IEEE Transactions on*

- Geoscience and Remote Sensing*, vol. 37, no. 1, pp. 538-542, 1999.
- [25] L. A. Klerk, A. Broersen, I. W. Fletcher, R. van Liere and R. M. A. Heeren, "Extended data analysis strategies for high resolution imaging MS: New methods to deal with extremely large image hyperspectral datasets," *International Journal of Mass Spectrometry*, vol. 260, pp. 222-236, 2007.
- [26] J. S. Tyo, A. Konsolakis, D. I. Diersen and R. C. Olsen, "Principal-Components-Based Display Strategy for Spectral Imagery," *IEEE Transactions on Geoscience and Remote Sensing*, vol. 41, no. 3, pp. 708-718, 2003.
- [27] S. Cai, Q. Du, R. Moorhead, M. J. Mohammadi-Aragh and D. Irby, "Noise-adjusted principal component analysis for hyperspectral remotely sensed imagery visualization," in *Proc. IEEE Vis. Conf.*, 2005.
- [28] Q. Du, N. Raksuntorn, S. Cai and N. Younan, "Color representation and classification for hyperspectral imagery," *Proc. Int. Geosci. and Remote Sens. Symp.*, pp. 537-540, 2006.
- [29] S. Minhayenud, S. Chitwong and F. Cheevasuvit, "A Fast Intensity-Hue-Saturation Fusion Approach via Principal Component Analysis for IKONOS Imagery," in *ASPRS Annual Conference*, Portland, 2008.
- [30] V. Tsagaris and V. Anastassopoulos, "Multispectral image fusion for improved RGB representation based on perceptual attributes," *International Journal of Remote Sensing*, vol. 26, no. 15, pp. 3241-3254, 2005.
- [31] S. Le Moan, A. Mansouri, Y. Voisin and J. Y. Harderberg, "A Constrained Band Selection Method Based on Information Measures for Spectral Image Color Visualization," *IEEE Transactions on Geoscience and Remote Sensing*, vol. 99, pp. 1-12, 2011.
- [32] Q. Du, N. Raksuntorn, S. Cai and R. J. Moorhead, "Color display for hyperspectral imagery," *IEEE Trans. on Geosci. and Remote Sens.*, vol. 46, pp. 1858-1866, 2008.
- [33] H. Zhang, D. W. Messinger and E. D. Montag, "Perceptual display strategies of hyperspectral imagery based on PCA and ICA," *Proc. of SPIE*, 2009.
- [34] Y. Zhu, P. K. Varshney and H. Chen, "Evaluation of ICA based fusion of hyperspectral images for color display," *Information Fusion 10th International Conference*, pp. 1-7, 2007.
- [35] P. Aspden, "So, what does 'The Scream' mean?," 21 April 2012. [Online]. Available: <http://www.ft.com/cms/s/2/42414792-8968-11e1-85af-00144feab49a.html#axzz2LNacnLmw>. [Accessed 13 July 2013].

- [36] A. Lubow, “Edvard Munch: Beyond The Scream,” March 2006. [Online]. Available: <http://www.smithsonianmag.com/arts-culture/munch.html>. [Accessed 13 July 2013].
- [37] E. Cohn, “The Scream Auction: Munch's Painting Is Not The Most Expensive Work Of Art Ever Auctioned,” 3 May 2012. [Online]. Available: [http://www.huffingtonpost.com/2012/05/03/the-scream-auction-munchs\\_n\\_1475918.html](http://www.huffingtonpost.com/2012/05/03/the-scream-auction-munchs_n_1475918.html). [Accessed 13 July 2013].
- [38] S. Esaak, “The Scream by Edvard Munch,” No Date. [Online]. Available: <http://arthistory.about.com/od/Edvard-Munch/ss/The-Scream-by-Edvard-Munch.htm>. [Accessed 13 July 2013].
- [39] E. Gamerman, “Selling 'The Scream',” *The Wall Street Journal*, 12 April 2012. [Online]. Available: <http://online.wsj.com/article/SB10001424052702303592404577364321881780342.html>. [Accessed 9 July 2013].
- [40] NorWaves, “Edvard Munch - The man behind "Scream" and The Munch Museum,” No Date. [Online]. Available: <http://www.norwaves.com/edvard-munch-man-behind-scream-and-munch-museum.html>. [Accessed 13 July 2013].
- [41] J. Jones and P. Allen, “Edvard Munch's The Scream analysed – interactive,” 3 May 2012. [Online]. Available: <http://www.guardian.co.uk/artanddesign/interactive/2012/may/03/edvard-munch-scream-interactive>. [Accessed 13 July 2013].
- [42] Bodkin Design & Engineering, “Hyperspectral Imaging Information,” 2013. [Online]. Available: <http://www.bodkindesign.com/products/hyperspectral-imaging/hyperspectral-imaging>. [Accessed 6 July 2013].
- [43] E. Munch, Artist, *The Scream*. [Art]. National Gallery.
- [44] Norsk Elektro Optikk A/S, “HySpex hyperspectral cameras,” [Online]. Available: <http://www.hyspex.no/products/>. [Accessed 6 July 2013].
- [45] J. Hernandez-Palacios, I. Baarstad, T. Løke, L. L. Randeberg and T. Skauli, “Design and Characterization of a Hyperspectral Camera for Low Light Imaging with Example Results from Field and Laboratory Applications,” Norsk Elektro Optikk A/S.
- [46] F. Deger, S. George and J. Y. Hardeberg, “Hyperspectral Image Capture and Analysis of The Scream,” Gjøvik University College, 2013.
- [47] Wikipedia, “Infrared,” 11 July 2013. [Online]. Available: <http://en.wikipedia.org/wiki/Infrared>. [Accessed 13 July 2013].

- [48] C. Bugli and P. Lambert, "Comparison between Principal Component Analysis and Independent Component Analysis in Electroencephalograms Modelling," *Biometrical Journal*, pp. 1-16, 2006.
- [49] P. Comon, "Independent Component Analysis," *Higher Order Statistics*, pp. 29-38, 1992.
- [50] ERDAS, "Feature Extraction & Classification," 2009. [Online]. Available: [www.erdas.com](http://www.erdas.com). [Accessed 9 July 2013].
- [51] H. C. Wu, L. H. Yu and W. K. Li, "An Independent Component Ordering and Selection Procedure Based on the MSE Criterion," in *Independent Component Analysis and Blind Signal Separation*, Berlin, Springer Berlin Heidelberg, 2006, pp. 286-294.
- [52] A. Delorme, "ICA (Independent Component Analysis) for dummies," No Date. [Online]. Available: <http://sccn.ucsd.edu/~arno/indexica.html>. [Accessed 9 July 2013].
- [53] J. V. Stone, *Independent Component Analysis: A Tutorial Introduction*, Massachusetts Institute of Technology, 2004.
- [54] A. Hyvärinen and E. Oja, "Independent component analysis: algorithms and application," *Neural Networks*, pp. 411-430, 2000.
- [55] S. Shimizu, A. Hyvärinen, P. O. Hoyer and Y. Kano, "Finding a causal ordering via independent component analysis," *Preprint submitted to Elsevier Science*, 2005.
- [56] A. Hyvärinen, P. O. Hoyer and M. Inki, "Topographic Independent Component Analysis," *Neural Computation*, pp. 1527-1558, 2001.
- [57] Y. Cheung and L. Xu, "Independent component ordering in ICA time series analysis," *Neurocomputing*, pp. 145-152, 2001.
- [58] A. Hyvärinen, "Survey on Independent Component Analysis," *Neural Computing Surveys* 2, pp. 94-128, 1999.
- [59] K. Delac, M. Grgic and S. Grgic, "A Comparative Study of PCA, ICA and LDA," University of Zagreb, FER, Unska 3/XII, Zagreb, Croatia, No Date.
- [60] A. García-Ferrer, E. González-Prieto and D. Peña, "International Institute of Forecasters," No Date. [Online]. Available: <http://www.forecasters.org/submissions08/GONZALEZ-PRIETOESTERISF2008.pdf>. [Accessed 10 July 2013].
- [61] ENVI, "ENVI User's Guide: Transforms. Minimum Noise Fraction Transform," *Vizuális Információ*, 12 Aug 2005. [Online]. Available: [http://geol.hu/data/online\\_help/Minimum\\_Noise\\_Fraction\\_Transform.html](http://geol.hu/data/online_help/Minimum_Noise_Fraction_Transform.html). [Accessed

10 July 2013].

- [62] **S. C. Vermillion and S. A. Sader**, “Use of the Minimum Noise Fraction Transform to Analyse Airborne Visible/Infrared Imaging Spectrometer (AVIRIS) Data of Northern Forest Types,” **Maine Image Analysis Laboratory, University of Maine, Orono, ME USA 04473**, No Date.
  
- [63] **J. W. Boardman and F. A. Kruse**, “Automated spectral analysis: A geologic example using AVIRIS data, north Grapevine Mountains, Nevada,” *Proceedings, ERIM Tenth Thematic Conference on Geologic Remote Sensing*, pp. 1-407-1-418, 1994.
  
- [64] **A. A. Green, M. Berman, P. Switzer and M. D. Craig**, “A Transformation for Ordering Multispectral Data in Terms of Image Quality with Implications for Noise Removal,” *IEEE Transactions on Geoscience and Remote Sensing*, vol. 26, pp. 65-74, 1988.
  
- [65] **V. Bruce, P. R. Green and M. A. Georgeson**, *Visual Perception (3rd ed.)*, Psychology Press, 1996.
  
- [66] **M. Pedersen**, “Image quality evaluation using psychophysical approaches,” **The Norwegian Color Research Laboratory, Gjøvik, Norway**, 2012.
  
- [67] **CIE**, “Guidelines for the Evaluation of Gamut Mapping Algorithms,” **CIE**, 2004.
  
- [68] **H. Y. Chong, S. J. Gortler and T. Zickler**, “The von Kries Hypothesis and a Basis for Color Constancy,” *Proc. IEEE International Conference on Computer Vision (ICCV)*, pp. 1-8, 2007.

## **Appendix A**

This Appendix contains the set of instructions and ranking sheet used for the psychophysical experiment. The individual images used during the experiment are omitted as these were part of the on the screen assessment. These images are however available from the author on request.

### Quality Assessment Experiment

You will be shown a series of images. The images aim to show information not explicitly visible to the human eye of the painting **The Scream** obtained using a variety of processing techniques. Different parts of the painting are denoted in an exemplary image. For each set of images the observer has to judge and rank the quality and the extent of the “invisible” information presented in terms of one specific detail. The observer is asked to mark the quality of the methods according to the level of the perceived “invisible” information of the specified detail. The scale values 3, 2, 1, 0, -1, -2, -3 are denoted as follows:

Category	Explanation
<b>3: Extremely Good</b>	<b>The described detail has excellent visibility:</b> The described detail is easily identifiable and is visible without explicitly pointing at it or prior knowledge of the detail.
<b>2: Very Good</b>	<b>The described detail has very good visibility:</b> The described detail is identifiable and is visible without prior knowledge of the detail.
<b>1: Good</b>	<b>The described detail has good visibility:</b> The described detail is visible without prior knowledge of the detail but is less explicit.
<b>0: Adequate</b>	<b>The described detail has adequate visibility:</b> The described detail is visible with prior knowledge of the detail and it is fairly identifiable without careful examination of the neighborhood.
<b>-1: Poor</b>	<b>The described detail has poor visibility:</b> The detail is not quite visible or partially visible. If prior knowledge is given, and careful examination of the neighborhood is conducted, the detail can be seen slightly.
<b>-2: Very Poor</b>	<b>The described detail has very poor visibility:</b> The detail is not visible even after a careful study of the neighborhood within the detail.
<b>-3: Extremely Poor</b>	<b>The described detail has very poor visibility:</b> The detail is not visible at all or seems only noise present.

#### Specified details to look at:

**Detail 1:** The **blue colour** was retouched with a darker blue; it is unknown if the artist intentionally painted it with darker blue or not.

**Detail 2:** A **tilted 4-shape scratch** on the head of the figure, probably because of careless handling of the painting in the past.

**Detail 3:** A **hook-shape scratch** on the eye of the figure, probably because of careless handling of the painting in the past.

**Detail 4:** A **horizontal line shaped scratch** on the chine of the figure **intersecting a vertical scratch to the right** of the figure inflicted probably because of careless handling of the painting in the past.

**Detail 5:** A **tallow dropping**.

**Detail 6:** A **cluster of tallow droppings** with possible intentional restoration, but could not be removed without harming the painting.

The details are marked on the exemplary RGB image on page 3. Other examples can be found from the folder Method Examples.

3	2	1	0	-1	-2	-3
Extremely Good	Very Good	Good	Adequate	Poor	Very Poor	Extremely Poor



			Details					
			1	2	3	4	5	6
With IR Camera								
With Raking light								
With RGB Camera								
<b>SWIR</b>	ICA	PC1						
		PC2						
		PC3						
		PC4						
		PC5						
		PC6						
	MNF	PC1						
		PC2						
		PC3						
		PC4						
		PC5						
		PC6						
	PCA	PC1						
		PC2						
		PC3						
		PC4						
		PC5						
		PC6						
With UV light								
<b>VNIR</b>	ICA	PC1	-					-
		PC2	-					-
		PC3	-					-
		PC4	-					-
		PC5	-					-
		PC6	-					-
	MNF	PC1	-					-
		PC2	-					-
		PC3	-					-
		PC4	-					-
		PC5	-					-
		PC6	-					-
	PCA	PC1	-					-
		PC2	-					-
		PC3	-					-
		PC4	-					-
		PC5	-					-
		PC6	-					-

